Bio-Based Engineered Adsorbents for Sequestration of Persistent Emerging Pollutants: Process Optimization and Practical Applications in Water Treatment

A Thesis

submitted for the partial fulfilment

of requirements for the award of

DOCTOR OF PHILOSOPHY

by

AJIT KUMAR

(196106002)

Under the supervision of
Dr. Selvaraju Narayanasamy

Biochemical and Environmental Engineering Laboratory
Department of Biosciences and Bioengineering
Indian Institute of Technology Guwahati
Guwahati, Assam - 781039, India
May 2024

This thesis is dedicated to

My Family and Friends

Indian Institute of Technology Guwahati
Department of Biosciences and Bioengineering
Guwahati – 781039, Assam, India

DECLARATION

I, hereby declare that the content embodied in this thesis entitled **"Bio-Based Engineered Adsorbents for Sequestration of Persistent Emerging Pollutants: Process Optimization and Practical Applications in Water Treatment"** is the result of investigations carried out by me in the Department of Biosciences and Bioengineering, Indian Institute of Technology Guwahati, Assam, India under the guidance of **Dr. Selvaraju Narayanasamy**.

In keeping with the general practice of reporting scientific observations, due acknowledgments have been made wherever the work of other researchers have been referred. Further, the data in the thesis are collected by me. I certify that there is no fabrication or manipulation of data in the thesis.

Ajit Kumar

Ajit Kumar

196106002

Date: April, 2024

Place: IIT Guwahati

Indian Institute of Technology Guwahati
Department of Biosciences and Bioengineering
Guwahati – 781039, Assam, India

CERTIFICATE

This is to certify that the work presented in the thesis entitled **"Bio-Based Engineered Adsorbents for Sequestration of Persistent Emerging Pollutants: Process Optimization and Practical Applications in Water Treatment"** by **Ajit Kumar (196106002)** represents an original work under the guidance of **Dr. Selvaraju Narayanasamy**, **Department of Biosciences and Bioengineering, Indian Institute of Technology (IIT) Guwahati, Assam, India**. This study has not been submitted elsewhere for a degree.

Signature of student:
Date:
Place:

Ajit Kumar

Ajit Kumar (196106002)

Signature of supervisor:
Date:
Place:

N. Sy

Dr. Selvaraju Narayanasamy

Associate Professor (Thesis Supervisor)
Department of Biosciences and Bioengineering
Indian Institute of Technology Guwahati
Guwahati, Assam, India.

Acknowledgment

The journey of my Ph.D. program has been a roller coaster ride with its ups and downs, and the successful completion of the ride was only possible because of several instrumental people. I want to take this opportunity to express my sincere gratitude to everyone for making this journey worthwhile. First and foremost, I would like to thank ***my parents, sister, and brothers*** *for their patience, understanding, and inspiration. This would not have been possible without their unwavering and unconditional love and support always given to me, for which I shall forever remain grateful.*

During my journey toward my Ph.D., I have been fortunate to have had the guidance and support of an exceptional supervisor, ***Dr. Selvaraju Narayanasamy****, Associate Professor in the Department of Biosciences and Bioengineering at IIT Guwahati. Selva Sir has been a teacher, an inspiration to me, a role model, and a pillar of support. I am highly grateful to him for providing me with the opportunity to grow under his guidance over the past few years. Whenever I faced any difficulties in my research work, he went above and beyond to assist and bring me out of the lag phase. This Ph.D. work and thesis would not have been possible without his outstanding guidance and support. I shall be eternally grateful to him for his assistance.*

I sincerely thank my Doctoral committee members, ***Prof. Debasish Das****,* ***Prof. Lingaraj Sahoo,*** *and* ***Prof. Sudip Mitra,*** *for their constructive criticism, precious suggestions, motivation, and support throughout this work. I owe my gratitude to former HOD* ***Prof. Latha Rangan*** *for her administrative capability. I would like to thank the present HOD,* ***Prof. Rakhi Chaturvedi,*** *for providing departmental facilities. I am grateful to the* ***Department of Biosciences and Bioengineering*** *and* ***Central Instruments Facility****, IIT Guwahati, for providing technical and instrumental support for my research work. I wish to thank all the non-teaching staff and teaching assistants who helped with different instrumentations. I would gratefully acknowledge the* ***IIT Guwahati*** *and the* ***Ministry of Education, Government of India,*** *for providing me with the Ph.D. fellowship during all these years.*

I will take this opportunity to express my gratitude to all my past and present ***Biochemical and Environmental Engineering Laboratory*** *members. My special thanks to my senior,* ***Dr. Chandi Patra,*** *for his endless help and support throughout my Ph.D. journey and particularly for guiding me in paper publications. I am grateful to my lab fellow* ***Vishnu Priyan V*** *for helping me with various projects. I express my sincere thanks to my lab juniors (****Ragavan C., Sandhya***

S., Harish Kumar R., Jyoti Prakash Ray., Jothika J., Mohammed Askkar Deen F, Jeevanantham S., Ajithkumar V., Debanjana Ghosh, and Anushka Singh*) for their valuable discussion and help provided during my tenure. Every result described in this thesis was accomplished with the help and support of fellow lab mates. I also want to extend my deepest gratitude to all the previous M. Tech students,* ***Rishabh Gupta, Anjali J., Nirvesh Patel, Bedadeep D****,* ***Ghurupreya R.,*** *and current M. Tech student* ***Pavithra P****. I want to express my gratitude to my friends, who provided bond, encouragement, and a sense of camaraderie throughout my time as a Ph.D student. Their insights and perspectives enriched my research and made the experience of doctoral study more enjoyable.*

I owe my special praises to my friends from IIT Guwahati, ***Chandi, Alok Kumar Pandey, Alok Senapati, Arman Mohanty, Suraj Panda, Pratik Nag, Md Rafi Uz Zama Khan, Nikhil Kulkarni, Siddhartha Neog, Sahil Dhull,*** *and* ***Rahul Bhagawati****. They have been there for me during difficult times and created beautiful memories I will cherish forever.*

Words cannot describe how much I appreciate the support of my life partner. I would like to thank my wife, ***Kanchan,*** *for her love and unwavering support. I also want to mention my daughter,* ***Subhlaxmi K.,*** *who has brought immense joy to our lives. I am thankful to God for blessing me with completing my doctoral work.*

May 2024 ***AJIT KUMAR***

ABSTRACT

The rapid growth of industries and cities puts significant strain on natural resources, leading to severe ecological impacts. One of the most pressing issues is water pollution caused by persistent emerging pollutants (PEPs). These pollutants include pharmaceuticals, pesticides, herbicides, personal care products, endocrine disruptors, illicit drugs, food additives, hydrocarbons, metabolites, microplastics, and more. PEPs are not typically regulated under current environmental laws as they occur in relatively low concentrations. However, their persistent or pseudo-persistent nature can lead to various environmental and health impacts on water ecosystems and living organisms. Therefore, it is imperative to sequester these contaminants from water systems.

While various treatment methods exist, adsorption emerges as a prominent approach for sequestering these contaminants due to its efficiency at low pollutant concentrations, ease of implementation, cost-effectiveness, selectivity, economic feasibility, and potential to achieve environmental sustainability without causing secondary pollution. The selection of precursors and modification of adsorbents/biosorbents are crucial factors that influence the efficiency of the adsorption process for different target pollutants. This thesis work primarily focuses on developing bio-based engineered adsorbents from natural derivatives, including agricultural byproducts (lignocellulosic wastes) and biopolymers (Chitosan and Carboxymethyl cellulose), addressing the significant challenges associated with adsorbents include difficulties in their recovery post-treatment and limited surface functionality, which hinder the applicability of the adsorption process for selectively targeting pollutants. These limitations could be overcome by developing magnetic adsorbents or transforming precursors into bead form.

Optimizing process parameters such as pH, adsorbent/biosorbent dosage, initial pollutant concentration, contact time, and temperature helps establish suitable conditions for pollutant

sequestration. The second significant aspect of this thesis involves phytotoxicity evaluation before and after treatment using model organisms to assess the safety and efficacy of the adsorption process. Furthermore, this thesis aims to bridge the gap between laboratory-scale studies and practical applications by considering real-time factors such as reusability and column studies. The research findings contribute to a theoretical understanding of the adsorption process for various PEPs and offer practical insights into the feasibility and sustainability of using bio-based engineered adsorbents for large-scale water treatment. These findings are expected to have significant implications for water quality management and environmental sustainability, potentially influencing the regulation of persistent emerging pollutants in water ecosystems.

ORGANIZATION OF THESIS

The present thesis is divided into six chapters:

Chapter 1 provides an introduction to persistent emerging pollutants (PEPs), their presence in various water sources, and their harmful effects on the environment, animals, and human health. The chapter also discusses different methods to remove PEPs from aqueous solutions, including physical, chemical, and biological techniques, and outlines the aim and objectives of this thesis.

Chapter 2 presents a detailed overview of using magnetic acid-activated carbon (MAAC) for the adsorptive removal of Ciprofloxacin (CIP). The chapter describes the preparation of MAAC from *Sterculia villosa Roxb* shells, followed by magnetization via co-precipitation with $FeSO_4.7H_2O$ and $FeCl_3.6H_2O$.

Chapter 3 covers the synthesis of activated carbon/chitosan beads (ACCB) for the adsorptive removal of Diclofenac (DIF) from aqueous solutions.

Chapter 4 describes the fabrication of carboxymethyl cellulose (CMC)-T-CH adsorbent through the crosslinking of carboxymethyl cellulose (CMC) and chitosan (CH) with triethylenetetramine. The chapter also outlines the application of this adsorbent in remediating dye-containing synthetic water (Congo Red and Direct Blue 6).

Chapter 5 investigates the effectiveness of a continuous packed bed adsorption process for removing Direct Blue dye from water using a biosorbent of chitosan and carboxymethylcellulose (CMC-T-CH).

Finally, **Chapter 6** provides a summary and conclusion based on the thesis work, highlighting some recommendations for future research in this field.

Contents

Chapter 3: Activated carbon-chitosan based adsorbent for the efficient removal of the emerging contaminant Diclofenac: Synthesis, characterization and phytotoxicity studies

List of Figures

List of Tables

Glossary of Acronyms

AFM	Atomic Force Microscopy	**CPCB**	Central Pollution Control Board
AAC	Acid-activated carbon	**CR**	Congo red
ACCB	Activated carbon-chitosan beads	**DB**	Direct blue
AOPs	Advanced Oxidation Processes	**DIF**	Diclofenac
BET	Brunauer-Emmett-Teller	**DR**	Dubinin Radushkevich
BOD	Biochemical oxygen demand	**ECs**	Emerging Contaminants
CAC	Commercial activated carbon	**EDCs**	Endocrine-disrupting compounds
CECs	Contaminants of Emerging Concern	**EDS**	Energy-dispersive X-ray spectroscopy
CH	Chitosan	**FESEM**	Field emission scanning electron microscopy
CIP	Ciprofloxacin	**FTIR**	Fourier-transformed infrared spectroscopy
CMC	Carboxymethyl cellulose	**MAAC**	Magnetic acid activated carbons
CMC-T-CH	Carboxymethyl cellulose-triethylenetetramine - chitosan adsorbent	**NSAID**	Non-steroidal anti-inflammatory drugs
COD	Chemical oxygen demand	**PCPs**	Personal Care Products
PEPs	Persistent Emerging Pollutants	**TGA**	Thermal gravimetric analysis

PPs	Pharmaceutical products	**US EPA**	United States – Environmental Protection Agency
SEM	Scanning Electron Microscopy	**VSM**	Vibrating Sample Magnetometer
TDS	Total dissolve solids	**WHO**	World Health Organisation
TEM	Transmission Electron Microscopy	**WWTP**	Wastewater Treatment Plant
TETA	Triethylenetetramine	**XRD**	X-ray diffraction

List of Notations

Ms	Saturation magnetization	**qe**	quantity of adsorbate adsorbed
Q_t	Adsorption capacity	**K_L**	Langmuir isotherm constant
%R	Removal efficiency	**K_F**	Freundlich isotherm constant
t	time	**q_m**	maximum adsorption capacity
C_t	Concentration of adsorbate at time 't'	**k_1**	pseudo-first-order rate constant
C_o	Initial concentration of adsorbate	**k_2**	pseudo-second-order rate constant
V	Volume	**F**	Flow rate
m	Mass of adsorbent	**t_{total}**	Total time for column saturation
g	Gram	**m_{total}**	Total amount of dye introduced into the column
h	Hours	**Q_{total}**	amount of dye molecules adsorbed by adsorbent in the column experiment
J	Joule	**$q_{e(exp)}$**	Maximum adsorption capacity in column studies
K	Kelvin	**V_{eff}**	Total volume of the effluent

Chapter 1

General Introduction

And

Theoretical Background

1.1 Introduction

Water is a critical component of life, and its importance has been amplified by the rapid pace of modernization, urbanization, and industrialization. The cumulative impact of these factors has led to a water shortage in many regions worldwide. As per the UN World Water Development Report 2023, approximately 2 billion individuals, constituting 26% of the global population, lack access to safe drinking water (*Imminent Risk of a Global Water Crisis, Warns the UN World Water Development Report 2023 | UNESCO*, n.d.). Additionally, 3.6 billion people, accounting for 46% of the population, do not have access to properly managed sanitation facilities (*Imminent Risk of a Global Water Crisis, Warns the UN World Water Development Report 2023 | UNESCO*, n.d.).

The report also highlights that between two and three billion people experience water shortages for at least one month annually. These shortages pose significant risks to people's livelihoods, particularly concerning food security and electricity availability. Projections indicate that the number of people in urban areas facing water scarcity is likely to double from 930 million in 2016 to between 1.7 and 2.4 billion by 2050. The escalating frequency of extreme and prolonged droughts is straining ecosystems, leading to dire consequences for various plant and animal species (*Imminent Risk of a Global Water Crisis, Warns the UN World Water Development Report 2023 | UNESCO*, n.d.).

In India, the situation is particularly alarming. According to a 2023 report by the World Bank, many Indians face high to extreme water stress (*UN World Water Development Report 2023 | UN-Water*, n.d.). Approximately 600 million individuals, nearly half of the country's population, experience severe water stress. Additionally, three-fourths of rural households in India lack access to piped, safe drinking water, relying instead on sources that pose significant health hazards (*Flagship UN Report Extolls Win-Win Water Partnerships to Avert Global Crisis | UN News*, n.d.). India has also become the leading global extractor of groundwater, accounting for 25%

of the total extracted worldwide. Moreover, around 70% of India's water sources are contaminated, contributing to the deterioration of major rivers due to pollution (*Flagship UN Report Extolls Win-Win Water Partnerships to Avert Global Crisis | UN News*, n.d.). Industries often discharge their wastewater uncontrollably into water bodies, contaminating both surface and groundwater (Zhu et al., 2023). These pollutants, known as Persistent Emerging Pollutants (PEPs), are xenobiotic and persistent in nature (Arman et al., 2021; M. Kumari et al., 2022; Shah et al., 2020). Their concentration has increased from ng L^{-1} to µg L^{-1}, posing a significant threat to the environment and public health.

The presence of these contaminants in our water supplies poses a significant challenge to public health and environmental sustainability. Ensuring access to clean, safe water at an affordable cost is a critical humanitarian goal, and arguably one of the most pressing challenges in our global landscape. As we move forward, it will be essential to develop and implement effective strategies for monitoring, managing, and mitigating the impact of these emerging contaminants.

This thesis explores a variety of adsorbents that have been proposed for the effective removal of Persistent Emerging Pollutants (Ciprofloxacin, Diclofenac, Congo red dye and Direct Blue dye). The proposed adsorbents have demonstrated high removal efficiency. The primary focus of this work is on the synthesis, characterization, and application of these materials for wastewater remediation. Engineered adsorbents, which undergo individualized modifications during synthesis to enhance their physicochemical properties, could potentially serve as a long-term solution for environmental clean-up.

1.2. Persistent Emerging Pollutants (PEPs)

'Emerging Contaminants (ECs)', or 'Persistent Emerging Pollutants (PEPs)', or 'Contaminants of Emerging Concern (CECs)' represent a broad spectrum of pollutants that include, but are not limited to, pharmaceuticals, pesticides, dyes, heavy metals, herbicides, personal care

products, endocrine-disrupting compounds, hydrocarbons, metabolites, and microplastics. These substances have the potential to infiltrate our water bodies, leading to a range of toxic effects that can harm both aquatic life and human health.

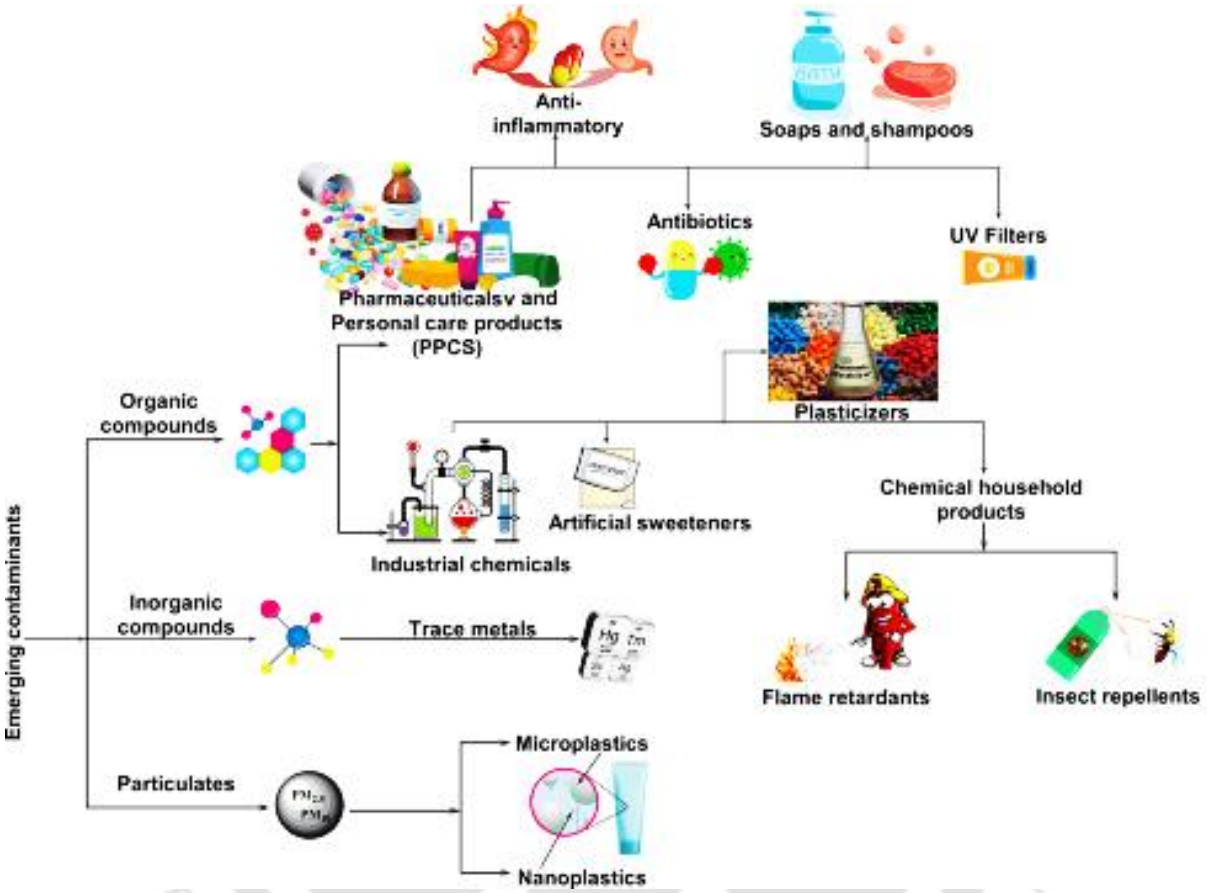

Figure 1.1: Examples of Persistent Emerging Pollutants

1.2.1. Pharmaceuticals Pollutants

Pharmaceuticals are a group of chemical substances that are used extensively in human and animal healthcare to prevent, treat, and cure various illnesses and diseases. This category consists of various compounds, including steroids, antibiotics, painkillers, legal and illegal drugs, and beta-blockers. Their distinct function causes them to remain in human and animal bodies, leading to potential environmental pollution. Many pharmaceutical substances have been observed in different environmental matrices, such as sediments, effluents, drinking water, and both natural and groundwater. These substances can boost the production of antibiotic-resistant genes in soil bacteria. Over 160 unique pharmaceuticals have been

identified in aquatic environments at concentrations ranging from nanograms to micrograms per liter. A comprehensive list of these pharmaceutical pollutants and their adverse effects can be found in Table 1.1.

India's pharmaceutical industry is primarily located in cities like Ahmedabad, Bangalore, Dehradun, Hyderabad, and Mumbai. Among these, Hyderabad stands out as the top producer of pharmaceuticals (Mathew & Unnikrishnan, 2012). For instance, in the wastewater treatment plant (WWTP) of Patancheru, Hyderabad, ciprofloxacin was found at concentrations of up to 31 mg per liter (Larsson et al., 2007). Similarly, studies by Deo and Halden (2013) revealed that Okhla WWTP's effluent had ciprofloxacin concentrations exceeding the predicted no-effect concentration (PNEC) of 0.005 µg/L. In Delhi's Yamuna River, both influents and effluents from wastewater showed a maximum concentration of ampicillin (104.2±98.11 µg/L and 12.68±8.38 µg/L, respectively) (Mutiyar & Mittal, 2014). Groundwater in Punjab, according to Jindal et al. (2015), contained diclofenac ranging from 6 to 48 ng/L. Guwahati's surface water was found to have high concentrations of acetaminophen (5.9 µg/L), caffeine (22.7 µg/L), and carbamazepine (75 ng/L) (Kumar et al., 2019). Furthermore, Subedi et al. (2015) reported elevated levels of amphetamine (0.984 µg/L), atenolol (3.18 µg/L), ibuprofen (2.32 µg/L), and triclocarban (6.18 µg/L) in Chennai's Cooum river. The Kaveri River was detected with carbamazepine at 13.0 ng/L (Ramaswamy et al., 2011). Finally, Diwan et al. (2010) identified various pharmaceuticals and personal care products (PPCPs) in Ujjain Charitable Trust Hospital's effluents, including ofloxacin (73 µg/L), levofloxacin (81 µg/L), and ceftriaxone (60 µg/L).

Table 1.1: Pharmaceutical pollutants and their adverse effects.

Pharmaceuticals	Examples	Function	Harmful effects
Analgesic	Acetaminophen, phenazopyridine, non-steroidal anti-inflammatory drugs (NSAID) such as diclofenac, ibuprofen, naproxen	Pain relief, NSAID also reduce inflammation	Ibuprofen could interfere with cardiac benefits of aspirin (Jones et al., 2005); analgesics can cause negative developmental effects (Bruce et al., 2010); diclofenac can be bioaccumulated (Escher et al., 2005)
Antibiotics	Tetracycline, ciprofloxacin, ofloxacin, sulfonamides (ex. sulfadiazine), amoxicillin, cefixime, metronidazole, trimethoprim	Kill or inhibit bacterial growth	Antibiotics have been shown to create antibiotic-resistant bacteria (tetracycline-resistant enterococci, antibiotic-resistant *Escherichia coli*) and can negatively affect plant growth (Baquero et al., 2008). Sulfonamides are found to be associated with birth defects (Crider et al., 2009)
Anticoagulant	Warfarin	Disrupt blood clotting factor synthesis or function to avert formation of blood clots	Warfarin, after prolonged exposure, could lead to severe bleeding due to its prolonged inhibition of vitamin K (WHO, 1989).
Anticonvulsant	Carbamazepine	Treat epileptic seizures	Could cause cancer (Bruce et al., 2010; Bull et al., 2011) and negatively affect reproduction and development (Bruce et al., 2010)
Antidiabetic	Metformin, insulin, pramlintide, acarbose, chlorpropamide	Lower glucose levels in the blood	Antidiabetics, such as metformin, can act as an endocrine disruptor, and is not easily degradable and is highly mobile in the environment (Lopez et al., 2015)
Antihistamine	Diphenhydramine	Block histamine action to treat allergic reactions	Diphenhydramine has been shown to cause acute and chronic toxicity to a variety of aquatic organisms (Du et al., 2014)
Antipsychotic	Loxapine Olanzapine Risperidone Chlorpromazine, Clozapine	Treat psychosis and other emotional or mental health conditions	Olanzapine, risperidone, chlorpromazine, clozapine are shown to be persistent, bioaccumulative, and toxic to human health and the ecosystem (David et al., 2018; Reichert et al., 2019). They are up-taken from hospital effluent contaminated soil and bioaccumulate in plant tissues (Xiang et al., 2018).
Antipyretic	Antipyrine, NSAIDs	Lower fever	Antipyrine is toxic to the mucosa and lungs and can cause organ damage (Tan et al., 2013)
Beta-blocker	Metoprolol, propranolol	Lower blood pressure	Can be toxic on organisms in aquatic environments and shows more toxicity to phytoplankton and zooplankton (Fent at al., 2006)
Fibrate	Gemfibrozil	Lower blood triglyceride levels	Developmental side effects and carcinogenic in rodents (Bruce et al., 2010) toxic to aquatic organisms (Fent at al., 2006)
X-ray contrast agent	Iopromide, diatrizoic acid	Enhance visibility of internal organs or structures for diagnostic X-rays	While x-ray contrast agents are generally non-toxic (Steger et al., 1999), they persist in the environment and chlorination has been shown to cause mutagenicity and acute toxicity of iopromide (Matsushita)

1.2.2. Personal care products

Personal care items encompass a variety of everyday household chemicals utilized for diverse functions such as beautification, health maintenance, and sanitation. This category also comprises a range of cosmetics, fragrances, and products for personal and skin care (Table 1.2). The extensive use of these skincare and personal care items leads to the frequent disposal of substantial quantities of waste from these products into our surroundings.

A significant portion of these personal care items are bioactive and are categorized based on their potential for retention and bioaccumulation, posing a threat to both the environment and the public at large (Dey et al., 2019; Juliano & Magrini, 2017). It is estimated that each year, the global production of triclosan and triclocarban amounts to approximately 15,000 tonnes and 227,000–454,000 kg respectively (Lehutso et al., 2017; Tchounwou et al., 2022). Typically, products from European countries contain triclocarban and triclosan concentrations of 0.2% and 0.3% respectively.

Table 1.2: Personal Care Products and their adverse effects.

Personal Care Products	**Examples**	**Function**	**Harmful Effects**
Shampoos and Soaps	Phthalates (Hoyett & Hoyett, 2017)	Used to clean our hair and skin	Associated with gestational diabetes, gestational hypertension, preterm birth, and developmental issues in children (Hoyett & Hoyett, 2017)
Perfumes and Lotions	Phthalates (Hoyett & Hoyett, 2017)	Used to add fragrance and moisturize the skin	Can lead to language and behavioral issues as well as changes in reproductive development (Hoyett & Hoyett, 2017)
Hair Dyes	Coal Tar (Mishra et al., 2020)	Used to change the color of hair	Associated with pigmented cosmetic dermatitis, folliculitis, and even cancers (Mishra et al., 2020)
Cosmetics	Diethanolamine (DEA) (Parlakidis et al., 2022)	Used to enhance or alter the appearance	Associated with detrimental effects on brain development and increased incidence of liver neoplasms and renal tubule adenoma in mice (Parlakidis et al., 2022)
Skin Lightening Creams	Mercury (Pramanik et al., 2021)	Used to lighten the skin tone	Can damage the kidneys, liver, and brain (Pramanik et al., 2021)

1.2.3. Dyes

Dyes are widely used across industries worldwide, including tanneries, food production, cosmetics, textiles, and medicine, with a global production of 1,000,000 tons (Maheshwari et al., 2021). Among these industries, textiles have a significant impact, releasing about 7.5 metric tons of dyes into the environment each year (Al-Tohamy et al., 2022; Maheshwari et al., 2021). The presence of dyes in water streams can severely affect living organisms. Due to their complex structures, which include aromatic rings bonded with different functional groups, dyes can absorb light within the 380–700 nm spectra (Qurrat-Ul-Ain et al., 2020; Sarkar et al., 2017). This absorption can hinder photosynthesis for aquatic plants, impacting the food chain (Hernández-Zamora & Martínez-Jerónimo, 2019). Furthermore, some dyes can be highly carcinogenic. For example, the proliferation of azo groups has been associated with the release of amines and benzidines. Since dye molecules are not easily broken down, they can persist in the environment, posing long-term hazards.

Directly releasing untreated dye-containing wastewater into natural water bodies can lead to harmful effects on aquatic organisms and fish due to the presence of metals and aromatic compounds. It can also impact human health, causing conditions like cancer, mutations, allergies, dermatitis, and kidney diseases (Al-Tohamy et al., 2022; Chung, 2016; Puvaneswari et al., 2006).

Additionally, the disposal of dye wastewater without proper treatment can also contribute to water pollution, affecting biodiversity, water quality, and ecosystem balance. Efforts to reduce dye pollution involve implementing stricter regulations on dye usage, promoting eco-friendly dyeing processes, and improving wastewater treatment technologies.

1.2.4. Pesticides

Pesticides play a vital role in protecting crops from insects, weeds, fungi, and other pests, which helps increase crop production. However, their excessive and improper use has caused

significant environmental contamination and negative effects on humans and other life forms. When it rains or crops are irrigated, water can carry pesticide residues to nearby surface water bodies or groundwater sources, either through runoff or leaching (Pradhan et al., 2022). This can lead to a range of issues, such as acute and chronic health problems in people of all ages due to exposure to pesticides through contaminated water. Additionally, pesticide residues can disrupt the ecosystem balance in water bodies (de Souza et al., 2020; Pradhan et al., 2022; Taha et al., 2014).

Contaminated irrigation water can also affect other crops and their environment, which is especially concerning in regions of intensive agriculture (Helmecke et al., 2020). Leaks of highly toxic substances into water supplies can have adverse effects on human and animal health. There are over 1,000 pesticides used worldwide to protect food from damage or destruction by pests (de Souza et al., 2020; Taha et al., 2014). Each pesticide has different properties and toxicological effects. Some of the older, cheaper pesticides can stay in the soil and water for years.

Organochlorine insecticides, like DDT and HCH, are the main pesticides used in India, making up over 70% of the total (Agarwal et al., 2015; Dutta Gupta et al., 2018). Residues of these pesticides have been discovered in public water supplies in cities like Delhi, Kanpur (in Uttar Pradesh), and Bhagalpur (in Bihar) (Agrawal et al., 2010; Aleem & Malik, 2005; Bakore et al., 2004; B. Kumari et al., 2007). Specifically, high levels of γ-HCH and malathion were found in surface water samples from the Ganga River in Kanpur (Malik et al., 2009; PK Mutiyar, 2012). Samples from the Bhagalpur River contained elevated levels of methyl parathion, endosulfan, and DDT. A study by the Industrial Toxicology Research Centre (ITRC) in Lucknow also identified 0.5671 parts per billion (ppb) concentrations of endosulfan in the river at Allahabad, Uttar Pradesh (Agarwal et al., 2015).

1.3. Sources of PEPs

PEPs can originate from various sources, including industrial activities, households, hospitals, and agricultural practices, and can enter the soil, atmosphere, or water bodies through several routes (Priya et al., 2022). The extent of their infiltration is largely dependent on their properties such as polarity, volatility, and persistence, as well as the characteristics of the environmental compartments.

The origins of these pollutants are diverse (Figure 1.2). They can come from various sources including (Arman et al., 2021; M. Kumari et al., 2022):

- **Agriculture**: Agricultural activities could introduce various contaminants into the environment, including pesticides and other chemicals used in farming.
- **Urban Runoff**: Urban areas could contribute a variety of contaminants, including those from industrial processes, residential areas, and transportation.
- **Household Products**: Ordinary household products such as soaps, disinfectants, and pharmaceuticals could become contaminants when they are disposed of in sewage treatment plants and subsequently discharged to surface waters.
- **Industrial and Agricultural Sources**: The pollutants mainly from industrial and agricultural sources, including micropollutants, synthetic dyes, compounds containing hazardous dyes, toxins, hormones, pharmaceuticals, endocrine disruptors, and pesticides.

Improper disposal of PEPs can lead to their entry into the water cycle through various means, such as being carried by runoff into rivers, direct discharge into water bodies, or seepage into the groundwater, which can then contaminate public water supplies. Even sewage systems and wastewater treatment plants can contribute to the presence of PEPs in surface and groundwater sources. These chemicals can cause harm to aquatic ecosystems and pose risks to human health when consumed through contaminated water sources. It is therefore crucial to implement proper disposal methods and effective wastewater treatment to minimize the environmental impact of PEPs on water quality and ecosystem health.

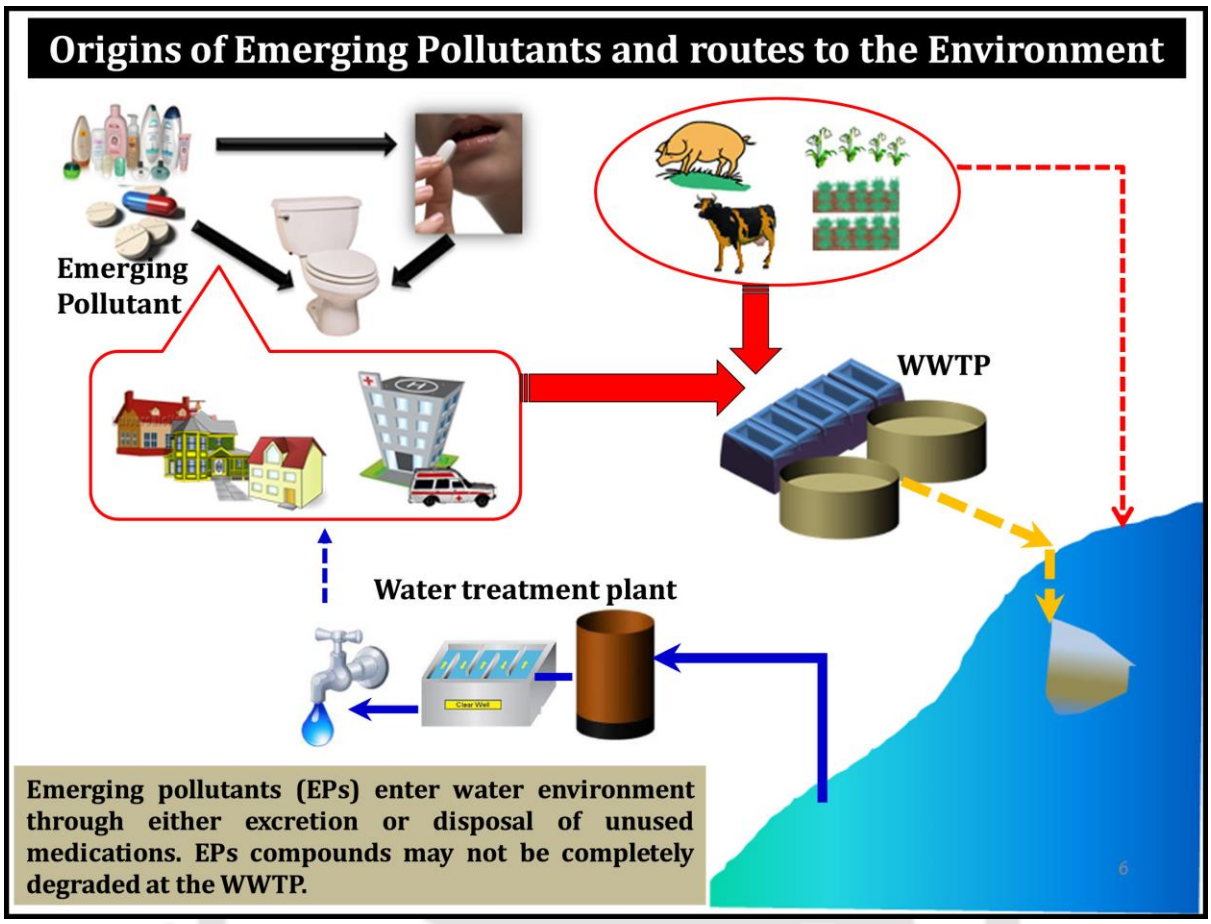

Figure 1.2: Conceptual illustration of the origin and pathway of emerging pollutants to the environment.

1.4. Remediation methods for removing PEPs

Removing PEPs from water is a complex task, as conventional water purification techniques are not designed for this purpose. However, several technologies and treatment strategies have shown potential in addressing this issue.

1.4.1. Advanced Oxidation Processes (AOPs)

AOPs are water treatment methods that use powerful oxidizing agents, such as hydrogen peroxide and ozone, to decompose and eliminate organic pollutants in water. This process generates highly reactive oxygen species that target the organic compounds in the water, either through a direct electrophilic assault via molecular ozone or an indirect attack through hydroxyl radicals (•OH). Recent research has assessed the effectiveness of AOPs in eliminating PEPs from various water sources (Anumol et al., 2016; Arman et al., 2021; Salimi et al., 2017).

1.4.2. Membrane Filtration

Technologies based on membrane filtration, including reverse osmosis and nanofiltration, have proven to be highly efficient in extracting PEPs from water. These methods employ a semi-permeable membrane to segregate and eliminate pollutants from water, capable of removing a broad spectrum of PEPs, including pharmaceuticals and endocrine-disrupting compounds. The application of membrane technology for PEPs is challenging due to the varied physicochemical properties of substances and the extensive range of parameters required to enhance the separation process (Shah et al., 2020). Suitable separation mechanisms and target pollutants narrow down the membrane selection. Furthermore, modifying the membrane surface with a specific compound may improve the separation efficiency.

1.4.3. Ozonation

Ozonation is a method used to treat water by using ozone gas. This process helps disinfect water and remove various types of contaminants, such as pharmaceuticals, personal care products, and compounds that disrupt the endocrine system. One interesting aspect of ozonation is its ability to break down these contaminants effectively. Ozone can undergo a process called autocatalysis, where its decomposition rate increases with higher pH levels. This leads to the formation of hydroxyl radicals, which are highly reactive and can target a wide range of pollutants.

Catalytic ozonation is a technique that enhances ozone decomposition and hydroxyl radical production by using catalysts. This method helps overcome some of the limitations of regular ozonation. There are two types of catalytic ozonation processes: homogeneous and heterogeneous. While homogeneous catalytic ozonation involves dissolved metal ions and may lead to secondary pollution, heterogeneous catalytic ozonation is considered more promising because it avoids this issue (Shah et al., 2020; Wang & Bai, 2017).

1.4.4. Ultraviolet (UV) treatment

UV treatment is a powerful method for disinfecting water and eliminating harmful contaminants. It has been proven to be highly effective in removing PEPs, such as pharmaceuticals and personal care products, from water. However, the success of UV treatment depends on various factors, including the intensity of the UV radiation, water quality parameters, and the type of reactor in use. There are multiple types of UV reactors used for water treatment, including low-pressure mercury lamps, medium-pressure mercury lamps, and UV-LEDs (Rizzo et al., 2019). Each reactor has its own unique advantages and limitations. The combination of UV treatment with hydrogen peroxide, known as the UV/H_2O_2 process, is an especially effective method for removing emerging contaminants. However, it is important to note that this process can also lead to the formation of disinfection by-products, which can be harmful to human health. Despite this, UV treatment offers many benefits over other treatment methods, including energy efficiency, low chemical consumption, and environmental friendliness (Shah et al., 2020). Nevertheless, it is important to conduct further research to optimize the UV treatment process for specific contaminants and water quality parameters.

1.4.5. Biological treatment

Biological treatment processes such as activated sludge process (ASPs), microalgae-based treatments, biological activated carbon (BAC), and membrane bioreactors (MBRs) have been proven effective for removing various PEPs. Bioreactors and constructed wetlands (CWs) use microorganisms to break down and eliminate contaminants in water. BAC is effective in removing analgesics, antibiotics, and pesticides, while MBRs have shown better removal of certain PEPs like PCPs, EDCs, and betablockers compared with CWs (Besha et al., 2017; Luo et al., 2014; Nguyen et al., 2022). However, these treatments have limitations such as long

retention time, membrane fouling, large area requirement, poor removal of some PEPs, and final disposal of the sludge that contains PEPs.

1.4.6. Adsorption

Adsorption is a widely used method for removing emerging contaminants from water in both drinking water and wastewater treatment processes. In this process, contaminants are attracted to the surface of a solid material called an adsorbent. Commonly used adsorbents for eliminating emerging contaminants include activated carbon, zeolites, and graphene-based materials. Activated carbon is favoured due to its large surface area, porous structure, and easy availability. However, recent research has shown that zeolites and graphene-based materials also perform well in this regard.

Several factors influence the efficiency of adsorption, such as the properties of the adsorbent, the concentration and type of contaminants, and the water's pH and temperature. The adsorption capacity of an adsorbent depends on its surface area, pore structure, and surface chemistry. A higher surface area allows an adsorbent to attract more contaminants, while a well-defined pore structure enhances its adsorption capacity. Additionally, the surface chemistry of the adsorbent affects its affinity for different types of contaminants.

Different contaminants exhibit varying adsorption efficiencies. Polar contaminants like pharmaceuticals and personal care products are more readily adsorbed compared to non-polar contaminants such as pesticides. The pH and temperature of the water also play a role in adsorption efficiency. Changes in these parameters can alter the surface chemistry of the adsorbent and the properties of contaminants. For example, acidic conditions can boost the adsorption of basic contaminants, while high temperatures can decrease the adsorption capacity of the adsorbent.

It is crucial to recognize that each treatment method has distinct advantages and limitations, and their effectiveness can vary depending on the specific type of PEPs or water sources being treated. The implementation of these technologies can also incur significant costs and may demand specialized expertise. Hence, continuous research and development of emerging technologies and treatment methods are imperative to efficiently eliminate PEPs from water, safeguarding public health and the environment.

1.4.7. Why adsorption as a promising treatment process for PEPs removal?

Adsorption is a water treatment method that involves attaching or adhering contaminants onto a solid substrate, known as the adsorbent. Compared to other treatment methods, adsorption offers several advantages, making it an effective option for removing PEPs (Kumar et al., 2022; Vishnu Priyan et al., 2022).

Selective Capability: Adsorption operates as a discerning process capable of targeting specific PEPs within water matrices, while preserving innocuous compounds unaltered. This attribute proves particularly consequential when confronted with low PEP concentrations or coexisting chemical species.

Broad Spectrum PEP Removal: Adsorption exhibits versatility in eliminating a diverse array of PEPs from water, encompassing pharmaceuticals, personal care products, and endocrine-disrupting compounds, among others. This broad applicability renders it a versatile option for addressing various PEP types.

High Removal Efficiency: Adsorption mechanisms can yield notable removal efficiencies reaching up to 99%, thereby positioning it as a highly effective treatment strategy for PEP removal from water.

Cost-Effectiveness: Adsorption typically presents a cost-efficient alternative to other treatment methodologies due to its reduced energy and chemical requirements. Furthermore,

the capacity for facile regeneration and reuse of adsorbents contributes to further cost reduction in the treatment cycle.

Simplicity of Implementation: Adsorption stands out for its straightforward and easily deployable nature as a water treatment modality. Its scalability enables seamless adjustment to accommodate varying plant sizes, while necessitating minimal operator training.

Synergy with Complementary Techniques: The compatibility of adsorption with adjunctive water treatment methodologies, such as advanced oxidation processes (AOPs) and membrane filtration, facilitates synergistic enhancement of overall treatment efficiency.

Environmental Considerations: Adsorption emerges as an environmentally sustainable treatment solution, characterized by minimal to negligible waste production. Moreover, its operability with renewable energy sources, such as solar or wind power, underscores its alignment with environmental sustainability principles.

In summary, adsorption emerges as a robust and economically viable water treatment modality, presenting numerous advantages over alternative techniques in the context of Persistent Emerging Pollutants (PEPs) removal. Its attributes, including selectivity, broad spectrum of PEP removal, high removal efficiency, cost-effectiveness, ease of implementation, compatibility with complementary treatment modalities, and environmental sustainability, collectively render it an appealing choice for PEP mitigation in aqueous environments.

1.5. Theoretical aspects

1.5.1. Isotherm models

Isotherm refers to the relationship between the equilibrium adsorbate concentrations in the liquid-phase and the equilibrium adsorption amount on the solid-phase at a certain temperature. Various isotherm models with their linear and non-linear equations were tabulated in the Table A1.

1.5.1.1. Langmuir isotherm model

The Langmuir isotherm model assumes that adsorption occurs through a reversible process in which the pollutant molecules attach to the surface of the adsorbent via weak chemical bonds. The Langmuir model also assumes that the surface of the adsorbent is homogeneous, and that the adsorption of one molecule does not affect the adsorption of another molecule. The Langmuir isotherm model is often used to analyze data from batch adsorption experiments, in which a fixed amount of adsorbent is exposed to a range of pollutant concentrations. The Langmuir isotherm model has several limitations, including the assumption of a homogeneous surface, the assumption of a fixed number of adsorption sites, and the assumption of reversible adsorption. However, the Langmuir isotherm model is a useful tool for understanding the adsorption of pollutants onto solid surfaces and for designing adsorption systems for pollution control (Guo et al., 2019; Langmuir, 1918).

1.5.1.2. Freundlich isotherm model

The Freundlich isotherm model is another commonly used model to describe the adsorption of pollutants onto solid surfaces. Unlike the Langmuir isotherm model, the Freundlich model does not assume a homogeneous surface or a fixed number of identical adsorption sites. Instead, it assumes that the adsorption occurs on a heterogeneous surface with a range of adsorption energies. The Freundlich model assumes that the amount of pollutant adsorbed increases with increasing concentration, but at a decreasing rate. This reflects the fact that as more pollutant

molecules are adsorbed onto the surface, the available adsorption sites become more limited, and the energy required to adsorb additional molecules increases.

The Freundlich isotherm model has several advantages over the Langmuir isotherm model, including its ability to account for the heterogeneity of the adsorption surface and the non-reversible nature of adsorption. However, it is important to note that the Freundlich model also has limitations, including its inability to account for saturation effects and its sensitivity to changes in the adsorbent surface properties (Freundlich, 1907; Zaheer et al., 2019).

1.5.1.3. Dubinin Radushkevich (DR) isotherm model

The Dubinin Radushkevich (DR) isotherm model is another commonly used model to describe the adsorption of pollutants onto solid surfaces. The DR model assumes that the adsorption occurs on a heterogeneous surface with a range of adsorption energies, similar to the Freundlich model. However, it also takes into account the variation of the adsorption potential with the degree of surface coverage. The DR model assumes that the adsorption potential decreases as the degree of surface coverage increases, due to the increasing competition between adsorbate molecules for available adsorption sites (Dubinin, 1947). This results in a characteristic downward curvature in the DR isotherm plot.

The DR isotherm model has several advantages over the Langmuir and Freundlich models, including its ability to account for the variation of the adsorption potential with the degree of surface coverage and the heterogeneity of the adsorption surface. However, it also has limitations, including its inability to account for the effects of surface diffusion and pore size distribution on the adsorption process (Chabani et al., 2006).

1.5.1.4. Temkin isotherm model

The Temkin isotherm model is another commonly used model to describe the adsorption of pollutants onto solid surfaces. The Temkin model assumes that the adsorption occurs on a homogeneous surface with a uniform distribution of adsorption energies (Temkin, 1940). The

Temkin model assumes that the heat of adsorption decreases linearly with coverage due to adsorbate-adsorbate interactions on the surface, resulting in a decrease in the adsorption energy for each additional adsorbate.

The Temkin isotherm model has several advantages over the Langmuir and Freundlich models, including its ability to account for adsorbate-adsorbate interactions on the surface and the effect of temperature on the adsorption process. However, it also has limitations, including its inability to account for the effects of surface heterogeneity and pore size distribution on the adsorption process (Yang, 1993).

1.5.2. Kinetic models

The adsorption kinetic study provides information of the adsorption rate, the performance of the adsorbent used, and the mass transfer mechanisms. Knowing the adsorption kinetic is essential for the design of the adsorption systems. Various kinetic models with their equations were tabulated in the Table A2.

1.5.2.1. Pseudo-first-order model

Pseudo-first-order assumes of the rate of number of filled adsorption sites to unfilled sites in most biosorption process, this model is not significant for whole contact time, and it suits for the biosorption process only at the initial stage. As the pollutant is adsorbed onto the surface, the number of unoccupied sites decreases, causing the rate of adsorption to slow down. It is important to note that the pseudo-first-order kinetics model assumes that the concentration of the pollutant in the surrounding solution remains constant throughout the adsorption process, which may not always be the case in real-world situations. Additionally, the model may not accurately describe the adsorption behavior of all pollutants and surfaces (Wang and Guo, 2020).

1.5.2.2. Pseudo-second-order model

Pseudo-second-order model states about the behavior of the biosorption process for the entire time. In this model it is assumed that due to the sharing of electrons between the adsorbate and adsorbent which involves some valence forces considered to be the rate limiting step. Unlike the pseudo-first-order model, the pseudo-second-order model does not assume that the concentration of the pollutant in the surrounding solution remains constant throughout the adsorption process. This makes it a more accurate model for describing real-world situations where the concentration of the pollutant may change over time. However, it is important to note that the pseudo-second-order kinetics model may not accurately describe the adsorption behavior of all solutes and surfaces. Other factors such as temperature, pH, and the presence of other compounds can also affect the adsorption process. Therefore, it is important to use caution when applying this model and to validate its assumptions with experimental data (El-Khaiary et al., 2010).

1.5.2.3. Elovich kinetic model

The Elovich kinetic model is a commonly used model to describe the adsorption mechanism of pollutants onto surfaces. It assumes that the adsorption process occurs through two steps: (1) a surface reaction that is relatively fast and (2) a diffusion step that is slower. It is useful for describing the complex adsorption process that involves both surface reactions and diffusion, and can provide insight into the mechanisms underlying the adsorption process. It is useful for providing insight into the underlying mechanisms of the adsorption process and can be used to predict the behavior of the adsorption system over time (Wu et al., 2009).

1.5.2.4. Intra-particle diffusion model

The intra-particle diffusion model is a commonly used kinetic model for describing the adsorption of solutes onto solid surfaces. It assumes that the adsorption process occurs through several steps, including (1) transport of solute molecules from the bulk solution to the external

surface of the adsorbent, (2) diffusion of solute molecules through the pores of the adsorbent, and (3) adsorption of solute molecules onto the surface of the adsorbent. The intra-particle diffusion model is often used to describe the adsorption behavior of solutes onto porous materials, such as activated carbon or zeolites. It is useful for providing insight into the mechanisms underlying the adsorption process (Wang and Guo, 2022).

1.5.3. Thermodynamic analysis

Thermodynamic studies in adsorption are important for understanding the energy changes that occur during the adsorption process. These studies help to determine the feasibility and spontaneity of the adsorption process, and provide insight into the factors that influence the adsorption behavior. The thermodynamic parameters that are commonly studied in adsorption include the Gibbs free energy change (ΔG), the enthalpy change (ΔH), and the entropy change (ΔS). These parameters can be calculated using experimental data such as the adsorption isotherm and the temperature dependence of the adsorption process.

The Gibbs free energy change (ΔG) is an important parameter that determines the spontaneity of the adsorption process. If ΔG is negative, the adsorption process is thermodynamically favourable and spontaneous. If ΔG is positive, the adsorption process is not favourable and non-spontaneous.

The enthalpy change (ΔH) is related to the heat absorbed or released during the adsorption process. It provides information about the energy required for the adsorption process to occur. If ΔH is negative, the adsorption process is exothermic, and if it is positive, the adsorption process is endothermic.

The entropy change (ΔS) is related to the degree of disorder in the system during the adsorption process. It provides information about the change in the degree of freedom of the adsorbate and adsorbent. If ΔS is positive, the adsorption process is accompanied by an increase in the

degree of disorder, which suggests that the adsorption process is more favourable at higher temperatures (Myers and Monson, 2014).

Thermodynamic studies in adsorption can be used to optimize the design and operation of adsorption systems, as well as to understand the fundamental mechanisms of the adsorption process. However, it is important to note that the thermodynamic parameters may be affected by experimental conditions such as the initial concentration of the adsorbate and the surface properties of the adsorbent, and thus caution must be taken when interpreting the results (REN et al., 2007).

1.5.4. Continuous column models

Continuous column models are commonly used to study the process of adsorption in industrial and laboratory settings. In these models, a fixed-bed column is packed with a solid adsorbent material, and a liquid or gas stream containing the target species to be adsorbed is passed through the column. These studies are used to determine the performance of the adsorbent material for removing pollutants from the water under different conditions.

The experimental setup typically involves measuring the influent and effluent concentrations of the pollutant, and monitoring the breakthrough curve, which is the time-dependent change in effluent concentration as the adsorbent becomes saturated with the pollutant. By analyzing the breakthrough curve data, various parameters such as the breakthrough time, the adsorption capacity, and the rate of adsorption can be determined (Bunluesin et al., 2007; Lim and Aris, 2014).

Continuous column studies can also be used to optimize the operating conditions for the adsorption process, such as the flow rate, bed height, and contact time. These studies can provide valuable information for designing and scaling up adsorption systems for the treatment of contaminated water.

1.5.4.1. Thomas model

The Thomas model is a mathematical model that is commonly used for column studies in adsorption processes. It is particularly useful for describing the adsorption of solutes from dilute solutions in continuous-flow systems. The model assumes that the adsorption of solutes occurs on a surface with a finite capacity, and that the driving force for adsorption is the concentration difference between the bulk liquid phase and the adsorbent surface (Soetaredjo et al., 2014). The equation can be mathematically represented as:

$$\ln\left(\frac{C_o}{C_t} - 1\right) = \frac{k_{TH} Q_o w}{F} - k_{TH} C_o t \qquad (1.1)$$

Where, k_{TH} (mL min^{-1} mg^{-1}) and Q_o (mg g^{-1}) are the Thomas model constant and the adsorption capacity of adsorbent, respectively; F (mL min^{-1}) represents the flow rate of adsorbate in the column; w (g) is the weight of adsorbent in the fixed bed column; and C_o/C_t denotes the ratio of influent to an effluent concentration of adsorbate.

The Thomas model assumes that the adsorption process is controlled by two steps: transport of the solute from the bulk liquid phase to the adsorbent surface, and adsorption of the solute onto the surface. The model can be used to determine the breakthrough time, which is the time required for the effluent concentration of the solute to reach a certain level, as well as the rate of adsorption and the adsorption capacity of the adsorbent (Calero et al., 2009). Column studies using the Thomas model can be used to optimize the design and operation of adsorption systems, as well as to evaluate the performance of different types of adsorbents for the removal of pollutants from water. The model can be applied to a wide range of solutes and adsorbents and can provide valuable insights into the adsorption process.

1.5.4.2. Adams-Bohart model

The Adams-Bohart model is a mathematical model used to describe the behavior of a fixed-bed column during the adsorption of solutes from a fluid stream (Foroughi-dahr et al., 2016). This model is useful for predicting the breakthrough behavior of a fixed-bed adsorbent and can

be used for design and optimization of adsorption systems. The linear expression can be presented mathematically as:

$$\ln\left(\frac{C_o}{C_t}\right) = k_{AB}C_o t - \frac{k_{AB}N_{AB}z}{u} \quad (1.2)$$

where C_o (mg L^{-1}) and C_t (mg L^{-1}) are influent and effluent adsorbate concentrations, adsorbent bed height is z (cm); superficial velocity u (cm min^{-1}) that were derived by dividing flow rate of the column by the cross-sectional area of the bed. k_{AB} (L mg^{-1} min^{-1}) and N_{AB} (mg L^{-1}) are the kinetics constant and saturation constant.

The Adams-Bohart model assumes that the adsorption process is a combination of external mass transfer and intraparticle diffusion. The model assumes that the adsorption capacity of the bed is uniform throughout the bed and the rate of adsorption is proportional to the concentration difference between the bulk fluid and the adsorbent surface. The Adams-Bohart model is useful for determining the breakthrough time of the adsorption process, as well as the maximum adsorption capacity of the bed. It can also be used to optimize the design of the fixed-bed column, such as the bed height and diameter, flow rate, and adsorbent characteristics (Chu, 2020).

1.5.4.3. Yoon-Nelson model

The Yoon-Nelson model is used to simulate the behavior of particles in a packed column. In a packed column, particles are packed into a fixed bed and a fluid flow through the column, causing the particles to move and interact with each other. The Yoon-Nelson model considers the hydrodynamic interactions between the particles and the fluid and is used to predict the motion and behavior of the particles in the column (Yu et al., 2015). Mathematical equation of this model is given below,

$$\ln\left(\frac{C_t}{C_o - C_t}\right) = k_{yN}t - k_{yN}\tau \quad (1.3)$$

Here, k_{yN} (min^{-1}) and τ (min) are the rate constant and time needed for 50% adsorbate breakthrough respectively whereas t represents the processing time.

The Yoon-Nelson model is based on the concept of a two-phase flow, where the fluid is treated as one phase and the particles are treated as another phase. The model uses equations that describe the motion and behavior of the particles and the fluid, and includes terms that account for the interactions between the particles and the fluid. The Yoon-Nelson model is generally used in column studies, to predict the behavior of particles in a packed column under various operating conditions.

1.6. Problem statement and related objectives

Water pollution is a growing concern due to the increase in persistent emerging pollutants (PEPs) such as dyes, heavy metals, personal care products, pharmaceuticals, and endocrine-disrupting compounds in water sources. These pollutants pose a significant threat to the environment, living organisms, and public health. The conventional water treatment methods fail to eliminate PEPs completely, which makes it essential to find innovative and sustainable solutions. One promising solution for the removal of PEPs is adsorption via bio-based engineered adsorbents because they can be tailored to specific surfaces and are environmentally sustainable. However, there are several challenges such as bioadsorbents recovery and toxicity, target specificity, interaction studies between adsorbate and adsorbent, absence of column studies, desorption, and reusability studies that hinder the widespread application of these adsorbents for PEPs removal. This thesis aims to investigate the adsorption efficiency, mechanisms, and scalability of bio-based engineered adsorbents in the context of removing emerging pollutants from aquatic systems. By filling these knowledge gaps, this thesis seeks to contribute to the development of effective and sustainable water treatment strategies for mitigating the impact of PEPs on environmental and public health. Hence, the current research work has been designed with specific objectives based on the discussed problem statements.

Aim and Objectives

1. Synthesis, characterization, and optimization of engineered adsorbents from bio-based materials to maximize removal efficiency through batch studies.
2. Investigating the mechanisms and possible interactions via isotherm and kinetic modelling.
3. Performing regeneration studies to evaluate adsorbents' recyclability.
4. Examining the toxicity before and after adsorption process through Phytotoxicity.
5. Continuous packed bed column studies and real-time sample studies for industrial setup.

Chapter 2

Preparation of Magnetic adsorbent for adsorptive removal of Ciprofloxacin from aqueous solution

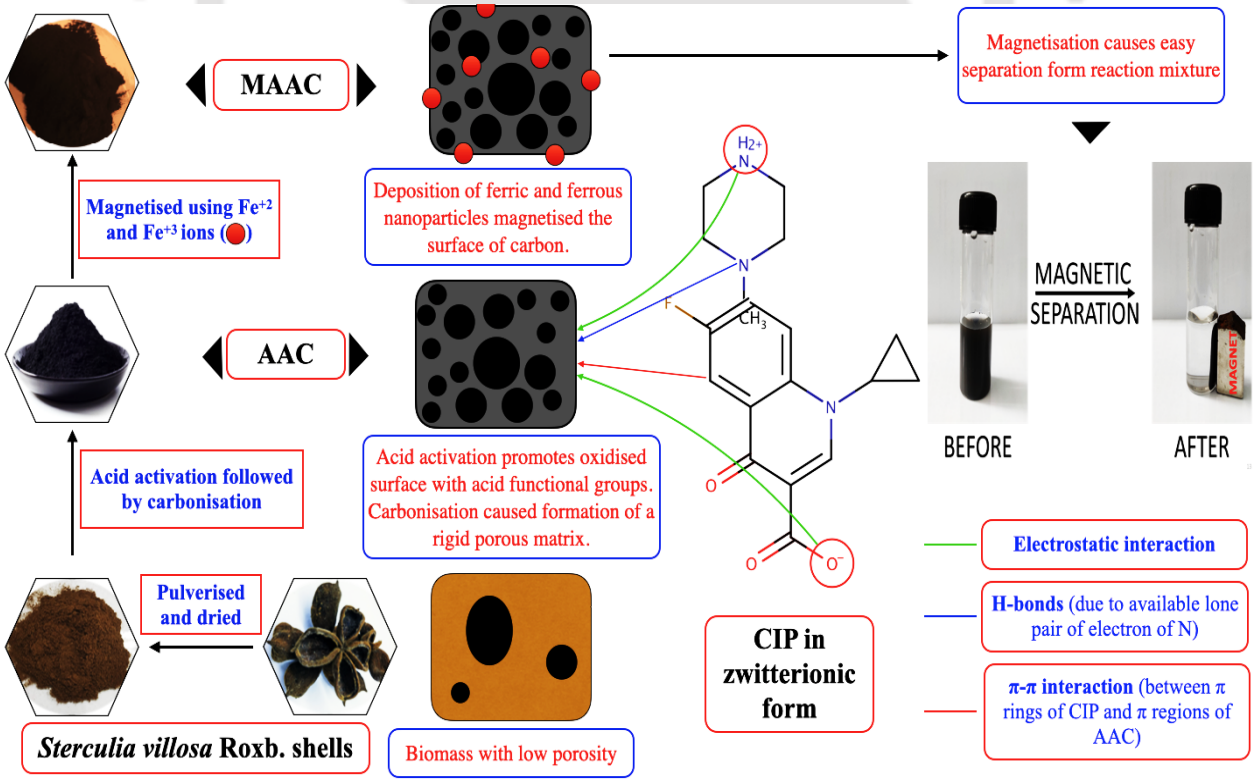

ABSTRACT

Magnetic acid activated carbons (MAAC) were prepared from the shells of *Sterculia villosa Roxb* by activating the biomass and magnetizing it using the co-precipitation technique. Characterization of MAAC prior and post adsorption was performed using various microscopic and spectroscopic analytical techniques, and they verified the formation of magnetic aggregates over porous activated carbon surface. Vibrating Sample Magnetometer (VSM) analysis confirmed the superparamagnetic behavior of the adsorbent with saturation magnetization (Ms) value of 18.2 emu/g, causing an easy and rapid recovery from the adsorption setup in the presence of an external magnetic field. Langmuir isotherm and pseudo-second-order kinetic model best fit the experimental data with theoretical Langmuir maximum adsorption capacity as 81.97 mg/g and verifying chemisorption type of adsorption process, respectively. Thermodynamic analysis verified the interaction among adsorbate and adsorbent as endothermic, spontaneous, and thermodynamically favourable. Co-existing metal cations showed a significant reduction in ciprofloxacin removal efficiency; co-existing anions, though, showed a negligible influence on the adsorption efficiency of MAAC. Recyclability studies verified that the adsorption efficiency fell from 98% in the first cycle to 43% in the fifth cycle. The Ms value fell to 7.6 emu/g (after five adsorption cycles), affecting the adsorbent's recovery. The Phyto-toxicological assessment was performed to evaluate the environmental risk to human and aquatic life using *Vigna mungo* seeds. MAAC proved to be an effective and magnetically separable adsorbent for removing antibiotics.

2.1. Introduction

The rapid pace of modernization, urbanization, and industrialization have strongly affected the quality and quantity of our water reservoirs. Industries discharge their untreated wastewater into such water reservoirs, thus contaminating both the surface and groundwater bodies. In recent times pharmaceutical wastes have been a major concern due to their bulk disposal. A major component of such wastes is the antibiotic species, which may have a long-term impact on the ecosystem and its living beings if left untreated.

Antibiotics used for animal production and disease control account for two-thirds of globally produced antibiotics (Jubeen et al., 2019). According to World Health Organisation (WHO), the tally of antibiotics for non-human consumption (e.g., growth factors for poultry production, agriculture, and aquaculture) accounted for more than half of the production of the global antibiotics (WHO, 2014).

Also categorized as an 'emerging contaminant' (Varsha et al., 2022), antibiotic species can remain active in wastewater bodies due to their stable molecular configuration, which supplements them with properties like high water solubility and low degradability (de Oliveira Carvalho et al., 2019; Prasannamedha et al., 2021). Ciprofloxacin (CIP) is one such emerging antibiotic contaminant, which belongs to the fluoroquinolone class of antibiotics and is commonly recommended for treating bacterial infections. Its concentrations in wastewaters can reach up to 31 mg L^{-1} or more from the effluents of drug production plants (Chandrasekaran et al., 2020). It inhibits large freshwater producers such as duckweed (*Lemna minor*) and cyanobacteria (*Microcystis aeruginosa*) being at mere concentrations of 17–203 µg/L (Robinson et al., 2005). Also, the metabolic activities of a periphyton community (e.g., substrate utilization) were inhibited by 18–199 µg/L of CIP (Johansson et al., 2014). Hence, the efficient removal of ciprofloxacin (CIP) is required as it occurs beyond tolerance limits in

various wastewaters; and is also resistant to natural degradation, and has the potential to affect the ecosystem (Yang et al., 2017; Igwegbe et al., 2020).

When it comes to treatment, conventional wastewater treatment plants are inefficient in removing such antibiotic species since they lack recent technology and fail to detect their trace levels in wastewater systems. Various biotic and abiotic methods have been researched and studied to remove such pollutants by filtration, flocculation, coagulation, sedimentation, or biodegradation process (Ding et al., 2016; Gerard et al., 2016; Sher et al., 2020; Prasannamedha et al., 2020). However, these techniques are deemed ineffective due to their non-specificity towards antibiotics or their inability to detect the antibiotic species at trace levels. Also, they are expensive due to their high maintenance and process costs (Sathishkumar et al., 2015).

Meanwhile, adsorption has been one such method of priority and research for almost a decade due to its in-expensive process, removal efficacy at trace levels, and ease to develop and design adsorbents based on the type of pollutant adsorbate molecules (Neeraj et al., 2016; Kumar et al., 2019). Activated carbon is one of the most preferred adsorbents by many researchers over the years, especially due to its porous structure, large surface area, and high adsorption capacity (Melliti et al., 2021; Elias et al., 2021). Activated carbon is primarily produced by activating lignocellulosic biomass via chemicals (acid/base) and carbonizing at high temperatures. Chemical activation enhances adsorbents' surface morphology by enhancing its porosity, and supplements with functional groups responsible for adsorption and carbonization promotes porous morphology with volatile matrices (Patra et al., 2019, Othmani et al., 2021). However, carbonaceous adsorbents suffer a disadvantage of loss of adsorbent species due to their removal from the adsorption setup via filtration or centrifugation, post adsorption process (Bayazit et al., 2017). To avoid such loss, an alternative is a subject of research of magnetizing activated carbon with magnetic material vis FeO, γ-Fe_2O_3, or Fe_3O_4. This enables magnetic separation of the adsorbate species from the reaction mixture using an external magnetic field (Demarchi

et al., 2019). Many researchers have reported the use of agricultural residue-based magnetic activated carbon for the removal of food, toxic organic compounds (Bhatia et al., 2018), heavy metals (Parlayıcı and Pehlivan, 2017), and antibiotics (Yegane Badi et al., 2018). Though a lot of studies are available when it comes to magnetic activated carbon over a wide range of pollutants, detailed adsorptive studies for antibiotics species are still scarce.

The present study involves the adsorptive removal of Ciprofloxacin (CIP) using magnetic acid-activated carbon (MAAC). *Sterculia villosa Roxb* shells were used to produce acid-activated carbon, following magnetization and precipitation with $FeSO_4.7H_2O$ and $FeCl_3.6H_2O$. The sorbate-sorbent interaction was optimized for efficient removal of CIP species, followed by isotherm, kinetics, and thermodynamics study, using the equilibrated data. A commercially obtained neodymium bar magnet was used to separate out the magnetized adsorbent from the reaction mixture. Pharmaceutical wastewater also contains various ionic salts and metal ions that may influence the uptake of antibiotic species from the wastewater setup. Thus, the influence of co-existing anions and metal cations on the adsorptive behaviour of MAAC was evaluated. MAAC recyclability studies were also investigated. Furthermore, the phytotoxic toxic assay was also performed to evaluate the potential efficacy of MAAC in eliminating CIP.

2.2. Materials and Methods

2.2.1. Chemicals and reagents

All the chemicals, salts and reagents required for the current study were of analytical grade and purchased from Sigma Aldrich, India and Himedia Laboratories Pvt. Ltd., India via local vendors (Table 2.1).

Table 2.1: Detail list of chemicals, reagents, and salts

Serial No.	*Chemical/Reagent/Salt*	*Purpose*
1.	Ciprofloxacin	Adsorbate
2.	0.1 M Sodium Hydroxide (NaOH)	Adjusting pH
3.	0.1 M Hydrochloric acid (HCl)	Adjusting pH
4.	Phosphoric acid	Surface modification of adsorbent
5.	Ferrous sulfate ($FeSO_4.7H_2O$)	Magnetization
6.	Ferric chloride ($FeCl_3.6H_2O$)	Magnetization and source of Ferric (Fe^{+3}) ions
7.	Lead Nitrate [$Pb(NO_3)^2$]	Source of lead (Pb^{+2}) ions
8.	Cobalt (II) Chloride ($CoCl^2$)	Source of cobalt (Co^{+2}) ions
9.	Sodium Sulphate (Na_2SO_4)	Source of sulphate (SO_4^{-2}) ions
10.	Sodium Nitrate ($NaNO_3$)	Source of nitrate (NO_3^{-1}) ions
11.	Sodium Carbonate (Na_2CO_3)	Source of carbonate (CO_3^{-2}) ions
12.	Sodium Chloride (NaCl)	Source of chloride (Cl^{-1}) ions
13.	Sodium Phosphate (Na_3PO_4)	Source of phosphate (PO_4^{-3}) ions
14.	1% Sodium Hypochlorite (NaClO)	Rinsing Vigna mungo seeds

2.2.2. Preparation of iron nanoparticles doped magnetic acid activated carbon (MAAC)

Acid-activated carbon (AAC) was synthesized by acid activating the shells of *Sterculia villosa Roxb.*, followed by its carbonization. Pulverized *Sterculia villosa Roxb.* shells were chemically

activated using phosphoric acid, then carbonization at 400 °C, resulting in acid-activated carbon formation (AAC). Acid treatment assists in developing a porous matrix and oxidizing the surface, thus rendering acidic functional groups. Further, carbonization assists in developing a porous matrix which attributes to enhanced surface porosity for the acid-activated carbon (Patra et al., 2019; Bhatnagar et al., 2013).

The magnetization process involved mixing 2.5 g of AAC with a mixture of 1.83 g of $FeSO_4.7H_2O$, and 3.33 g of $FeCl_3.6H_2O$ in 100 ml distilled water, and all the components were vigorously mixed at 65 °C, using a magnetic stirrer. The solution was then cooled to 40 °C and then its pH was adjusted to 11.0 with 5M NaOH solution. The resulting solution was mixed for 60 minutes and was left stable overnight. The supernatant was discarded, and the residue was thoroughly rinsed with distilled water followed by ethanol washing via filtration, until the pH of the filtrate reached 7.0. After washing, the prepared composite was dried in a hot-air oven at 80 °C and labelled MAAC.

2.2.3. Characterization of the prepared adsorbent

Morphology of MAAC, both before and after magnetisation and post adsorption process was evaluated via Scanning Electron Microscopy (SEM) (Zeiss, Gemini-300), Transmission Electron Microscopy (TEM) (JEOL-2100F), and Atomic Force Microscopy (AFM) (Oxford, Cypher). Elemental composition analysis was carried out by Energy-dispersive X-ray spectroscopy (EDS) (Zeiss Sigma-300). Fourier-transformed infrared spectroscopy (Nicolet iS10) and Raman (LabRam HR, Horiba Jobin Vyon) spectroscopy were also studied to understand the modifications on MAAC surface, and its interaction with CIP. The magnetic properties of MAAC were detailed by Vibrating Sample Magnetometer (VSM) (Lakeshore 7410S). Zeta-potential analysis (Delsa nano C, Beckman Coulter) was done to evaluate the surface charge behaviour of MAAC in aqueous systems. X-ray diffraction (Agilent, USA) was

done to understand the structural and sub-structural modifications that may have occurred due to magnetisation of AAC to form MAAC.

2.2.4. Sorbate-Sorbent adsorption and desorption studies

Variable parameters that directly influenced the CIP uptake by MAAC was studied. These parameters include the initial pH of CIP solution (2.0 - 10.0); initial concentration of CIP (20 mg/L - 100 mg/mL); variable dosage of MAAC (0.25 mg/mL-2.5 mg/mL) and MAAC-CIP interaction temperature (25 °C – 65 °C). Adsorption experiments were carried out in an shaker incubator (ORBITEK-LE) at 150 rpm for 24 h. After the reaction period, the spent adsorbent (MAAC) with the adsorbate species (CIP) were separated out using a strong neodymium bar magnet. The remaining solution was then analysed for any remnant CIP species. Detection of the CIP species was performed on a UV-Vis spectrophotometer at the spectral wavelength of 278 nm. Adsorption capacity (Q_t) and the removal efficient (%R) of MAAC towards CIP were calculated using the following equations (Anitha et al., 2016):

$$Q_t = \frac{(C_0 - C_t)V}{m} \quad (1)$$

$$\%R = \frac{(C_0 - C_t)}{C_0} 100 \quad (2)$$

The adsorption capacity of MAAC at a time ‘t’ was represented by Q_t (mg/g); ‘C_t’ (mg/L) is the CIP concentration at the time ‘t’; ‘C_o’ (mg/L) is the initial concentration of CIP; ‘m’ (g) represents the mass of the adsorbent (MAAC) and ‘V’ (L) represents the test volume of CIP solution.

Desorption of the spent MAAC was performed with 0.1 N NaOH (desorbing agent); in order to evaluate the recyclability potential of MAAC. NaOH was chosen as the desorbing agent due to the following reasons:

- Being an alkali, NaOH tends to neutralize the acidic functional groups developed on the surface of AAC; thus, interfering with the electrostatic interactions between the carbon surface and CIP species. This will cause the adsorbed CIP species to shed off; vacating the occupied active sites (Liu et al., 2016).
- Chemically, Ciprofloxacin is a carboxylic salt, and thus it forms sodium salts (R-COO-Na+) complexes with NaOH; resulting in CIP desorption from the MAAC surface (Berenguer et al., 2010).

Spent MAAC was treated with 0.1 N NaOH, after every adsorption cycle. The excess NaOH was then washed away with distilled water; followed by drying. Once dried, it was subjected to subsequent adsorption-desorption cycles. This process was repeated until the adsorption efficiency of MAAC was ≤ 50%.

2.2.5. Effect of co-existing ions

Real-time pharmaceutical wastewater may contain various anionic and metal cationic salts that may affect the uptake of the antibiotic species by the adsorbent. In order to evaluate the effect of co-existing ions, adsorption experiments were performed in the presence of different anions and metals. Chloride (Cl^{-1}), Carbonate (CO_3^{-2}), Sulfate (SO_4^{-2}), Nitrate (NO_3^{-1}), and Phosphate (PO_4^{-3}) were considered for co-existing anionic salts and Lead (Pb^{+2}), Ferric (Fe^{+3}), and Cobalt (Co^{+2}) were considered for co-existing metal cationic salts. The study was performed with experimental setups containing 100 mg/L of both salt solution and antibiotic solution in a 1:1 ratio.

2.2.6. Phytotoxicity assay

For phytotoxic assessment, *Vigna mungo* (black gram) seeds were germinated in untreated and MAAC treated solutions of CIP. Phytotoxicity assay was performed as per methods specified in USEPA, 1996 with some changes (Naraginti and Yong, 2019). Sodium hypochlorite (1%)

solution was used to wash seeds to prevent any fungal growth, followed by washing the seeds with distilled water. The seeds were then air-dried and stored at room temperature. For the experiment, *Vigna mungo* seeds were germinated in a petri dish (7.5 cm diameter) with cotton-soaked solutions. Seeds germinated with distilled water were marked blank; those germinated with untreated CIP solution were marked as control samples; and those treated with CIP solution were marked as test samples. For one week, all seeds were germinated in a dark environment at normal room temperature. After germination, the average root lengths of the seeds were measured as an outcome of the experiments, and further assessment was done.

2.3. Theoretical background

2.3.1. Analysis of Isotherm models

To investigate the nature of sorbate-sorbent interaction at a fixed temperature, two-parameter isotherm models viz. Langmuir, Freundlich, Frumkin and Dubinin-Radsuhkevich were evaluated using the obtained equilibrated data. The isotherm models detailed information and related equations have discussed in the Section 1.5.1.

2.3.2. Analysis of kinetic model

The kinetics of adsorbate-adsorbent interaction was determined using kinetics models viz. pseudo-first-order, pseudo-second-order, and intra-particle diffusion. The Section 1.5.2. has briefly discussed the related theory and equations of the kinetic models.

2.3.3. Analysis of thermodynamic parameters

Thermodynamic parameters viz. the change in the entropy ($\Delta S°$), enthalpy ($\Delta H°$) and Gibb's free energy ($\Delta G°$), were examined in order to analyze the energy distribution, variation involved in heat of adsorbent-adsorbate interaction, and spontaneity related to the interaction. The detailed theory and related equations have discussed in the Appendix section.

2.4. Results and Discussion

2.4.1. Characterization

2.4.1.1. Surface morphology and elemental analysis

Figure. 2.1(A, B, and C) depicts the surface morphology of acid activated carbon (AAC), AAC post modification (MAAC), and MAAC after adsorption of CIP species (MAAC-CIP), respectively. AAC shows an irregular morphology with multiple pores of varying porosity throughout the carbon surface (Figure. 2.1A). Figure. 2.1B depicts the surface of MAAC with aggregates of iron oxides, which were formed by co-precipitation of ferrous (Fe^{+2}) and ferric (Fe^{+3}) particles on the surface of AAC. Figure. 2.1C represents the surface of the modified carbon surface (MAAC) post CIP adsorption. Post CIP adsorption, the surface of MAAC-CIP is relatively smooth with less irregularities and cavities as compared to AAC and relatively less intensity of ferrous/ferric aggregates as compared to MAAC. This was due to adsorption of CIP species over MAAC surface which caused the smoothening of it's surface.

Energy-dispersive X-ray spectroscopy (EDS) analysis confirms the formation of iron oxides post magnetisation of AAC, as verified due to increased elemental composition of Fe, from 1.1% for AAC to 58.2% for MAAC (Figure. 2.1 D and 1E). Presence of fluorine (F) peak for MAAC surface post CIP adsorption confirms CIP's adsorption as fluorine is an integral component of Ciprofloxacin (Figure. 2.1F).

Figure. 2.1(G and H) depicts the Transmission electron microscopy (TEM) image for MAAC at different magnifications. Iron aggregates can be observed assembled over relatively large particle, supposedly AAC. These aggregates are irregular and heterogeneous in shape and size, with an average particle size of less than 50 nm. Thus, it can be concluded that these iron aggregates are actually the aggregates of iron nanoparticles. Figure. 2.1H represents the

Selected-Area-Electron-Diffraction (SAED) image of MAAC that describes the sample as polycrystalline, i.e. having both amorphous and crystalline regions.

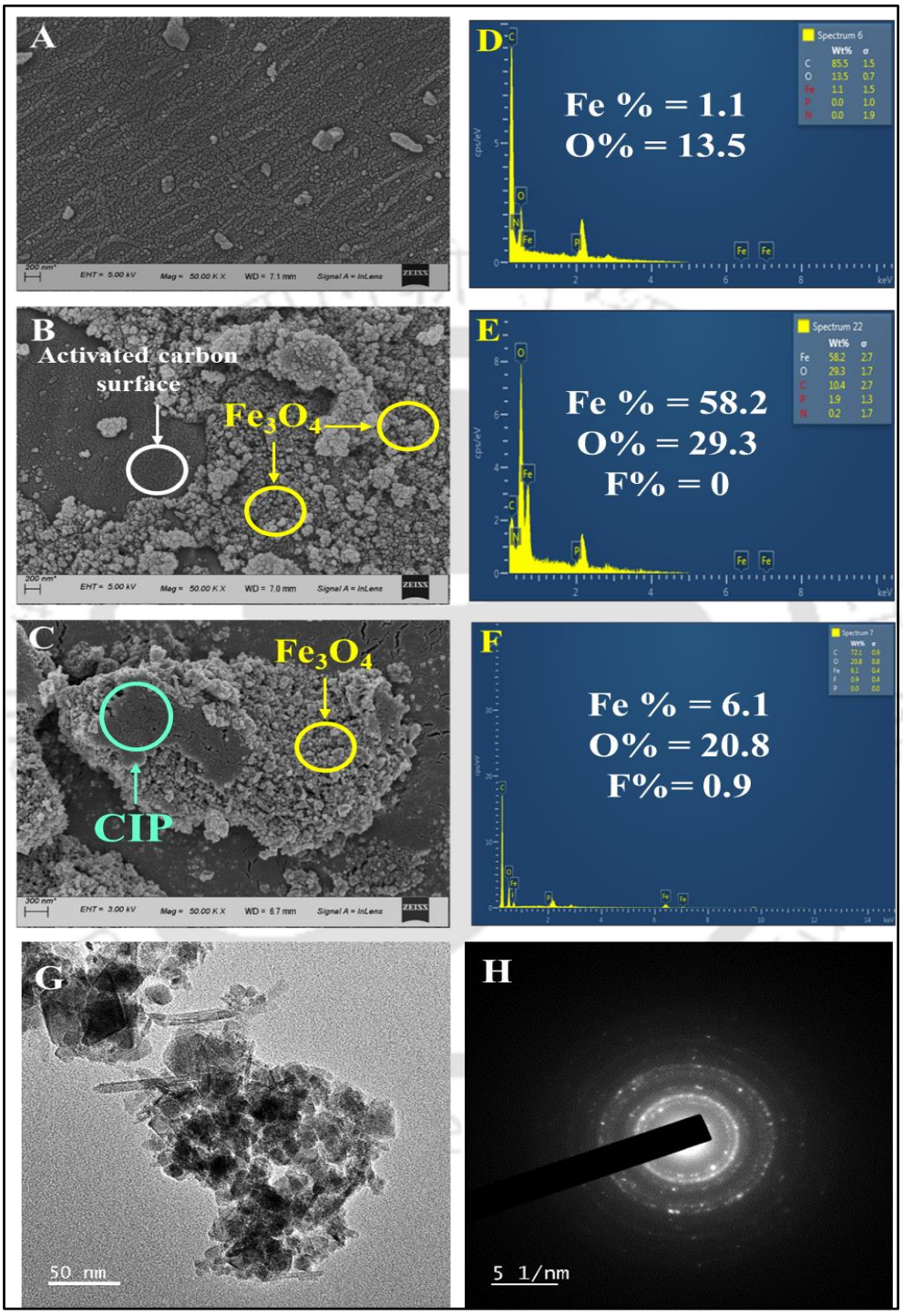

Figure. 2.1: (A) FESEM image of AAC, (B) after magnetic modification (MAAC); (C) after CIP adsorption (MAAC/CIP); (D) EDS analysis of AAC, (E) after magnetic modification

(MAAC); (F) after CIP adsorption (MAAC/CIP); (G) FETEM image of MAAC, (H) SCID image of MAAC.

Atomic force microscopy (AFM) analysis measures the surface topology of samples. Figure. 2.2 (A, B, C, D) represents the 2-D and 3-D topology of AAC and MAAC, respectively. The surface of AAC showed a rough irregular morphology. However, post modification, the surface of the MAAC showed multiple conical shaped aggregates protruding upwards. These conical aggregates showed an elevation from a height of 69.1 nm on AAC surface to a maximum height of 144.4 nm on the surface of the MAAC. These conical shaped aggregates were a result of ferrous nanoparticles formed over the surface of AAC.

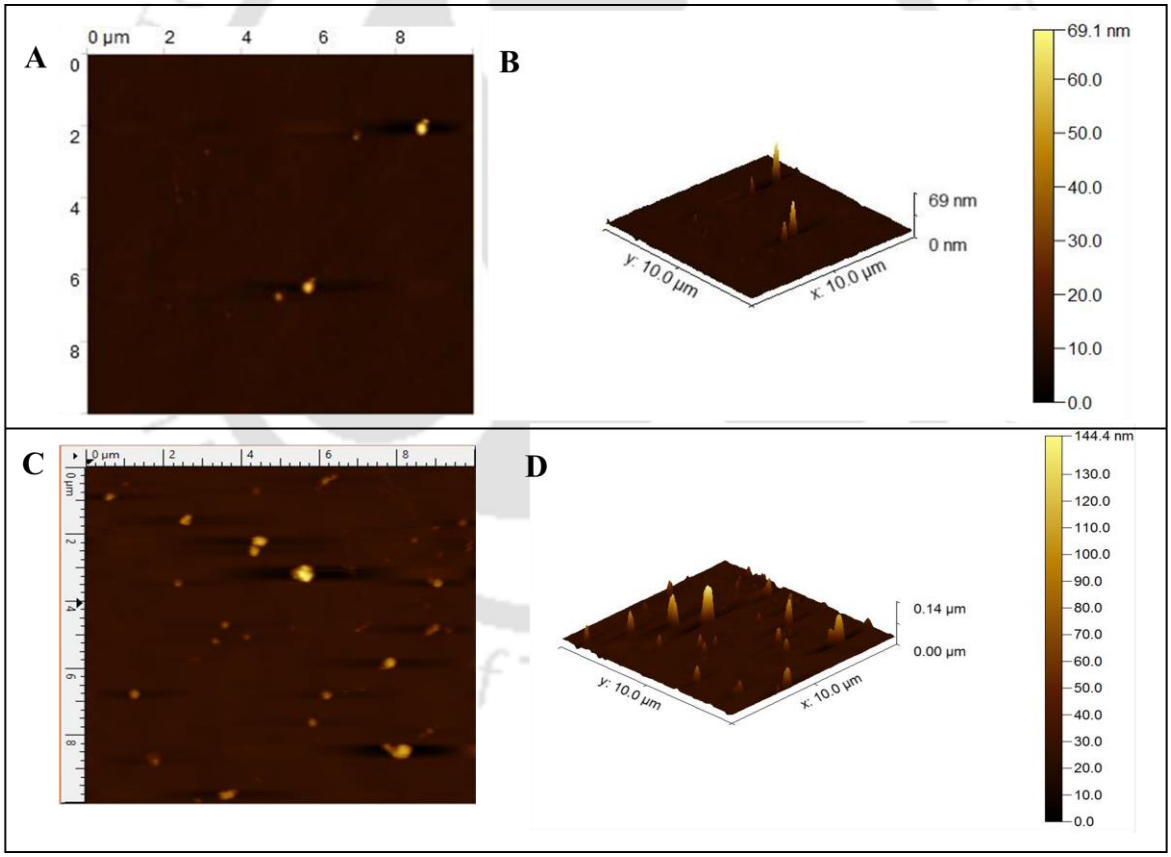

Figure. 2.2: (A, B) 2-D and 3-D AFM images of AAC; (C, D) 2-D and 3-D AFM images of MAAC.

Conclusively, SEM analysis verified the formation of iron aggregates on the surface of AAC resulting the formation of MAAC. SEM analysis also verified the smoothening of MAAC surface due to adsorption of CIP species. EDS analysis verified the aggregates to primarily contain Fe and O, signifying ferrous/ferric oxide aggregates over AAC surface. TEM imaging verified the aggregate particles to be well under 100 nm i.e. they are nano-particles. AFM verified the aggregates to be conical shaped with variable heights.

2.4.1.2. Adsorbent magnetic properties analysis

The magnetic behaviour of the MAAC, MAAC/CIP (after adsorption) and MAAC_D (after desorption) samples were recorded at ambient temperature by varying the applied magnetic field from -15 to +15 kOe. The vibrating sample magnetometer (VSM) analysis is depicted in Figure. 2.3, and as represented the hysteresis loop is similar to the alphabet 'S'. The magnetic properties of MAAC were investigated by Vibrating Sample Magnetometer (VSM) instrument. A magnetic hysteresis curved of the AAC, MAAC, MAAC/CIP (after adsorption) and MAAC_D (after desorption) samples were measured by varying the applied magnetic field from -20 to +20 kOe and saturation magnetization (Ms) was calculated. Ms is an intrinsic property of a magnetic material that shows maximum magnetic moment per unit volume for the analysis sample. From Fig. 2E, Ms of MAAC and AAC were found to be 18.2 emu/g and zero, respectively. The magnetization for MAAC is high enough to provide quick and easy separation from aqueous solution in the presence of an external magnetic field (neodymium bar magnet). After CIP adsorption (MAAC/CIP), Ms value almost remains constant, i.e., 18.0 emu/g. But after 5 cycles of adsorption-desorption, Ms value decreases to 7.6 emu/g (MAAC_D). The main reason for this behaviour could be the loss of magnetic nano-particle aggregates during the desorption process. However, the magnetic separation ability of the MAAC was active and was tested by placing a strong magnet next to the glass bottle of MAAC aqueous suspension.

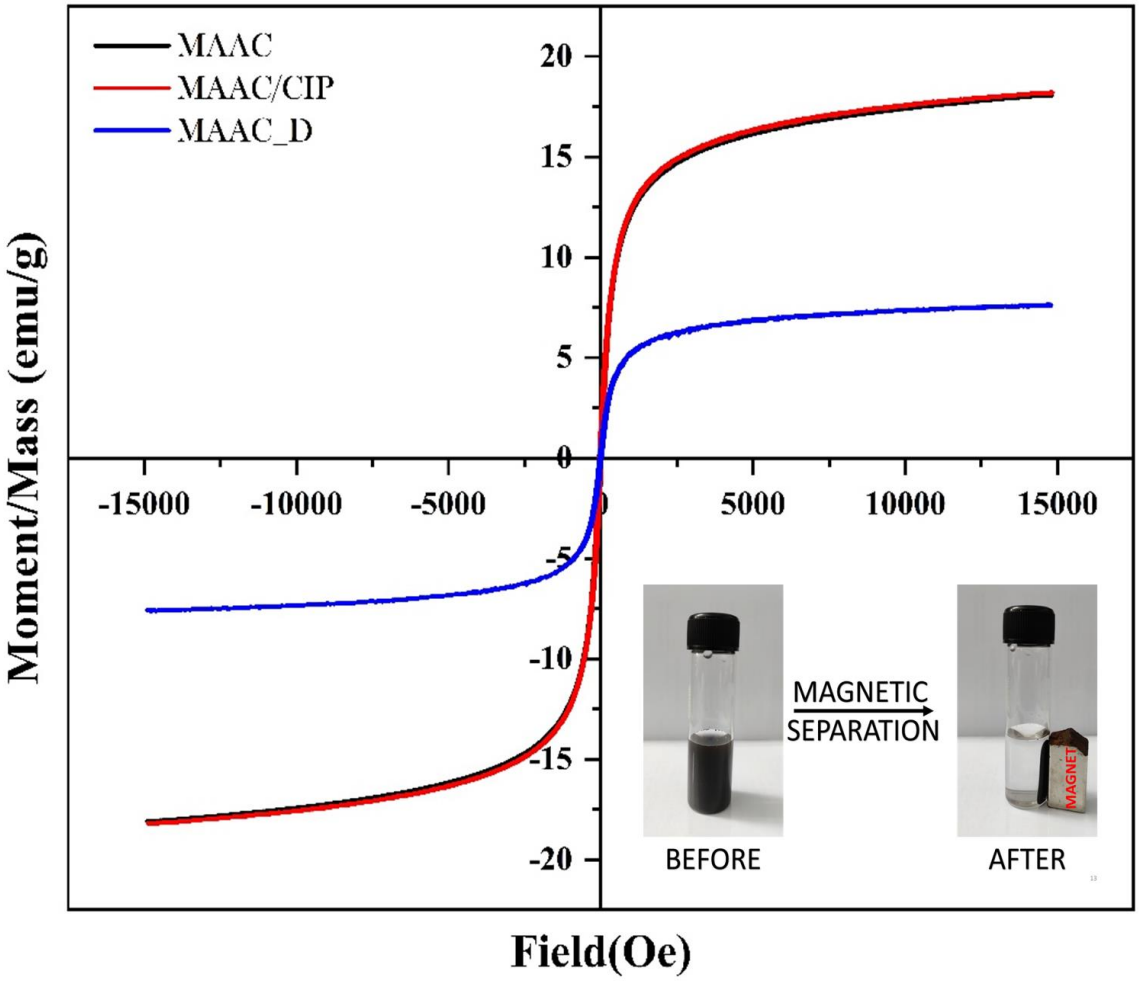

Figure. 2.3: VSM plot of MAAC, after CIP adsorption (MAAC/CIP) and after 5 cycles of adsorption/desorption (MAAC_D).

2.4.1.3. Powdered X-ray diffraction analysis

The X-ray diffraction peaks for AAC and MAAC are demonstrated in Figure 2.4C. AAC showed 2 major peaks at 2θ values of 20.80 and 26.60, which are the characteristic peaks for activated carbon (Mishra et al., 2019). MAAC showed distinct peaks at 26.60, 30.30, 35.60, 53.70, 57.20 and 62.80, which are equivalent to the characteristics pattern of standard iron oxide peaks (Altintig et al., 2018; Lin & Lee 2020). Hence, successful coating of magnetic nanoparticles can be confirmed on the surface of AAC with high purity as no other residuals

peaks were detected in the sample. Distinct peaks for AAC are not detected in MAAC due to the high-intensity peaks of Fe_3O_4.

2.4.1.4. Adsorbent thermal stability analysis

Thermogravimetric (TG) analysis of MAAC was used to investigate the general decomposition properties and activation temperature of the precursor during activation in a Nitrogen atmosphere (Figure 2.4D). The TG curve of the MAAC indicated that till ~220°C, MAAC showed a mere loss of weight (%). This slight reduction may be due to loss of water and elimination of surface O_2-containing functional groups of MAAC (Gholamiyan et al., 2020). However, further rise in temperature resulted to a continuous and gradual loss in weight (%). This drastic loss may be due to the combustion of the carbonaceous composition of the adsorbent. However, even at higher temperatures, a majority of MAAC still shows stability. Fe_3O_4 could be one the components that remains unburnt at such higher temperatures, even after burning of the carbonaceous material along with some impurities (Hu et al., 2019). TG analysis verified the thermal stability and integrity of the adsorbent at high temperatures, vis. as high as 220°C.

2.4.1.5. FTIR spectral analysis

FTIR spectroscopy was assessed to evaluate the modifications in the surface functional groups, prior (AAC) and after the surface modification (MAAC) and post CIP adsorption (MAAC/CIP), as represented in Figure 2.4 (A and B). The spectrum was recorded within the range of 400-4000 cm^{-1}. Acid activated carbon (AAC) showed a major broad peak from 3600 cm^{-1} to 3200 cm^{-1}. This peak was developed due to stretching of –OH of alcohol and carboxylic acid groups and stretching of N–H of amine and amide groups. This verifies the development of acidic functional groups due to surface oxidation caused due to the acid

treatment of biomass. Another major peak from 1200 cm^{-1} to 1020 cm^{-1} was developed due to stretching of C–OH groups of alcohol (Patra et al., 2020).

A strong peak in the range of 504-758 cm^{-1} was observed in MAAC and MAAC/CIP. This peak was due to Fe-O bond vibration of Fe_3O_4 (Peng et al., 2018); thus, verifying the presence of ferrous nanoparticles. After adsorption of CIP by MAAC, peak changes around 1000-1300 cm^{-1} were observed, showing strong C-O-C and C-OH stretches that may be involved in the binding of CIP species. Furthermore, the range of 1500-1800 $cm^{-1}$is associated to the C=C band aromatic ring stretching vibrations of the donor–acceptor π-π electrons. The CIP structure was known to consist of an aromatic ring structure, that could integrate with the remaining π-electrons on the MAAC. Additionally, it can also be attributed that hydrogen bonds could be formed due to stretching vibration of carbonyl groups (–C=O) on the surface of CIP (Hu et al., 2019). Conclusively, FTIR analysis verified the acid activation of biomass forming AAC and further magnetisation of AAC to MAAC via modification with ferrous nanoparticles. Also, it can be concluded that MAAC was rich in functional groups that were useful for CIP uptake.

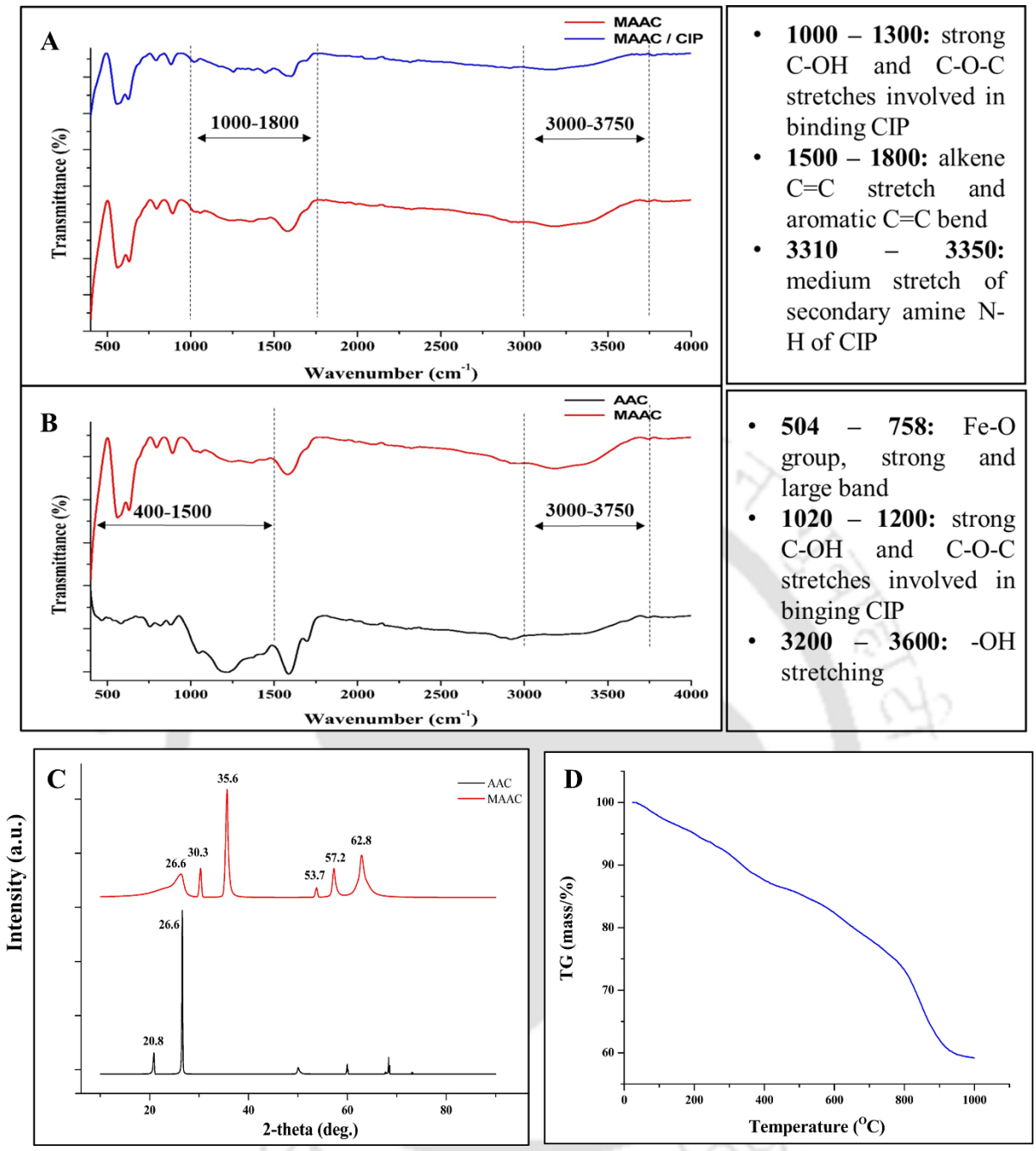

- **1000 – 1300:** strong C-OH and C-O-C stretches involved in binding CIP
- **1500 – 1800:** alkene C=C stretch and aromatic C=C bend
- **3310 – 3350:** medium stretch of secondary amine N-H of CIP

- **504 – 758:** Fe-O group, strong and large band
- **1020 – 1200:** strong C-OH and C-O-C stretches involved in binging CIP
- **3200 – 3600:** -OH stretching

Figure 2.4: (A) FTIR plot of MAAC, before and after CIP adsorption (MAAC/CIP); (B) FTIR plot of AAC and after magnetisation (MAAC); (C) XRD plot of AAC and MAAC; (D) Thermogravimetric analysis of MAAC.

2.4.1.6. Zeta potential analysis of the adsorbent

Figure 2.5A represents the zeta potential analysis plot for MAAC and as presented, the isoelectric pH (pH_{IPC}) for MAAC was determined to be at pH 7.1. At pH >7.1, MAAC showed negative zeta potential values, thus verifying MAAC surface to be negatively charged. Conversely, at pH<7.1, MAAC showed positively zeta potential values, thus verifying MAAC surface to be positively charged. This could be due to negatively charged acidic groups which attracts excess H+ ions at pH<7.1; thus, rendering MAAC with positive zeta potential values. However, with rise in pH values, the intensity of OH− ions also elevates. This neutralises the positively charged groups over the adsorbent's surface; rendering it's interface with negative charges. This causes negative zeta potential values to MAAC surface, as depicted in Figure 2.5A.

2.4.2. Influence of process parameters

2.4.2.1. Initial pH of adsorbate (CIP) solution

The influence of initial pH of the CIP solution on the adsorbate-adsorbent interaction included the protonation-deprotonation processes on the surface functional groups of MAAC and the functional groups of CIP. Initial pH ranging from 2.0 to 10.0 for CIP solution (100 mg/L) were incubated along with fixed dose of MAAC (10 mg for 20 mL CIP solution). Figure 2.5B represents the influence of initial pH of CIP solution on it's adsorptive removal efficiency and as represented MAAC shows maximum CIP adsorption efficiency at pH 6.0.

Ciprofloxacin (CIP) has 2 pka values, viz. 6.1 (pka1) and 8.7 (pKa2) (PubChem). At pH values <6.1 CIP tends to acquire a positive charge due to protonation of amine group (NH_2^+). At this pH range, MAAC tends to be positively charged (mentioned previously in section 2.4.1.6.); thus, at this pH efficient interaction between CIP and MAAC was not possible as reported in Figure 2.5B. Simultaneously, for pH values >8.7 CIP tends to acquire negative charges due to

the release of the hydrogen ions from the carboxyl group. At this pH range MAAC also acquires negative charged groups, thus resorting to inefficient adsorption. CIP acquires zwitterionic form between pH 6.1 to 8.7. It is at this pH range when MAAC also showed considerable removal efficiencies for CIP. At pH 6.0, positively charged MAAC surface is able to efficiently interact with negative oxygen groups of CIP species; thus, achieving the maximum removal efficiency as depicted in Figure 2.5B. This result also shows a process of inexpensive adsorption in an environmentally friendly manner for the treatment of loaded CIPs in wastewater by MAAC. In fact, the pH of most pharmaceutical wastewater and receiving water are nearly neutral (Alwared et al., 2021). Under such circumstances, the addition of additional bases or acids to adjust the pH value will not be required in the treatment process. Thus, pH 6.0 was set for the further experiments.

2.4.2.2. Dosage of the adsorbent (MAAC)

To investigate the effect of MAAC dosage, variable doses of MAAC in the range of 0.25 mg/mL to 2.5 mg/mL (with 20 mL of CIP solution) were used for the removal of CIP solution (100 mg/L) with an initial pH of 6.0; for an interaction period of 24 hours. The maximum CIP adsorption efficiency of 98.4% was observed at the MAAC dosage of 2.0 mg/mL. As depicted in Figure 2.5C, the removal efficiency (%) of MAAC increased with increasing dose of MAAC, until it ceases to saturation. Such behaviour could be associated to the dosage gradient of the adsorbent influencing the accessibility of the active sites for adsorption process thus driving the adsorption process. Elevated dosage resorts to increased accessibility of available binding sites for a fixed concentration of CIP species, causing elevated adsorption efficiencies. However, after a certain limit, fixed CIP concentration tends to cease the driving force causing adsorption capacity to reach a stage of equilibrium (Patra et al., 2021).

2.4.2.3. Initial concentration of the adsorbate (CIP) solution

The influence of the variable initial CIP concentration (20 mg/L to 100 mg/L) over its adsorption on the optimised dosage of MAAC (2.0 mg/mL for 20 mL of CIP) was studied at optimised interaction pH of 6.0 for CIP solution for an incubation period of 24 h. It is clear from Figure 2.5D that as the initial CIP concentration increased, the adsorption capacity (mg/g) of MAAC also elevated. However, the adsorption efficiency (%) showed an opposite trend with slight reduction as the initial concentration increases. Such behaviour could be due to the limited amount of available active sites on the surface of MAAC, which gets filled up with increase in initial concentration of CIP. These filled up active sites drives the adsorbent's adsorption capacity. Thus, with the increase in initial concentration of CIP, the filled up active sites also increases and so does the adsorption capacity of the adsorbent (mg/g). Conversely, the adsorption efficiency (%) for MAAC was driven by the number of available active sites. As the initial concentration for CIP increases, the number of available active sites over the adsorbent reduces; and so, does the adsorption efficiency.

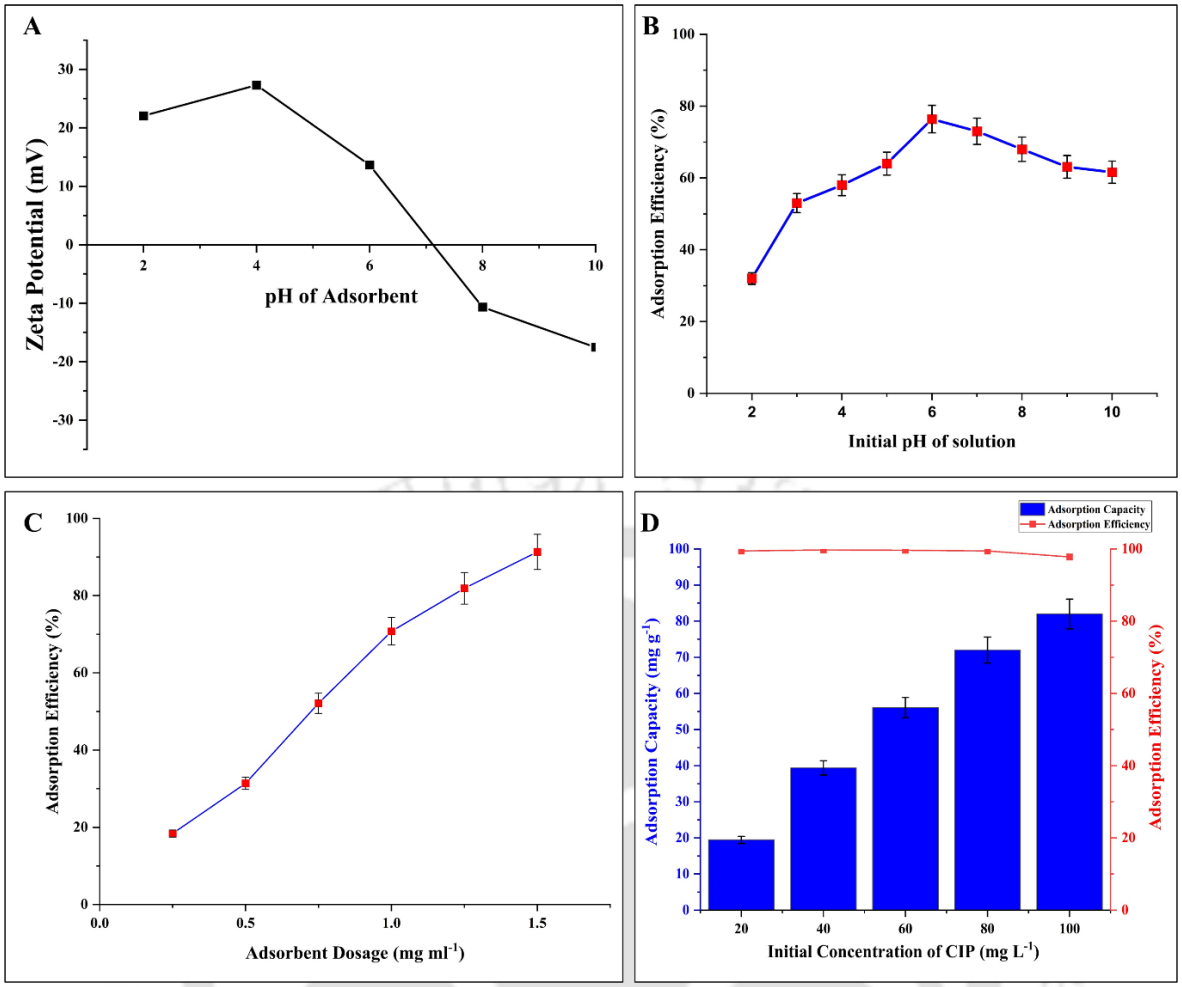

Figure 2.5: (A) zeta potential plot of MAAC; Influence of process parameters viz. (B) initial pH of CIP solution, experimental conditions: pH 2 to 10, dosage 0.5 mg ml^{-1}, MAAC concentration 100 mg L^{-1}, temperature 35°C; (C) dosage of MAAC, experimental conditions: pH 6, dosage 0.25 to 1.5 mg ml^{-1}, MAAC concentration 100 mg L^{-1}, temperature 35°C; (D) initial concentration of CIP solution, experimental conditions: pH 6, dosage 2.0 mg ml^{-1}, MAAC concentration 20 to 100 mg L^{-1}, temperature 35°C.

2.4.2.4. Effect of reaction temperature and interaction thermodynamics

The influence of the reaction temperature on the CIP-MAAC interaction was investigated by varying the reaction temperatures from 30°C to 60°C for various initial CIP concentrations from 20 mg/L to 100 mg/L, while the other variables were kept as optimized. Table 2.2 shows the calculated values of ΔG°, ΔH° and ΔS° for different temperatures (°C) and initial CIP

concentrations (mg/L) of the experimental solution. Negative values of ΔG° for CIP adsorption by MAAC confirmed the interaction between CIP and MAAC as spontaneous and thermodynamically favourable. The adsorption process was endothermic which was confirmed by positive values of ΔH°. Temperature-dependent active sites are formed during acid activation of MAAC precursor. The energy involved in forming such active sites must be greater than the energy released during the adsorption process; which may have led the adsorption process to be endothermic in nature. Finally, positive values of ΔS° for CIP adsorption by MAAC indicates an increase in the degree of disorderness and randomness.

Table 2.2: Thermodynamics Parameters (ΔG°, ΔH°, and ΔS°) for adsorption of CIP by MAAC.

Temp. (°C)	C_i (mg/L)	ΔG° kJ/mol	ΔH° kJ/mol	ΔS° J/mol
30	20	-25.62	14.25	39.56
	40	-26.00		
	60	-27.48		
	80	-26.80		
	100	-22.12		
40	20	-26.46	-3.70	102.45
	40	-28.19		
	60	-28.82		
	80	-28.80		
	100	-26.36		
45	20	-29.67	2.63	84.67
	40	-33.10		
	60	-32.30		
	80	-32.06		
	100	-25.27		
50	20	-25.09	-7.27	115.16
	40	-27.85		
	60	-29.13		
	80	-28.51		
	100	-26.65		
60	20	-27.30	-34.24	188.55
	40	-29.27		
	60	-30.04		
	80	-30.59		
	100	-28.22		

2.4.3. Interaction studies

2.4.3.1. Sorbent-sorbate interaction mechanism and magnetic separation

Various interactions determine the adsorption of the adsorbate species on the adsorbent's surface. Acid activation of biomass results to formation of oxidised regions. These oxidised regions primarily participate in the adsorption process and thus adsorb the CIP species via H-bonding and electrostatic interactions. The carbonaceous surface also possess π regions and these regions interact with the π rings of the CIP species via π–π stacking. Other interactions assisting the adsorption process involved formation of complex, pore-filling, acid–base and hydrophobic interactions etc. (Cazetta et al., 2016). Based on the actual CIP molecular structure and the determined MAAC structure (based on FTIR analysis), the adsorption interactions promoting CIP's adsorption over MAAC has been illustrated in Figure 2.6.

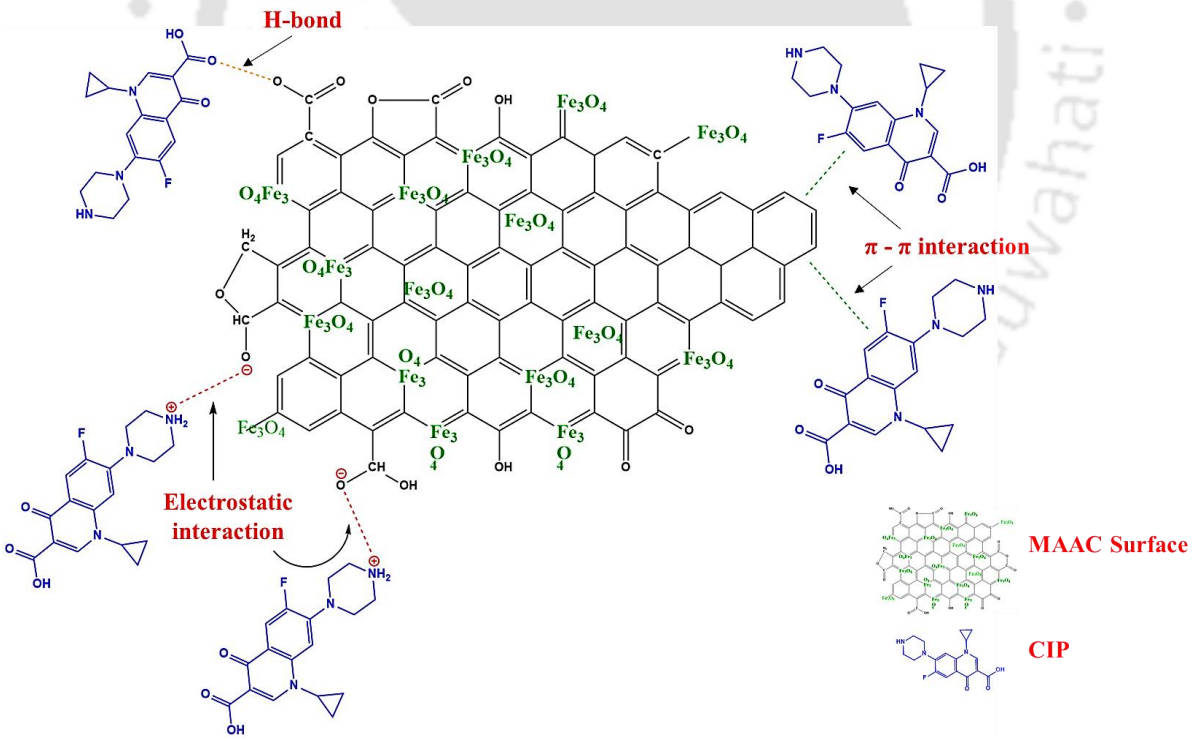

Figure 2.6: Adsorptive interaction between CIP and MAAC.

Another important feature of the produced MAAC is that it can be easily separated from the reaction mixture using a bar magnet as illustrated in Figure 2.3. This minimised any loss caused due to conventional separation methods involving filtration or centrifugation. Magnetic separation also minimised any loss/desorption of adsorbate species that could be caused due to filter papers or high rpm centrifugation.

2.4.3.2. Adsorption isotherms

The isotherm modelling of adsorbate-adsorbent interactions was investigated from the equilibrated data achieved from adsorption experiments done in optimised parameters. Table 2.3 presents the coefficients of regression (R2) and isothermal constants values. Langmuir isotherm model (0.99) was the best fit to represent the adsorption behaviour. Theoretically, Langmuir isotherm model suggest the adsorbate molecules to form a monolayer in homogenous manner over the adsorbent's surface. The maximum theoretical adsorption capacity (QL) that was calculated by Langmuir isotherm was 81.97 mg/g. Langmuir constant (KL) for CIP adsorption was 0.78 (less than unity); thus, suggesting the conditions to be favourable for CIP adsorption. It can be reported that when the adsorbate molecules first reached saturation on the outer surface of adsorbent, then they enter the adsorbent pores and get adsorbed onto the inner surface. Freundlich isotherm model (0.68) gave a very poor fit with the experimental data and thus the possibility of multilayer adsorption can be ruled out. However, the Freundlich constant (1/n) was less than unity, which represents the bond distribution and indicates a favourable chemisorption process. Positive values for Frumkin interaction parameter (α) confirms attractive forces among the adsorbate species. But since, Frumkin isotherm model (0.90) did not show a good fitting with the experimental data, any attractive interaction between the adsorbate (CIP) species can be denied. Dubinin-Radushkevich isotherm model (0.83) gave a poor fit with the experimental data; thus, rendering pore filling process non-applicable for the adsorption process (Wang et al., 2017, Hu et al.,

2019). Figure 2.7 shows the non-linear curve plotting for the isotherm models and as illustrated Langmuir isotherm model gave the best fitting with the experimental data.

Table 2.3: Adsorption isotherm models and their parameters.

	ISOTHERMS	ISOTHERM CONSTANTS	
TWO PARAMETERS ISOTHERMS	LANGMUIR	Q_L	81.97
		K_L	0.78
		R^2	0.99
	FREUNDLICH	K_F	4.57
		1/n	0.21
		R^2	0.68
	FRUMKIN	K_{FK}	$3.2x10^{-8}$
		α	10.70
		R^2	0.90
	DUBININ RADUSHKEVICH	Q_{DR}	61.79
		K_{DR}	0.13
		R^2	0.83

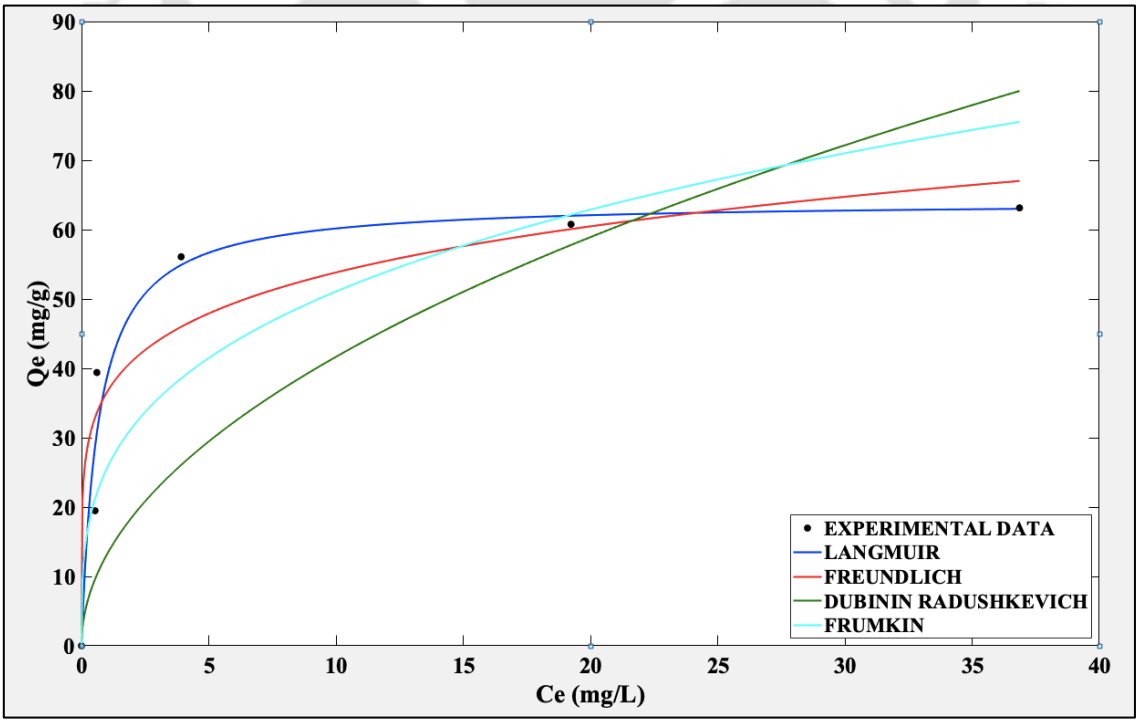

Figure 2.7: Non-linear isotherm modelling plots for CIP adsorption, experimental conditions: pH 6, dosage 2.0 mg ml^{-1}, MAAC concentration 20 to 100 mg L^{-1}, temperature 40°C.

2.4.3.3. Kinetics analysis

Kinetics of adsorbate-adsorbent interactions were investigated using various kinetics models such as pseudo-first order, pseudo-second order and intra-particle diffusion. Table 2.4 represents the regression coefficients (R^2) for the studied kinetics model. Among the different kinetic models, pseudo-second order kinetics model showed the best fitting with the experimental data; hence chemisorption is the rate limiting step for the adsorption process. Furthermore, the fitted data were validated with the similarity between the theoretical adsorption capacity (Q_e) values and the experimental adsorption capacity ($Q_{e\ expt.}$) values. Theoretical adsorption capacity (Q_e) values for pseudo-second order gave a near similarity with experimental adsorption capacity ($Q_{e\ expt.}$) values; thus, verifying its applicability with the adsorption process. The non-linear curve plots for the kinetic models are shown in Figure 2.8 and, it validates that the pseudo-second order model fits with the experimental data as compared to other models.

Table 2.4: Adsorption kinetics models and their parameters

C_i (mg/l)	Q_e Expt. (mg/g)	Pseudo-First Order			Pseudo-Second Order			Intra-Particle Diffusion		
		K_1 (1/min)	Q_e (mg/g)	R^2	K_2 (1/min)	Q_e (mg/g)	R^2	K_{id} (mg/g $min^{1/2}$)	C (mg/g)	R^2
20	13.187	0.001	0.773	34.30	153.294	19.508	99.60	0.186	13.723	78.08
40	25.568	0.002	8.228	20.51	9.881	40.177	98.94	0.621	19.212	92.95
60	39.707	0.001	22.802	16.83	2.377	57.860	98.28	1.065	18.263	95.43
80	53.407	0.002	25.008	21.98	2.066	63.583	98.45	1.198	18.986	92.84
100	64.982	0.002	28.455	17.67	1.712	65.490	97.81	1.220	18.881	96.67

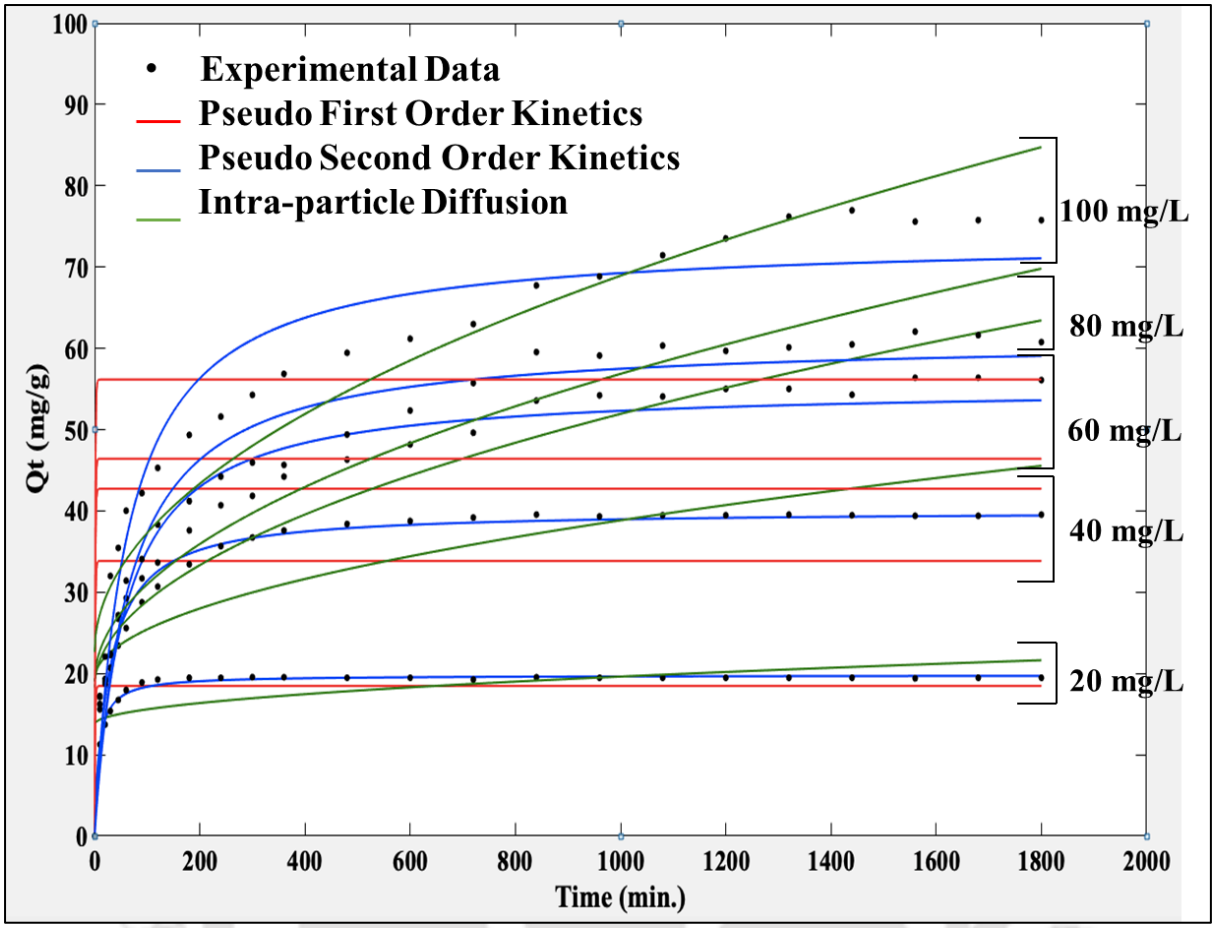

Figure 2.8: Non-linear kinetics modelling plots for CIP adsorption, experimental conditions: pH 6, dosage 2.0 mg ml^{-1}, MAAC concentration 20 to 100 mg L^{-1}, temperature 40°C.

2.4.4. Effects of co-existing ions

The adsorption process was slightly affected by the presence of co-existing anionic (SO_4^{-2}, NO_3^{-2}, CO_3^{-2}, Cl^{-1}, and PO_4^{-3}) and the cationic salts (Pb^{+2}, Co^{+2}, and Fe^{+3}), and the same has been depicted in Figure 2.9. Theoretically, adsorption of metal ions largely depends upon the size of the it's metal hydrate form in aqueous solutions. Larger the ionic radii of the metal ion in the aqueous medium, lesser would be the spread of it's metal hydrate form and thus higher will be it's ion-exchange over the MAAC surface; thus it will compete more with other

adsorbate species (Tobin et al., 1984). The ionic radii of the selected metal ions in Angstrom (Å) are in the sequence of; Co^{+2} (0.745 Å) < Pb^{+2} (1.20 Å) < Fe^{+3} (1.26 Å) (Web-Elements).

Thus accordingly, since Fe^{+3} ions has the highest ionic radii among the selected metal ions and thus it'll have the smaller metal hydrate form. Thus, it will show maximum competitive binding to the CIP species, thus limiting the MAAC's CIP uptake capacity efficiency. This was followed by Pb^{+2} ions and Co^{+2} ions as illustrated in Figure 2.9. Co^{+2} ions having the smallest ionic radii will have a greater metal hydrate form and thus compete less with the CIP species.

Another supporting theory could be that positively charged metal ions could neutralize the negatively charged groups of zwitterionic form of CIP species; thus, rendering the CIP species with no negative charge to undergo electrostatic interaction with the positively charged MAAC surface at pH 6.0 (Zeta potential analysis). This also supports the reduction in adsorption efficiency of CIP species by MAAC.

Minimal effect was reported by co-existing anionic salts due to competitive adsorption among negatively charged anionic salts and negatively charged CIP molecules on the surface of MAAC, as depicted in Figure 2.9. This nominal reduction could possibly be due to the zwitterionic form of CIP. Anionic salts could have been neutralised by the positively charged amine groups of zwitterionic CIP species, thus limiting the effect of anionic salts.

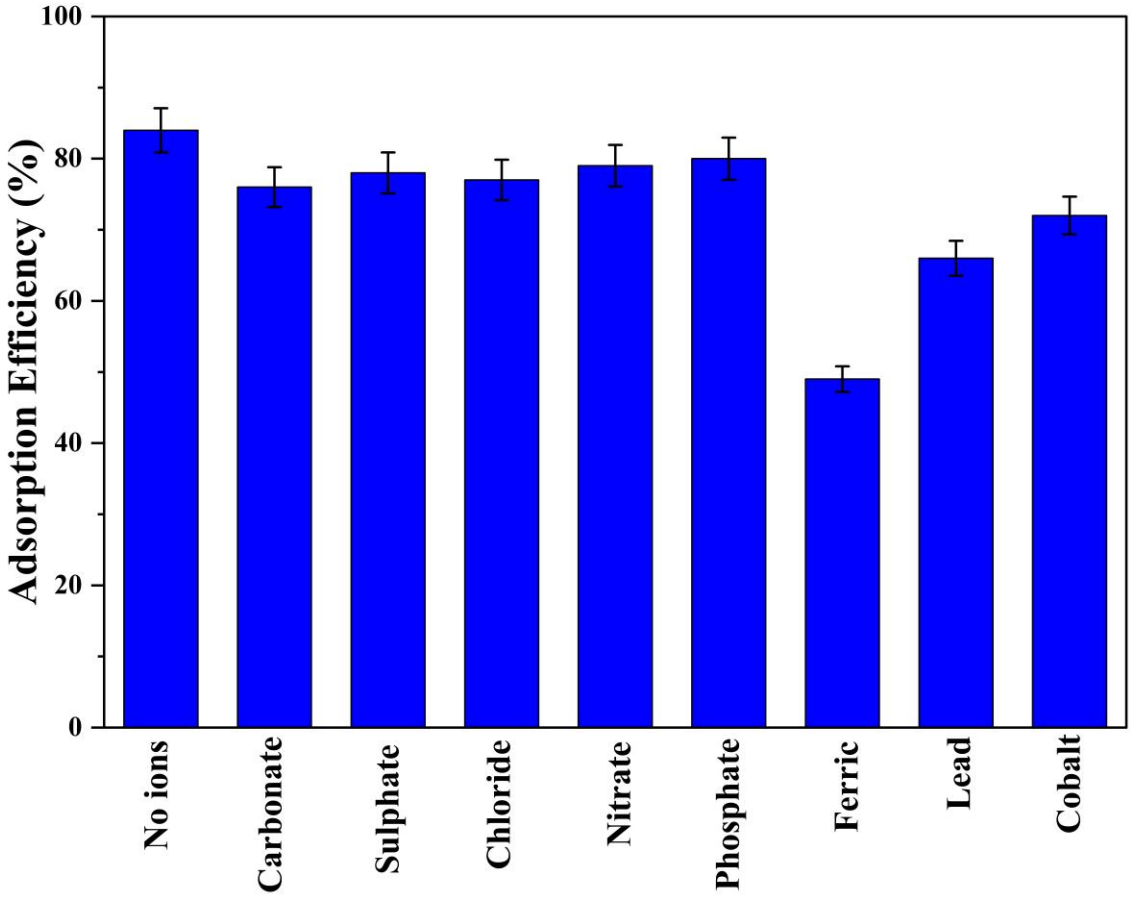

Figure 2.9: Effects of co-existing metal cations and anionic salts on CIP adsorption by MAAC, experimental conditions: pH 6, dosage 2.0 mg ml^{-1}, MAAC concentration 100 mg L^{-1}, ions concentration 100 mg L^{-1}, temperature 40 °C.

2.4.5. Adsorbent desorption and recyclability studies

The regenerative capacity of MAAC was investigated to understand the reusability of the adsorbent using 0.1 N NaOH as the desorption agent. A single cycle of adsorption involved the optimised dosage of MAAC (2.0 mg/mL) added to 100 mg/L of CIP solution at pH 2.0. The spent adsorbents after each cycle were treated with 0.1 NaOH, followed by thorough washing with distilled and then used for the next cycle. Washing with distilled water helped in removing any remaining antibiotics from the surface of MAAC, thus making the adsorbent available for reuse. Figure 2.10 illustrates the adsorption efficiency of MAAC after each adsorption-

desorption cycle. The analysis of this experiment shows a significant drop in the adsorption efficiency after the first cycle. This trend followed for all consecutive cycles after which regeneration of the adsorbed MAAC surface was not relevant; as the adsorption efficiency was too low. The CIP adsorption efficiency went down from 98% in first cycle to 43% in the fifth cycle. The main reason for this may be the morphological alteration and the continuous degradation of the active sites, with consecutive cycles. Another possible reason could be the blockage of pores, as some amount of CIP species fail to desorb or escape during the desorption cycles. Thus, with every cycle such molecules tend to block the active sites, making them unavailable for the consecutive cycles.

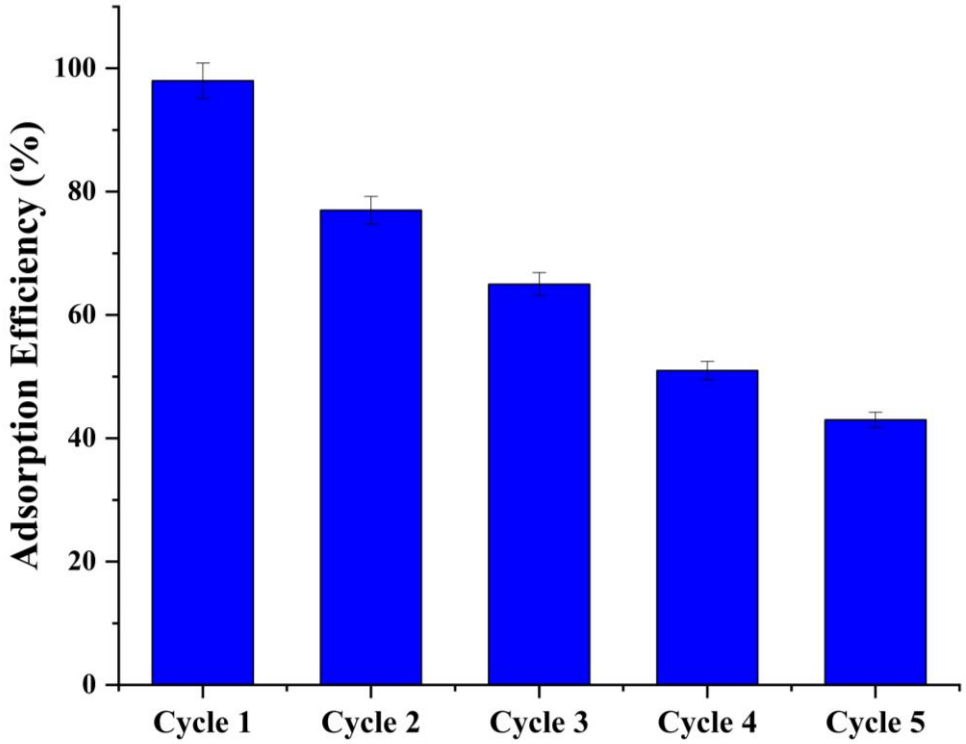

Figure 2.10: Desorption and recyclability of MAAC, experimental conditions: pH 6, dosage 2.0 mg ml^{-1}, MAAC concentration 100 mg L^{-1}, temperature 40 °C.

Also, after each consecutive cycle the adsorbent loses some amount of magnetic aggregates, causing a decline in its magneticity and thus the magnetic separation is also disrupted. The

same can be verified from Vibrating Sample Magnetometer (VSM) analysis, where the saturation magnetization (Ms) value of MAAC fell down from 18.2 emu/g (before first cycle) to as low as 7.6 emu/g (after fifth cycle), and the same has been illustrated in Figure 2.3.

2.4.6. Phytotoxicity assay

Phytotoxicity is the study of the adverse effect of phytotoxins (specific substances) on plant growth, seed germination, or any related effects on plant (Blok et al., 2019). The effectiveness of adsorbent (MAAC) in removing the adsorbate (CIP) was investigated by the phytotoxicity assay involving germination analysis of the *Vigna mungo* seeds. The analysis was performed by analyzing the antibiotics before and after treatment (adsorption). For the analysis, seeds germinated in distilled water labelled as a blank; in CIP solutions before treatment were labelled as control samples; and CIP solutions after the adsorptive treatment were labelled as test samples. The duration of this investigation was seven days. After the experiment, the root length was measured and recorded, as shown in Figure 2.11 (A and B). The mean root length of the germinated seeds in CIP solution prior to treatment was 6.35 cm, 4.8 cm, 4.6 cm, 3.6 cm, and 3.1 cm for 20, 40, 60, 80, and 100 mg/L of CIP solutions, respectively as compared to 26.4 cm for seeds germinated in distilled water. Conclusively, it can be reported that a higher concentration of antibiotics is harmful to the germination of seeds. However, mean root length for seeds germinated with CIP solution post adsorptive treatment with MAAC resulted in improved mean seed root length. The average root lengths improved to 24.7 cm, 18.8 cm, 14.1 cm, 13.2 cm, and, 12.4 cm for 20, 40, 60, 80, and 100 mg/L CIP solutions, respectively. Conclusively, seeds germinated with CIP solution post adsorptive treatment showed relatively better seed root length, thus resorting to efficiently removing CIP by MAAC. Similar results were reported in the literature (Dhaouefi et al., 2019; Shahnaz et al., 2021).

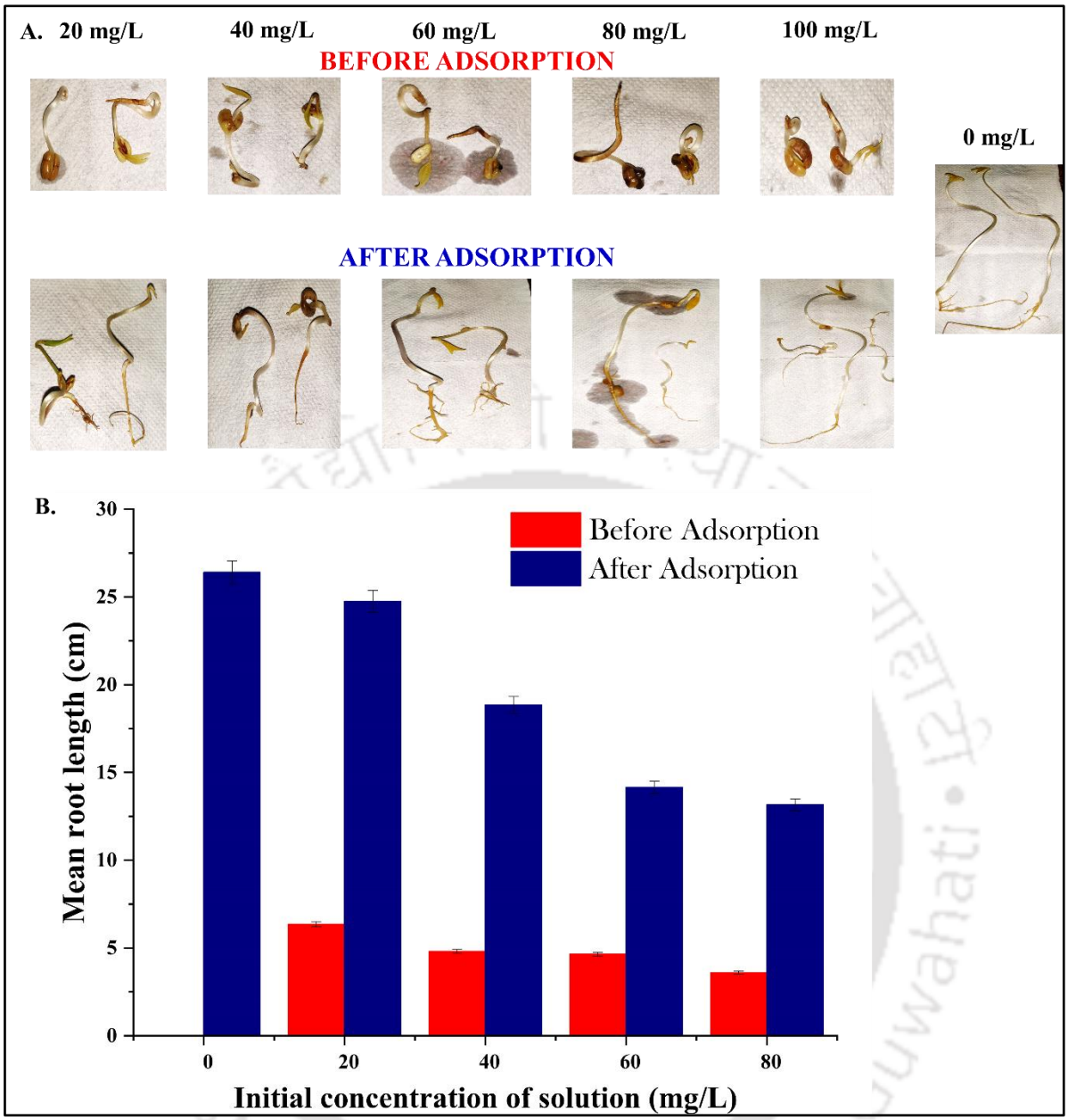

Figure 2.11: (A) Phytotoxic assessment of MAAC removing CIP using *Vigna mungo* (black gram) seeds; (B) comparison of seed germination root length.

2.5. Conclusion

Magnetic activated carbon (MAAC) was curated by a simple method of co-precipitation over activated carbon for the efficient elimination of emerging antibiotic contaminant Ciprofloxacin. Characterisation of MAAC surface verified the adsorbent's porous surface with enhanced magnetic properties. Process parameters such as pH of the CIP solution, temperature of adsorbate-adsorbent interaction, initial concentration of CIP and MAAC dosage influenced

the efficient adsorption of CIP by MAAC. Langmuir isotherm and pseudo-second order kinetics verified the formation of CIP monolayer over MAAC surface under optimal conditions and the sorbate-sorbent interaction was influenced by chemisorption. Thermodynamically, the adsorbate-adsorbent interaction was spontaneous, endothermic, with increased degree of randomness and disorderedness, that favoured the adsorption process. A significant reduction of the adsorption efficiency was reported in the presence of co-existing metal ions with CIP. However, in presence of anionic salts the reduction was nominal. Recyclability studies verified the loss in adsorption capability of MAAC towards CIP after consecutive cycles (for upto 5 cycles) and the associated loss of magneticity. Phytotoxic assay verified the ability of MAAC in adsorbing CIP, resulting from the effective germination of the *Vigna mungo* seeds. Table 2.5 represents a comparative data verifying the efficient applicability of the produced adsorbent (MAAC) in eliminating Ciprofloxacin species.

Table 2.5: Comparison table for adsorption capacities of various magnetic adsorbents for Ciprofloxacin.

Adsorbent	***Adsorption capacities (mg/g)***	***Reference***
Magnetic mesoporous carbon	74.68	Shi et al., 2013
Reduced graphene oxide/ magnetite composites	18.22	Tang et al., 2013
Fe_3O_4/Carbon composite	90.1	Mao et al., 2016
Fe_3O_4 coated polymer clay composite	39.1	Arya and Philip, 2016
MOF^C/ Fe_3O_4	63.2	Bayazit et al., 2017
M-BC	68.9	Kong et al., 2017
Fe_3O_4-MoO_3-AC nanocomposite	44.64	Mahmoud et al., 2021
Ferrites modified carbon nanotubes (MFe_2O_4/CNTs; M=Co, Cu, Mn)	63.32 (Co), 61.60 (Cu), and 46.35 (Mn)	Yao et al., 2021
MAAC	**81.97**	**This study**

Overall, MAAC proved to be an effective adsorbent for CIP removal. Impregnation of ferric/ferrous nanoparticles ensured easy, convenient and rapid recovery of the adsorbent from the sorbate-sorbent reaction mixture, by applying an external magnetic field. However, further studies are required to enhance its capabilities and its effectivity against other emerging contaminants of varying grades.

Chapter 3

Activated carbon-chitosan based adsorbent for the efficient removal of Diclofenac: Synthesis, characterization and phytotoxicity studies

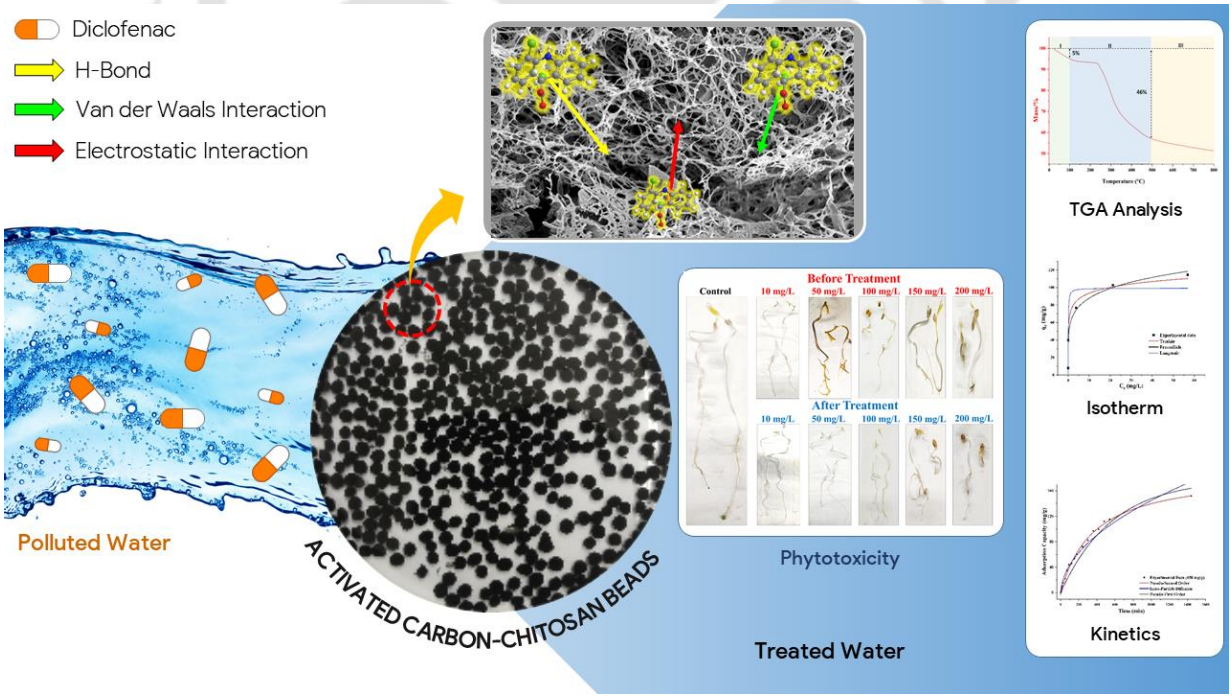

ABSTRACT

The rise in pharmaceutical pollutants due to their unregulated discharge in pharmaceutical wastewater has landed them as emerging contaminants that would gradually affect the aquatic ecosystem and human life. The current study emphasizes the adsorptive elimination of one such emerging pharmaceutical pollutant, i.e., Diclofenac (DIF), using a synthesized adsorbent vis. Activated carbon-chitosan beads (ACCB). The morphological and physicochemical properties of the prepared adsorbent, ACCB and its interaction with the DIF species were investigated. Process parameters influencing the adsorptive interactions between ACCB and DIF were optimized. DIF was efficiently adsorbed at optimized initial DIF pH of 6.0 and ACCB dosage of 1.5 mg/mL at an incubation temperature of 40°C. Freundlich isotherm model showed the best fit (R^2 = 0.98) with the experimental data to conclude that the adsorbent surface is heterogenous, promoting multilayer adsorption. As depicted from the Langmuir isotherm model, the maximum theoretical adsorption capacity was 99.29 mg/g. The seed toxicity assay confirmed the efficacy of ACCB in the adsorptive removal of DIF species from aqueous setups, making the post-treated solution fit enough for seed germination.

3.1. Introduction

Freshwater sources are depleting due to various factors, such as industrial and domestic use, population growth and urbanisation, constant water abstraction, climate change and drought. These sources are getting polluted by emerging contaminants. Among many emerging contaminants, pharmaceutical products (PPs) are the main concern for today's world as they negatively affect humans and other living beings (Priya et al., 2022). Emerging contaminants, or contaminants of emerging concern, can refer to many different kinds of chemicals, primarily including pharmaceuticals, personal care products (PCPs), endocrine-disrupting compounds (EDCs) and agricultural products (Bexfield et al., 2019).

What makes them a severe threat is that their risks to human health and the environment are not yet fully understood (Emerging Contaminants). According to US EPA (US EPA), they are increasingly being detected at low levels in surface water, and there is concern that these compounds may have an impact on aquatic life. The emerging contaminants may also demonstrate low acute toxicity but cause significant reproductive effects at deficient levels of exposure. The U.S. EPA is working to improve its understanding of several emerging contaminants, pharmaceuticals, PCPs and EDCs.

PPs are the formulated drugs used to prevent microbial infection, especially bacteria. They have a wide range of animal husbandry and aquafarming applications, i.e., disease control and growth enhancement (Alnajrani & Alsager, 2020). In recent decades, the use of PPs in the non-medical sectors has increased. In animal husbandry, sick animals were treated by providing them with food or water and washing the remains, which were then mixed with drain water, which eventually increased the wastewater's PPs concentration. In aquaculture, PPs are used to improve the fishes' immune systems and promote their growth. These are mixed with the feed and given to them. The unconsumed PPs will increase the risk of antibiotic resistance bacteria. Many household products contain antibiotics to kill potentially harmful bacteria, such as

triclosan, a synthetic component found in various shampoos and soaps (Meek et al., 2015). The disposed-off PPs residues are in an un-metabolized state that remains active and persistent even at low concentrations. The PPs residues cause the pathogenic microbes and bacteria to induce antibiotic resistance (AMR), thus resulting in potential health risks to humans and other living forms (Xu et al., 2020).

The present study focuses on Diclofenac (DIF), a nonsteroidal anti-inflammatory drug (PubChem) and one of the most prescribed pharmaceutical products (approximately 940 tons/year) in the world which is used to treat mild to moderate acute pain. It is one of the emerging pollutants found in the effluent of pharmaceutical industries, treatment plants, sewage, household drains, hospitals as in parent form or its metabolites (Sathishkumar et al., 2020). The continuous discharge of DIF increased the concern for scientific communities. Thus, various strategies have been employed to eradicate DIF from the water (Li et al., 2021; Sathishkumar et al., 2020).

Traditional wastewater treatment techniques used to eliminate the contaminants, including sedimentation, filtration, coagulation or biological treatment, are ineffective in removing pharmaceutical residues as they cannot detect such contaminants in trace levels (Alnajrani & Alsager, 2020; Isik et al., 2022; Spiliotopoulou et al., 2021). Moreover, advanced wastewater treatment technologies such as advanced oxidation process (AOP) (Yabalak et al., 2022), membrane bioreactor, UV photolysis, etc., have high efficiency for their removal but process cost, catalyst management, toxic by-products and residues produced during the treatment process makes the technologies non-feasible (Alnajrani & Alsager, 2020; Antoniou et al., 2016).

Over the past decade, adsorption has been exploited as an efficient and cost-effective process to effectively eliminate numerous organic and inorganic pollutants, primarily based on the type of adsorbent selected for the target adsorbate (Arslan et al., 2022; Shahnaz et al., 2021).

Activated carbon has been opted as an ideal adsorbent, as it has an extensive surface area and a well-developed porous structure which renders it with effective adsorption capacities (Patra et al., 2020). The activated carbon/carbon-based adsorption has also been reported as a unique process for removing antibiotics from water (Yu et al., 2016). However, carbon-based adsorbents have a disadvantage, as filtration or centrifugation separates the spent adsorbent after the adsorption process from an aqueous solution, causing a loss of some adsorbents (Aydin et al., 2019). To overcome this, the current study emphasises encapsulating activated carbon within a strong polymeric framework. This shall prevent the loss of adsorbent post adsorption separation process. For this, the activated carbon was encapsulated within a chitosan framework. The choice of chitosan as an encapsulating material is due to its cost-effectiveness, bulk abundance, non-toxicity, and biodegradability nature (Afzal et al., 2018). Chitosan is prepared via chitin deacetylation methods, which involves the removal of the acetyl groups and replacing them with amino groups. The extent of free amino groups available in the chitosan structure can be determined via the chitin's degree of deacetylation (DDA). Such amino groups render the chitosan with adsorptive properties (Patra et al., 2021).

Thus, activated carbon/chitosan beads (ACCB) were synthesised for the adsorptive elimination of DIF species from aqueous setups in the present study. The goal is to investigate the feasibility of ACCB as an inexpensive adsorbent to remove DIF from water. The effects of various adsorption parameters such as pH of DIF solution, initial concentration of ACCB and ACCB-DIF interaction temperature was optimised for the effective removal of DIF species. Other studies like the influence of sorbate's ionic strength, desorption and recyclability analysis

of the adsorbent, and seed toxicity analysis were also studied. The ultimate goal was to reuse the spent adsorbent to remove DIF multiple times.

3.2. Materials and Methods

3.2.1. Chemicals and reagents

All the chemicals, salts and reagents required for the current study were of analytical grade (purity > 99%) and purchased from Sigma Aldrich, India and Himedia Laboratories Pvt. Ltd., India via local vendors (Table 3.1).

Table 3.1: Detail list of chemicals, reagents, and salts.

Serial No.	*Chemical/Reagent/Salt*	*Purpose*
1.	Diclofenac	Adsorbate
2.	Chitosan	Adsorbent
3.	Commercial activated carbon	Adsorbent
4.	0.1 M Sodium Hydroxide (NaOH)	Adjusting pH
5.	0.1 M Hydrochloric acid (HCl)	Adjusting pH
6.	Sodium Chloride (NaCl)	Ionic strength
7.	1% Sodium Hypochlorite (NaClO)	Rinsing Vigna mungo seeds

3.2.2. Preparation of activated carbon/chitosan beads (ACCB)

The adsorbent was prepared following the protocol described by Afzal et al., 2018, with some minor modifications (Figure 3.1). Commercially available activated carbon (CAC) was used to prepare the adsorbent as it is highly porous and inexpensive. 1 g of commercially available chitosan was vigorously mixed into acetic acid solution (2% v/v). This was followed by adding

commercial activated carbon (1 gram), and the mixture was mixed to obtain a homogenous mixture. The produced chitosan/ activated carbon suspension was then converted to beads by dropping it into sodium hydroxide (NaOH) solution (2.5% w/v, 200 mL) using a syringe and were incubated overnight. The prepared beads were then extracted from the NaOH solution and were rinsed with deionised water until the pH of filtrate water was equivalent to that of deionised water. The beads were lyophilised, and these freeze-dried beads were further used for the batch experiments.

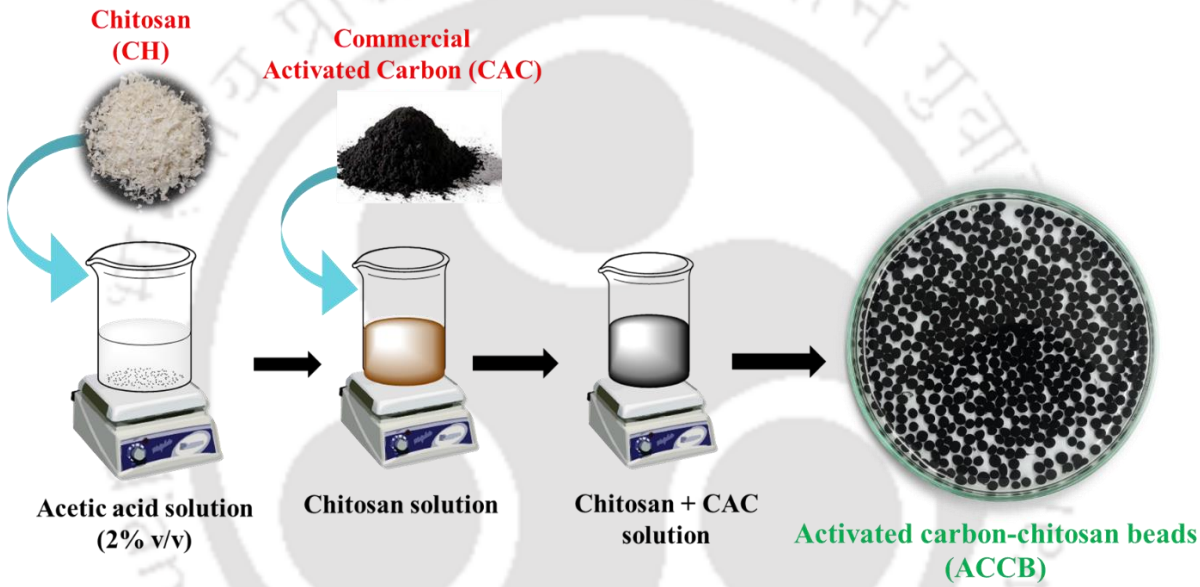

Figure 3.1: Schematic diagram of the ACCB preparation.

3.2.3. Characterization of the ACCB

Field emission scanning electron microscopy (FE-SEM) (Zeiss, Gemini-300) was used to assess the surface morphology, and Energy-dispersive X-ray spectroscopy (EDS) (Zeiss Sigma-300) was used to determine the elemental composition of the ACCB before and after the adsorption of DIF species. Brunauer-Emmett-Teller (BET) (Quantachrome-Autosorb-IQ MP, USA) analysis was performed to determined the surface area of prepared adsorbent (ACCB). Fourier-transformed infrared spectroscopy (FTIR) (Nicolet iS10) was used to analyse changes on the ACCB surface and its interaction with DIF species. X-ray diffraction (XRD)

(Agilent, USA) was used to determine the crystallographic structure that may have happened due to the encapsulation of CAC to create ACCB.

3.2.4. Batch adsorption, desorption, and effect of ionic strength analysis

Batch adsorption experiments were conducted to study the influence of various parameters for the adsorptive elimination of the DIF species by the prepared adsorbent (ACCB). In the present study, initial pH of DIF solution (2.0 - 10.0); ACCB's dosage (0.5 mg/mL - 3.0 mg/mL); DIF's initial concentration (10 mg/L - 200 mg/mL) and ACCB/DIF interaction temperature (30°C - 50°C) were studied. These experiments were conducted for 24 h in a rotator incubator (ORBITEK-LE) at 150 revolutions/min. After completing each batch experiment, the adsorbent was separated from the mixture, and the filtrate was analysed to detect any DIF species using UV-Vis spectrophotometer at 276 nm. The removal efficiency (%R) and the adsorption capacity (Qt) was calculated as follows (Kumar et al., 2022):

$$Q_t = \frac{(C_0 - C_t)V}{m} \quad (3.1)$$

$$\%R = \frac{(C_0 - C_t)}{C_0} 100 \quad (3.2)$$

Where, C_o (mg/L) represents the initial concentration of DIF; C_t (mg/L) represents the DIF concentration at the time t; m (g) represents the mass of ACCB (adsorbent), and V (L) represents the volume of the DIF solution (adsorbate).

Desorption study of ACCB was carried out with the desorbing agent, 0.1 N NaOH. The desorbed ACCB was then repeatedly rinsed with deionized water to normalise the adsorbent's surface to neutral pH. It was then re-used to adsorb DIF species. These adsorption-desorption cycles were repeated several times until the removal efficiency of ACCB dropped down to less

than 50%. The effect of ionic strength on the adsorption of DIF by ACCB was investigated in the presence of various concentrations of NaCl background electrolyte.

3.2.5. Seed toxicity assay

Validation of ACCB for the effective removal of DIF species and efficacy of the post-treated aqueous solution was analysed by seed toxicity assay using *Vigna mungo* (black gram). The seeds were rinsed in 1% sodium hypochlorite (NaOCl) solution to avoid fungal development. The seeds were then washed with deionised water to shed off any minute dust particle. The seed toxicity assay was conducted in Petri-dishes. Ten seeds were germinated in cotton soaked with deionised water (blank), untreated DIF solution (control) and treated DIF solution (test sample). The seeds were allowed to germinate for seven days in dark conditions at 22.5±2.5°C. After incubation, the average root length of each sample was calculated as the response of the experiment.

3.3. Theoretical background

The characteristics of adsorptive interaction of DIF by ACCB was investigated by different isotherm models. The models were tested on the acquired equilibrated data. The adsorption kinetics was determined using kinetics models. Thermodynamic parameters were investigated to analyse the heat and energy distribution of the interaction, and spontaneity of the interaction. The section 1.5. discusses the detailed theory as well as related equations.

3.4. Results and Discussions

3.4.1. Characterization of ACCB

3.4.1.1. Surface morphology and elemental analysis

Micrographs of the prepared activated carbon/chitosan beads (ACCB) are exhibited in Figure 3.2. Figure 3.2A and Figure 3.2B depict that most of the beads were almost spherical in shape with a smooth surface and an average diameter of about 3.6 mm. After freeze-drying, the beads had a rough lacunar surface with prominent wrinkles, as shown in Figure 3.2C. Figure 3.2D depicts the outer surface of ACCB with 500x magnification showing multiple pores with a rough and irregular surface. Figure 3.2E shows the distribution of embedded CAC in the chitosan matrix. This reveals the formation of activated carbon/chitosan (ACCB) adsorbent. In addition, ACCB has a fibrous network (Figure 3.2F) which increases the surface area and contributes to adsorption. The structural morphology study revealed that ACCB has a rough and porous structure that may facilitate DIF adsorption. Elemental analysis was performed by Energy Dispersive X-ray Spectroscopy (EDS). Figure 3.2G and Figure 3.2H depict the EDS spectra of ACCB surface prior and post DIF adsorption, respectively. A clear, distinct Chlorine (Cl) peak can be observed in Figure 3.2H after DIF adsorption, confirming that ACCB successfully adsorbed DIF as 'Cl' is an integral component of DIF molecules. The ACCB and CAC specific surface areas were 617.48 m^2/g and 626.64 m^2/g, respectively. The ACCB's surface area was slightly reduced due to the encapsulation of CAC in the chitosan matrix. The prepared adsorbent has a mesoporous structure as the average pore size ranges from 2 to 5 nm.

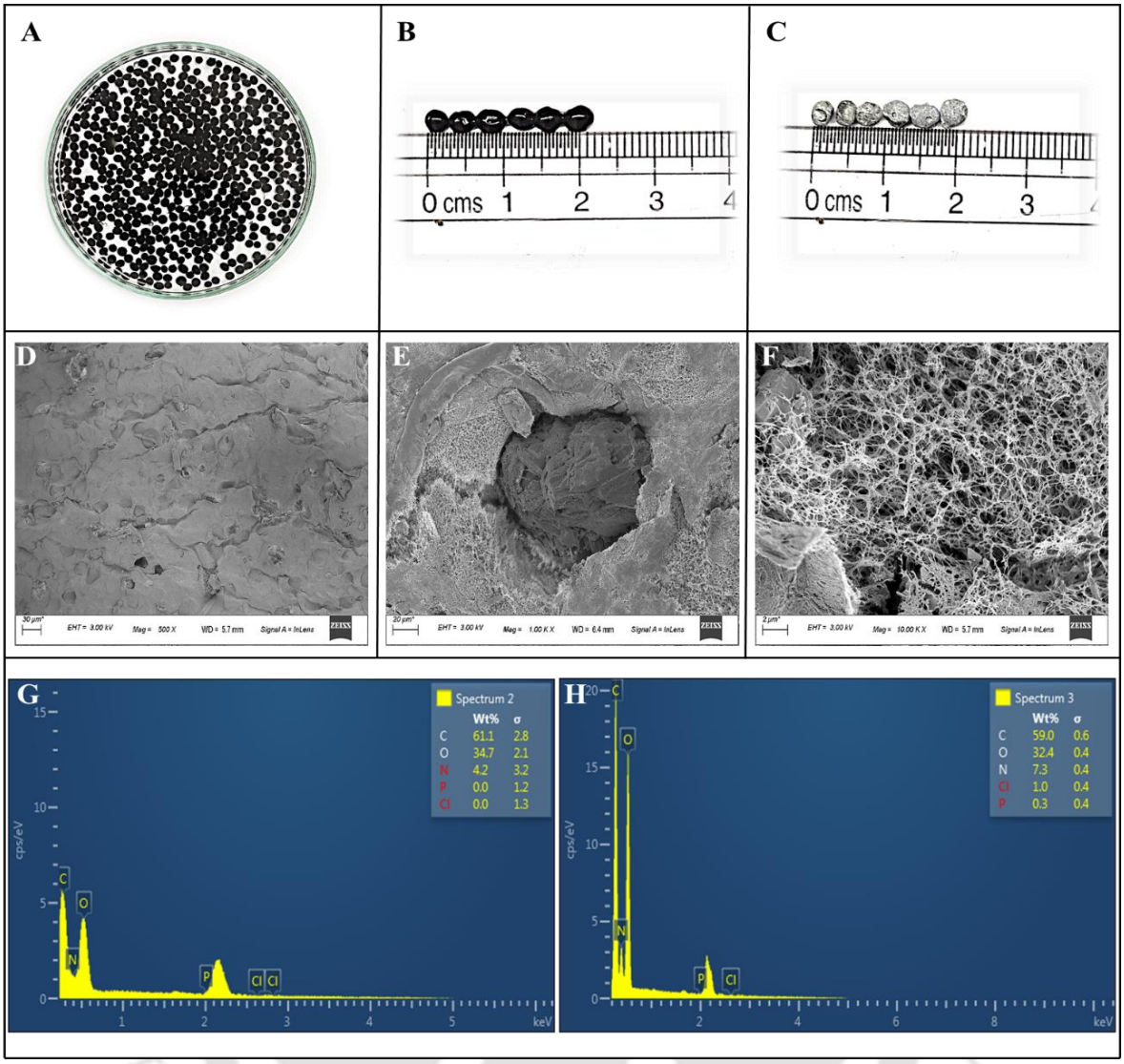

Figure 3.2: (A) Digital image of ACCB in petri dish; (B) Digital image of wet ACCB; (C) Digital image of lyophilized ACCB; (D), (E) and (F) FESEM images of ACCB at different magnification; (G) EDX spectrum of ACCB before adsorption; and (H) EDX spectrum of ACCB after adsorption.

3.4.1.2. Powdered X-ray diffraction (XRD) analysis

X-Ray Diffraction (XRD) analysis was used to determine the crystallographic structure of the adsorbent (ACCB) material based on its diffractive pattern. The peaks of the XRD analysis are shown in Figure 3.3A. Chitosan (CH) presents two distinct crystalline peaks at 9.80° and

20.04°, corresponding to form II crystallinity (Peng et al., 2020). A reflection peak at 43.8° was seen in both CAC and ACCB, suggesting CAC presence in ACCB beads (Idohou et al., 2020; Somsesta et al., 2020). Finally, the XRD results revealed that the prepared beads were moderately crystalline.

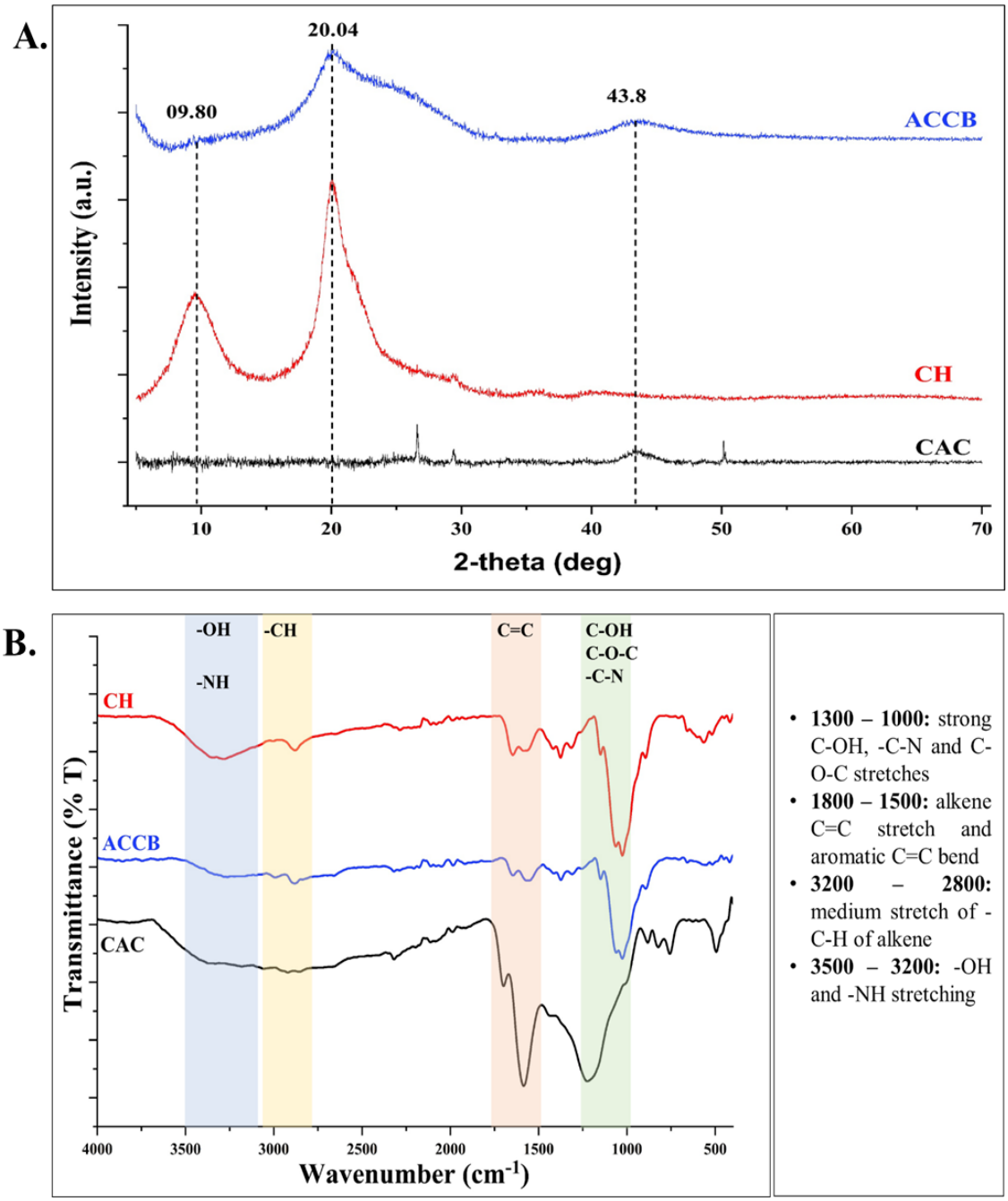

Figure 3.3: (A) XRD plot of ACCB, chitosan (CH) and commercial activated carbon (CAC) and (B) FTIR plot of ACCB, CH, and CAC.

3.4.1.3. Fourier-transformed infrared spectroscopic analysis

The FTIR analysis was performed to gain a clear information of the functional groups present on the material's surface. The FTIR spectrometer was measure the FTIR spectra of CAC, CH, and ACCB in the 400–4000 cm^{-1} region, as shown in Figure 3.3B. In 3500-3200 cm^{-1} region, all measured analytes showed peak that corresponds to -OH and -NH stretching due to presence of alcoholic and amine groups that will promote adsorption (Corazzari et al., 2015; Velusamy et al., 2021). In 3200-2800 cm^{-1} region, only CH and ACCB showed peak that belongs to the -CH stretching of alkene group (Kohli et al., 2019). In the range 1800-1500 cm^{-1}, -C=C- stretch of alkene and aromatic groups can be observed in all the spectra with strong band in CAC. Vibrational stretch of -C-OH, -C-N and C-O-C of carboxylic acids, aromatic amine and aromatic ester were observed in both CH and ACCB (Kaveeshwar et al., 2018; Renita et al., 2021). Introduction of various new function to ACCB surface will facilitate the adsorption capacity.

3.4.1.4. Thermal stability analysis

Thermal gravimetric analysis (TGA), is a thermal analysis that measures the changes in the physical and chemical properties of materials as a function of temperature. The TGA curve in Figure 3.4 depicts weight loss (in percentage) as a function of temperature. As the temperature rises, the weight percentage drops due to various reactions indicating mass changes due to the thermal process. As depicted in Figure 3.4 (region I), the initial decomposition starts at a lower temperature. It continues up to 100°C - 120°C, with 5% weight loss, corresponding to water evaporation from the adsorbent's surface. In region II, a logarithmic decomposition of approximately 46% for the adsorbent can be reported in the range of 100°C - 500°C. This could be due to the deterioration of the polymer chain caused by the deacetylation of glycosidic linkages. The last stage (region III), indicating the high temperatures (>500°C), corresponds to the thermal destruction of residual carbon material of the adsorbent (Moussout et al., 2016).

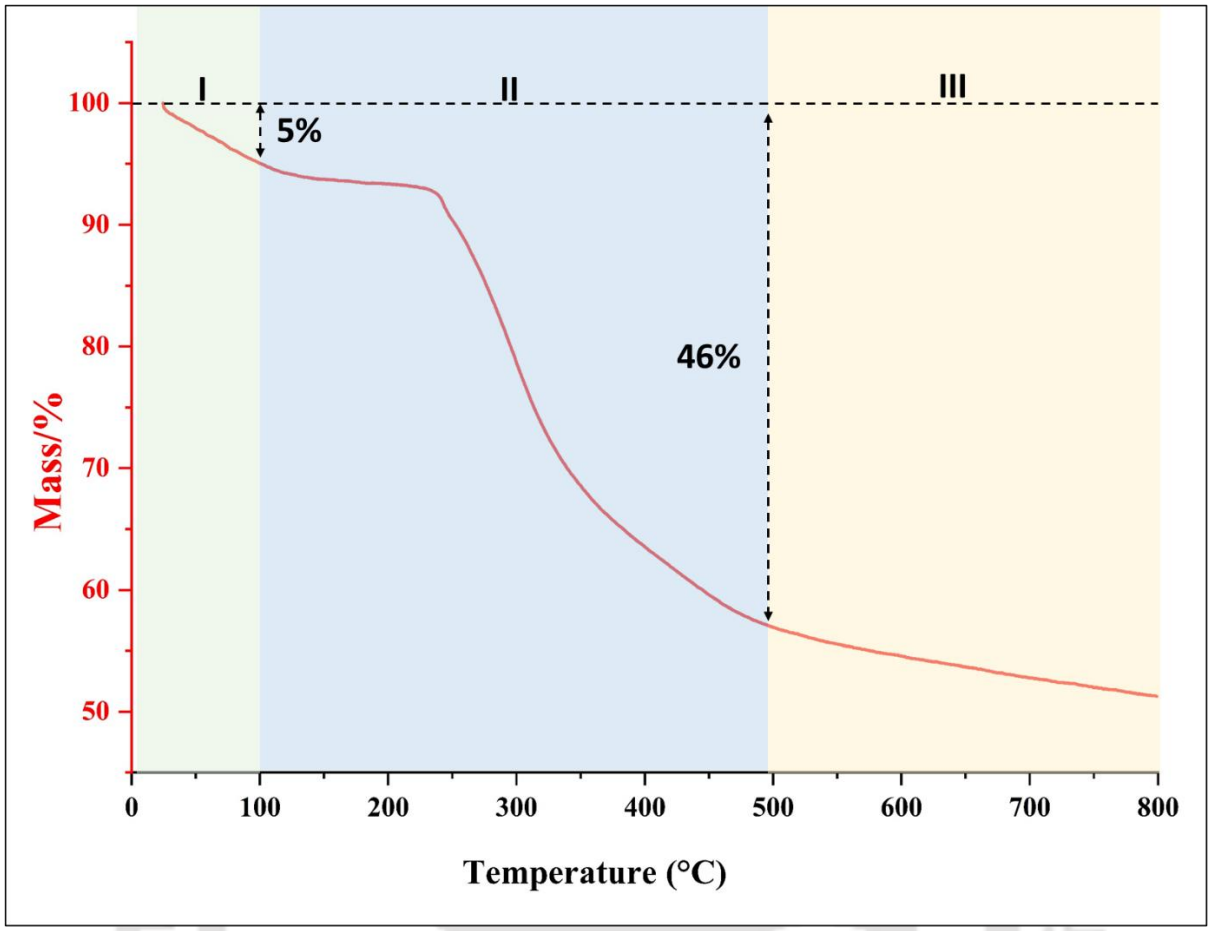

Figure 3.4: TGA plot of ACCB

3.4.2. Impact of adsorption parameters on DIF species removal by ACCB

3.4.2.1. Influence of pH of DIF solution on adsorption mechanism

The DIF solution's pH impacts the DIF species' charge intensity and the acquired charge on the adsorbent's surface, influencing the interaction between DIF species and the adsorbent in aqueous solutions (Soares et al., 2019). Figure 3.5 shows the adsorptive removal efficiency (%) of the DIF species between the pH values of 2.0-10.0. The removal efficiency of ACCB increases from pH 2.0 to 6.0, beyond which a slight reduction was reported. DIF molecules will acquire positive charges at pH values less than its pKa, and the ACCB surface should characteristically possess a positive charge at low pH. Therefore, a repulsive force will be generated between DIF and ACCB, thus resulting in low removal efficiencies of DIF at low

pH values, as shown in Fig. 4B. DIF species are negatively charged when the pH of the DIF solution is higher than its pKa value, i.e., 4.15 (Lu et al., 2020), and thus ACCB has a strong attraction for DIF species due to the acquired positive surface charges due to the presence of ammonium functional groups. The numerous protonated amine groups on the surface of ACCB resort to positive-negative charge interaction with DIF at pH 6.0, promoting efficient DIF adsorption on the ACCB surface. Since ACCB beads successfully removed the DIF species at pH 6.0, pH 6.0 was chosen as the best pH for this study.

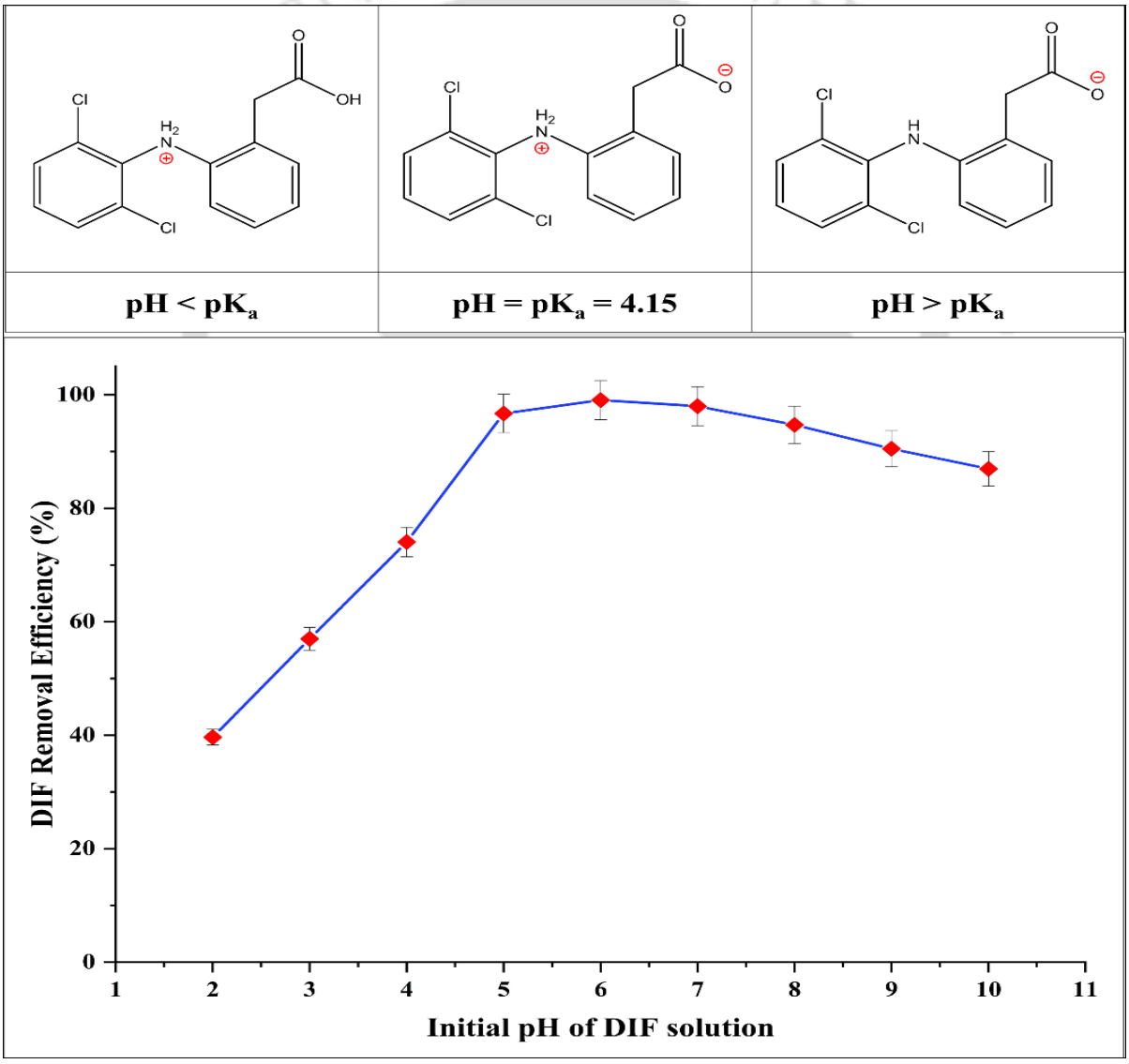

Figure 3.5: Effect of initial pH of DIF working solution, experimental conditions: pH 2 to 10, ACCB dosage 0.5 mg/mL, DIF concentration 100 mg/L, temperature 35 °C.

The proposed adsorption mechanism for ACCB adsorption of DIF is illustrated in Figure 3.6. At pH 6.0, most DIF species were positively charged, and the ACCB surface was negatively charged; therefore, the electrostatic interaction dominates the other interactions. Some DIF molecules will acquire a negative charge from the freely available polar group, -OH and -NH_2, forming a hydrogen bond with the adsorbent (Pereira et al., 2020). In addition, the aromatic rings of DIF interact with the aromatic groups of ACCB, resulting in a weak π–π interaction.

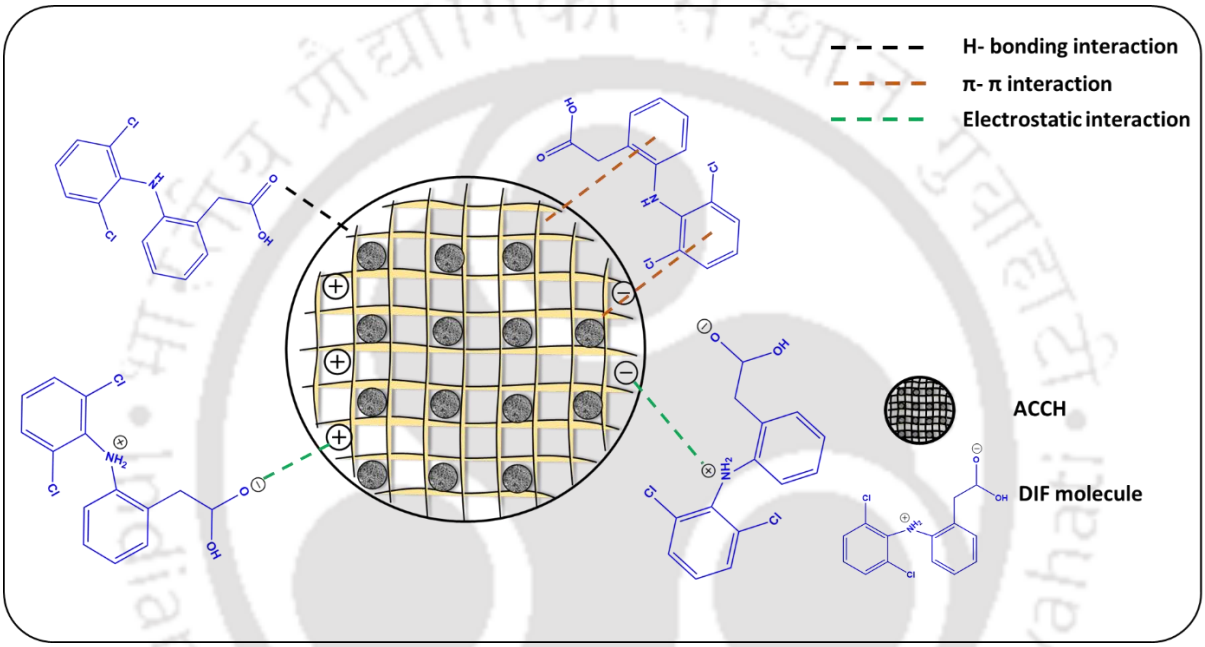

Figure 3.6: The proposed adsorption mechanism of DIF adsorption by ACCB.

3.4.2.2. Influence of ACCB dosage in the adsorption of DIF

The effect of ACCB dosage for the DIF adsorption was performed within the dosage ranging from 0.5 mg/mL to 3.0 mg/mL, with 100 mg/L of DIF solution at pH 6.0. From the plot (Figure 3.7A), at 1.5 mg/mL ACCB dosage, an optimum 97.02% DIF removal efficiency was observed. It can also be seen that with the increase of ACCB dosage concentration, the removal efficiency of DIF also increases. The main reason could be the increasing availability of free active sites as the ACCB dosage increases. However, adsorption capacity reaches equilibrium after a

certain dosage of ACCB. This was due to the limited number of DIF molecules; hence, all the DIF molecules are adsorbed on the surface of ACCB (Shirani et al., 2020).

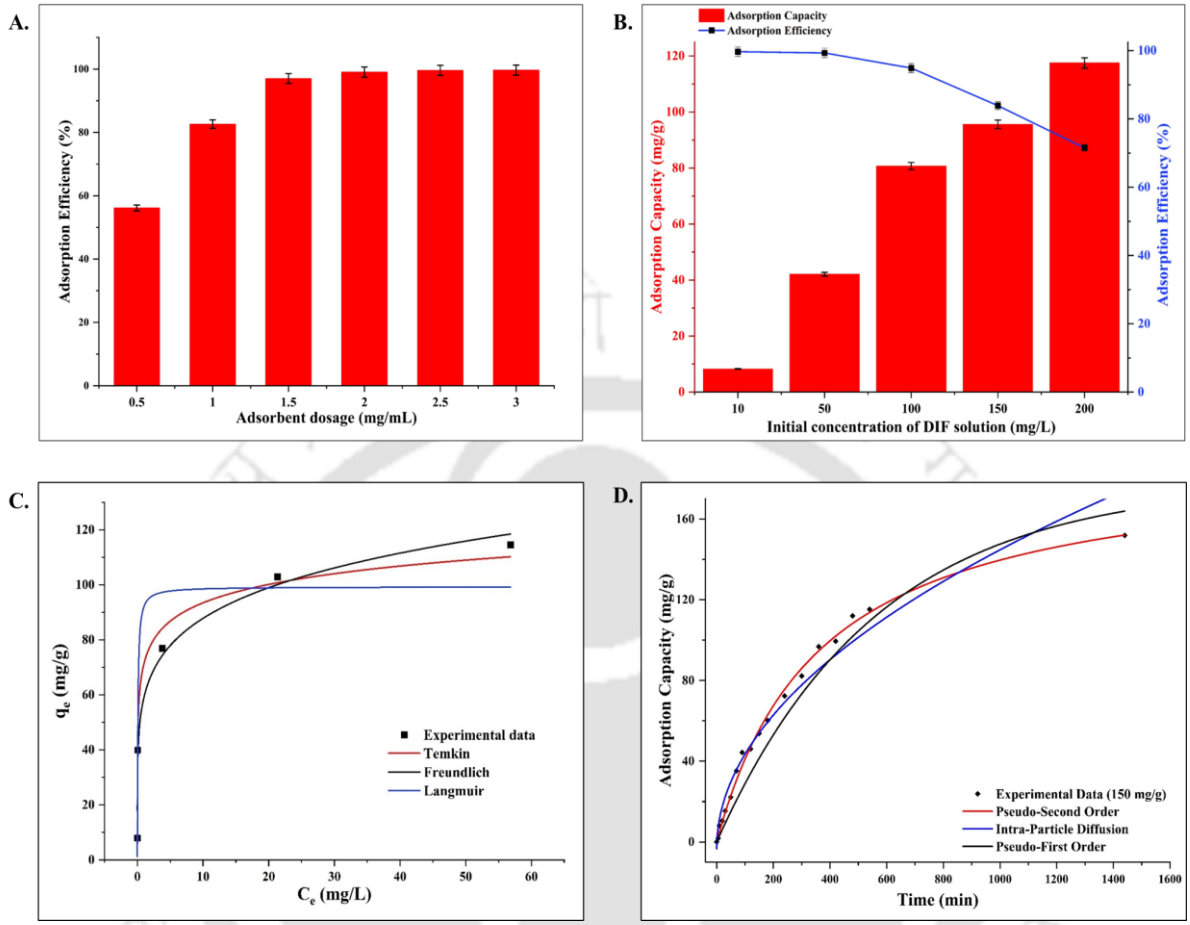

Figure 3.7: (A) Effect of ACCB Dosage, experimental conditions: pH 6, ACCB dosage 0.5-3.0 mg/mL, DIF concentration 100 mg/L, temperature 35 °C; (B) Effect of initial concentration of DIF solution, experimental conditions: pH 6, ACCB dosage 1.5 mg/mL, DIF concentration 10-200 mg/L, temperature 35 °C; (C) Non-modelling isotherm plot for DIF adsorption, experimental conditions: pH 6, ACCB dosage 1.5 mg/mL, DIF concentration 10–200 mg/L, temperature 40 °C; and (D) Non-linear Kinetic plot for DIF adsorption, experimental conditions: pH 6, ACCB dosage 1.5 mg/mL, DIF concentration 10–200 mg/L, temperature 40 °C.

3.4.2.3. Influence of Initial DIF concentration

The effect of initial DIF concentration was investigated under the following experimental conditions vis. 10 mg/L to 200 mg/L of DIF concentration; pH 6; 1.5 mg/mL ACCB dosage for the incubation of 24 h. From the plot (Figure 3.7B), it's clear that the adsorption capacity conjointly increased as the initial DIF concentration increased. However, a reduction in the adsorption efficiency can be seen with the increases in the initial concentration of DIF.

Such phenomenon is possible due to limitation in available active sites due to fixed dosage of ACCB for elevating initial concentrations of DIF species. These saturated active sites gradually influence the adsorption capacity of the adsorbent (ACCB). Hence with the gradual rise in the initial concentration of DIF species, the intensity of the occupied sites on the adsorbent (ACCB) increases and so does its adsorption capacity. Nevertheless, the adsorption efficiency of the adsorbent (ACCB) is the function of vacant active sites available on the adsorbent (ACCB) for adsorption. Thus, when the initial concentration of DIF species is elevated, the intensity of vacant active sites on the adsorbent's surface reduces. This causes a decline in the adsorption efficiency of the adsorbent.

3.4.2.4. Effect of reaction temperature and analysis of interaction thermodynamics

The effect of experimental temperature was studied at varying temperatures (30°C to 50°C) with different initial DIF concentrations, keeping the other parameters at optimised conditions. The outcome of the experiments is shown in Table 3.2, where the calculated values of $\Delta G°$, $\Delta H°$ and $\Delta S°$ are displayed. The reaction between DIF molecules and ACCB adsorbent were spontaneous and thermodynamically feasible as the negative values of $\Delta G°$ confirmed it. The positive values of $\Delta H°$ suggest that the adsorption process was endothermic. Finally, the DIF molecules get randomly adsorbed on the ACCB surface, as indicated by the positive values of $\Delta S°$.

Table 3.2: Thermodynamics Parameters (ΔG°, ΔH°, and ΔS°) for adsorption of DIF by ACCB.

C_i (mg/L)	Temp. (°C)	ΔG° kJ/mol	ΔH° kJ/mol	ΔS° J/mol
10	30	-40.12	-0.67	134.59
	40	-41.44		
	50	-42.81		
50	30	-38.43	-0.64	128.92
	40	-39.69		
	50	-41.01		
100	30	-24.01	-36.94	201.07
	40	-25.93		
	50	-28.04		
150	30	-20.58	0.48	67.01
	40	-21.88		
	50	-21.89		
200	30	-18.17	-16.67	115.55
	40	-19.87		
	50	-20.46		

3.4.3. Interaction studies

3.4.3.1. Adsorption isotherms

Interactions involved in the adsorption process of DIF by ACCB was investigated by adsorption isotherms. The equilibrated data was applied to Freundlich, Langmuir and Temkin adsorption isotherms. The values of the isothermal constants and the coefficients of regression (R^2) are shown in Table 3.3. The Freundlich isotherm model gave the best-fitted (R^2=0.98) with the experimental data. Theoretically, the Freundlich isotherm model suggests the adsorption phenomenon occur on heterogeneous systems with the possibility of adsorbate species adsorbed in a multilayer fashion. Accordingly, the value for the Freundlich constant

(1/n) is found to be more than 1, thus verifying the adsorption process to be feasible. Simultaneously, Langmuir isotherm model also gave a good fit with the equilibrated experimental data (R^2=0.91). This theoretically verifies the formation of adsorbate monolayer over the adsorbent surface due to sorbate-sorbent adsorptive interaction. The theoretical Langmuir maximum adsorption capacity (Q_L) for ACCB was 99.29 mg/g. Temkin isotherm values indicate that most of the adsorbate-adsorbent interaction occurred was endothermic (Kim & Kim, 2019). The non-linear plots for isotherm modelling, as depicted in Figure 3.7C, illustrate the Freundlich isotherm model to show a good fit with the equilibrated experimental data.

Table 3.3: Adsorption isotherm models and their parameters.

ISOTHERMS	***ISOTHERM CONSTANTS***	
LANGMUIR	Q_L (mg/g)	**99.29**
	K_L (L/mg)	**12.82**
	R^2	**0.91**
FREUNDLICH	K_F (mg/g) $(mg/L)^{-1/n}$	**59.09**
	1/n	**5.8**
	R^2	**0.98**
TEMKIN	A (L/g)	**1646.62**
	B (J/mol)	**270.28**
	R^2	**0.92**

3.4.3.2. Kinetics analysis

The equilibrated data were applied to analyse the kinetic behaviour of DIF adsorption. Pseudo-first-order, pseudo-second and intra-particle diffusion kinetics adsorption models were used to

investigate the kinetics of the adsorption process. All the calculated values of different models are shown in Table 3.4.

Table 3.4: Adsorption kinetics models and their parameters.

C_i (mg/l)	Q_e Expt. (mg/g)	Pseudo-First Order			Pseudo-Second Order			Intra-Particle Diffusion		
		K_1 (1/min)	Q_t (mg/g)	R^2	K_2 (1/min)	Q_t (mg/g)	R^2	K_{id} (mg/g $min^{1/2}$)	C (mg/g)	R^2
10	16.27	0.016	16.17	0.99	0.001	18.12	0.98	0.49	5.04	0.66
50	68.52	0.004	69.72	0.99	$4.85x10^{-6}$	87.19	0.98	2.43	13.58	0.88
100	126.33	0.002	134.8	0.96	$1.04x10^{-6}$	183.64	0.96	4.46	16.37	0.92
150	151.86	0.002	177.76	0.97	$1.43x10^{-6}$	190.64	0.99	4.68	17.18	0.96
200	169.27	0.002	181.67	0.98	$6.28x10^{-7}$	251.36	0.98	5.51	19.64	0.96

According to the analysed models, a plot was generated between adsorption capacity (mg/g) and time (min) to show the adsorption nature over time (Figure 3.7D). Pseudo-second-order kinetics gave the best fit over experimental values indicating that the adsorption process is governed by chemisorption between the adsorbate (DIF) and the adsorbent (ACCB). The validation of the result was given by the similarities between the values of experimental adsorption capacity (Q_e) and theoretical adsorption capacity (Q_t).

3.4.4. Effects of ionic strength

The adsorption of DIF species by ACCB adsorbent at different ionic strengths of NaCl (mol/L) is illustrated in Figure 3.8A. As the strength of NaCl increases, the adsorption of DIF decreases.

When the adsorbate and adsorbent charge is opposite, increasing ionic strength may reduce the electrostatic force between the adsorbate and adsorbent. This is because an increase in the ionic strength may cause the adsorbent particles to aggregate, resulting in a reduction in the adsorbent's functional adsorption sites, thus affecting its adsorption capabilities (He et al., 2018).

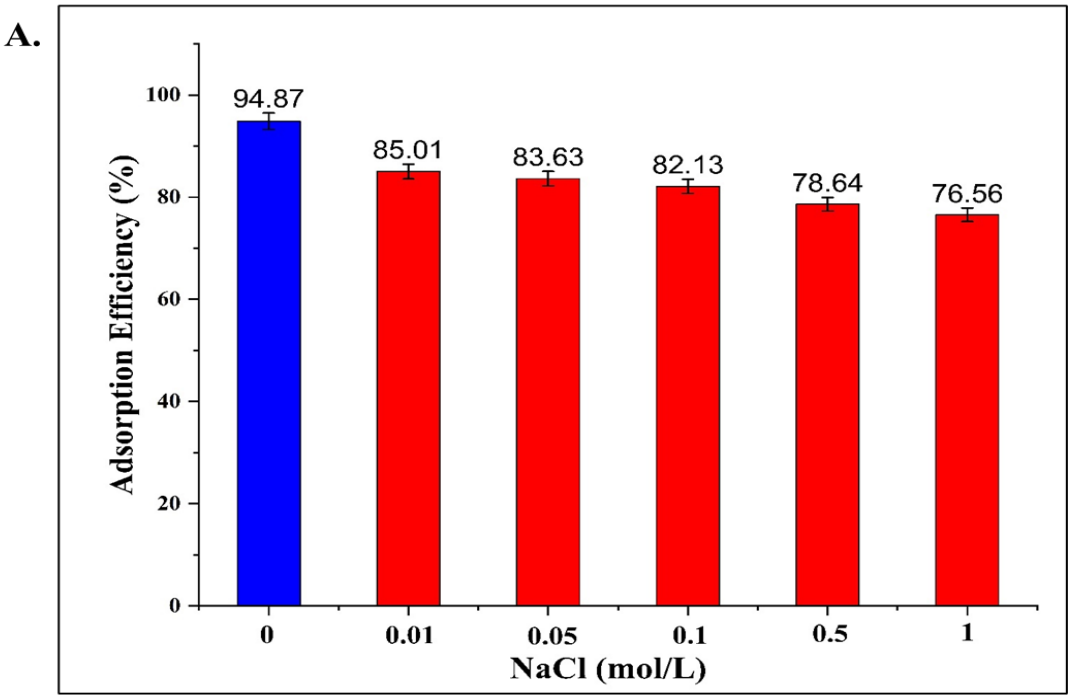

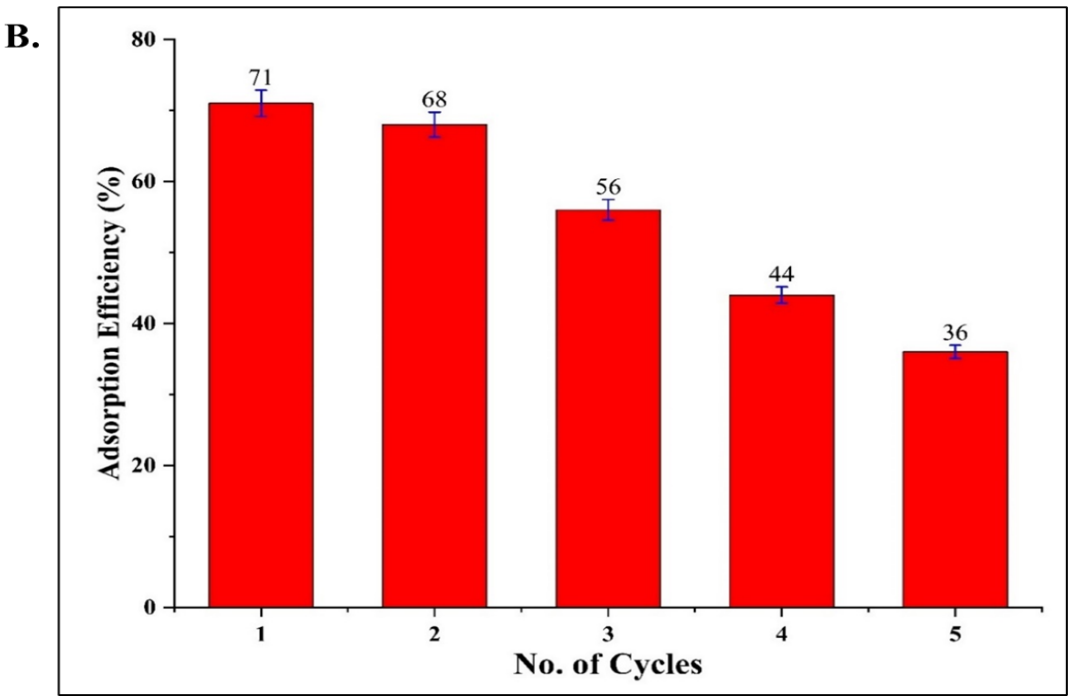

Figure 3.8: (A) Effect of ionic strength of NaCl in DIF adsorption, experimental conditions: pH 6, ACCB dosage 1.5 mg/mL, DIF concentration 100 mg/L, NaCl concentration 0.01-1 mol/L, temperature 40 °C; and (B) Desorption and Recyclability studies for ACCB, experimental conditions: pH 6, ACCB dosage 1.5 mg/mL, DIF concentration 100 mg/L, temperature 40 °C, NaOH concentration 0.1 mol/L.

3.4.5. Adsorbent recyclability studies

The recyclability study of the adsorbent (ACCB) was studied to analyse the numbers of cycles the adsorbent can be recycled. Adsorption was performed under optimised conditions, i.e., 1.5 mg/mL of ACCB was mixed to 100 mg/L of DIF solution maintained at pH 6.0. After each cycle, the used adsorbent was washed with 0.1 NaOH (desorbing agent). This desorbed adsorbent was then rinsed with deionised water. Rinsing with deionised water assisted in removing any remaining DIF molecules from the adsorbent, allowing the ACCB to be reused. The variation in adsorption efficiencies of ACCB with each desorption-readsorption cycle is depicted in Figure 3.8B. From the plot, it can be concluded that the adsorption efficiency shows a gradual decline with consecutive cycles. The adsorbent shows a significant adsorption capacity of >50% for the first three cycles, beyond which the adsorption efficiency declines rapidly. The DIF adsorption efficiency decreased from 71% in the 1st round to 36% in the 5th round. This decline was primarily due to the morphological degradation of the adsorbent's surface with successive adsorption-desorption rounds. Another possibility could be the pore obstruction, which occurs when some DIF molecules fail to desorb from the adsorbent's surface during the desorption process. As a result, such active sites fail to participate in the adsorption process for the consecutive cycle.

3.4.6. Phytotoxicity assay

The phytotoxicity experiment was done to assess the efficiency of the adsorbent (ACCB) in removing the adsorbate species (DIF), followed by checking the efficacy of the post-treated

DCF solution by germinating *Vigna mungo* seeds. The choice of *Vigna mungo* seeds was due to their multipurpose usage as a protein source in diet and one of the fast-growing crops. The investigation was carried out by comparing the prior and post adsorbent treated DIF solution. Seeds germination in deionised water were marked as blank; seeds germinated in non-treated DIF solution were tagged as control, and seeds germinated in post-treated DIF solution were tagged as test samples. The seeds were incubated for seven days in a dark, room-temperature environment. The root length of each sample was measured as an experimental response after the experiment, as shown in Figure 3.9. In non-treated DIF solution, the average root length of germinated seeds were 20.85 cm, 20.40 cm, 17.10 cm, 12.15 cm, and 7.10 cm for 10, 50, 100, 150, and 250 mg/L DIF solutions, respectively in comparison to 39.20 cm for seeds grown in deionised water (blank). Conclusively, a larger concentration of drugs is detrimental to seed germination. Mean root length for seeds germinated in post-treated DIF solution showed improved results. For 10, 50, 100, 150 and 250 mg/L DIF solutions, average root lengths increased to 30.50 cm, 27.60 cm, 22.00 cm, 18.75 cm, and 9.6 cm, respectively. Thus, seeds germinated in treated DIF solution had longer seed root length, suggesting that DIF was efficiently removed by ACCB.

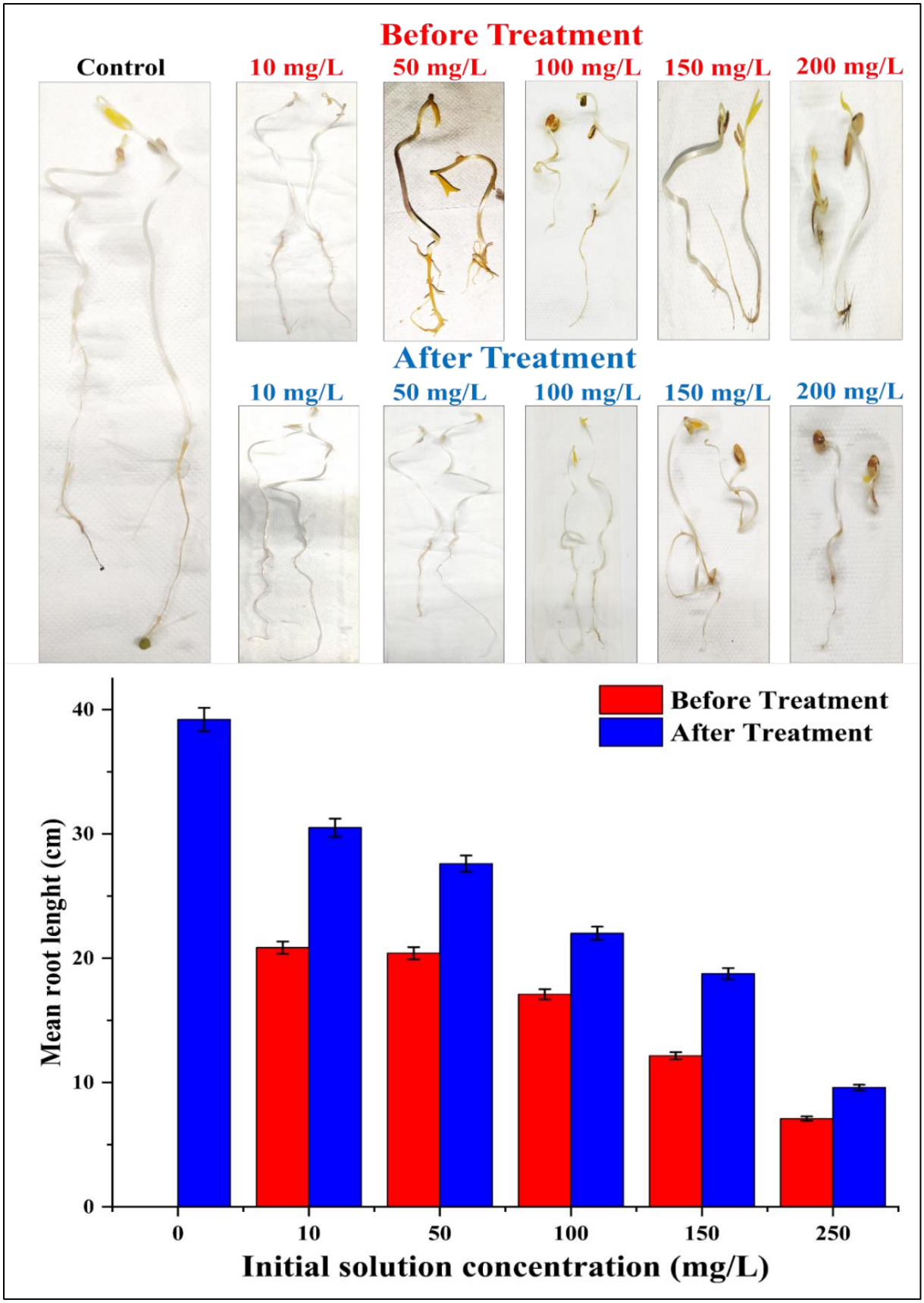

Figure 3.9: Phytotoxicity assay of ACCB.

3.5. Conclusion

The ACCB adsorbent was created by combining commercial activated carbon (CAC) with chitosan (CH) in a 1:1 ratio for the effective removal of the emerging pharmaceutical pollutant Diclofenac (DIF) from aqueous setups. The characterization of ACCB confirmed that it possesses a highly porous surface with enhanced physicochemical properties. The adsorbent exhibited a well-developed pore structure, high surface area, and the presence of functional groups that facilitate effective adsorption. The effective adsorption of DIF species by ACCB was regulated by process factors such as the pH of DIF solution, interaction temperature, initial DIF concentration and the ACCB dosage. Under optimised conditions, Freundlich isotherm and pseudo-second order kinetics confirmed the multilayer adsorption via chemisorption interaction between the adsorbate and adsorbent species. The theoretical maximum adsorption capacity (Q_L) for ACCB was 99.29 mg/g. Thermodynamically, the interaction of DIF and ACCB was spontaneous, endothermic, and facilitated the adsorption process due to an increased degree of disorderness. The decrease of ACCB's adsorption capacity towards DIF after multiple cycles was confirmed by recyclability experiments. The seed toxicity investigation confirmed the efficacy of the adsorbent treated solution, which verified that seeds germinated in post-treated solution showed better results than seeds germinated in pre-treated solutions. Further research is needed to improve its capabilities and efficacy against other developing toxins of various grades.

Chapter 4

Fabrication of a novel adsorbent CMC-T-CH for organic dyes wastewater treatment

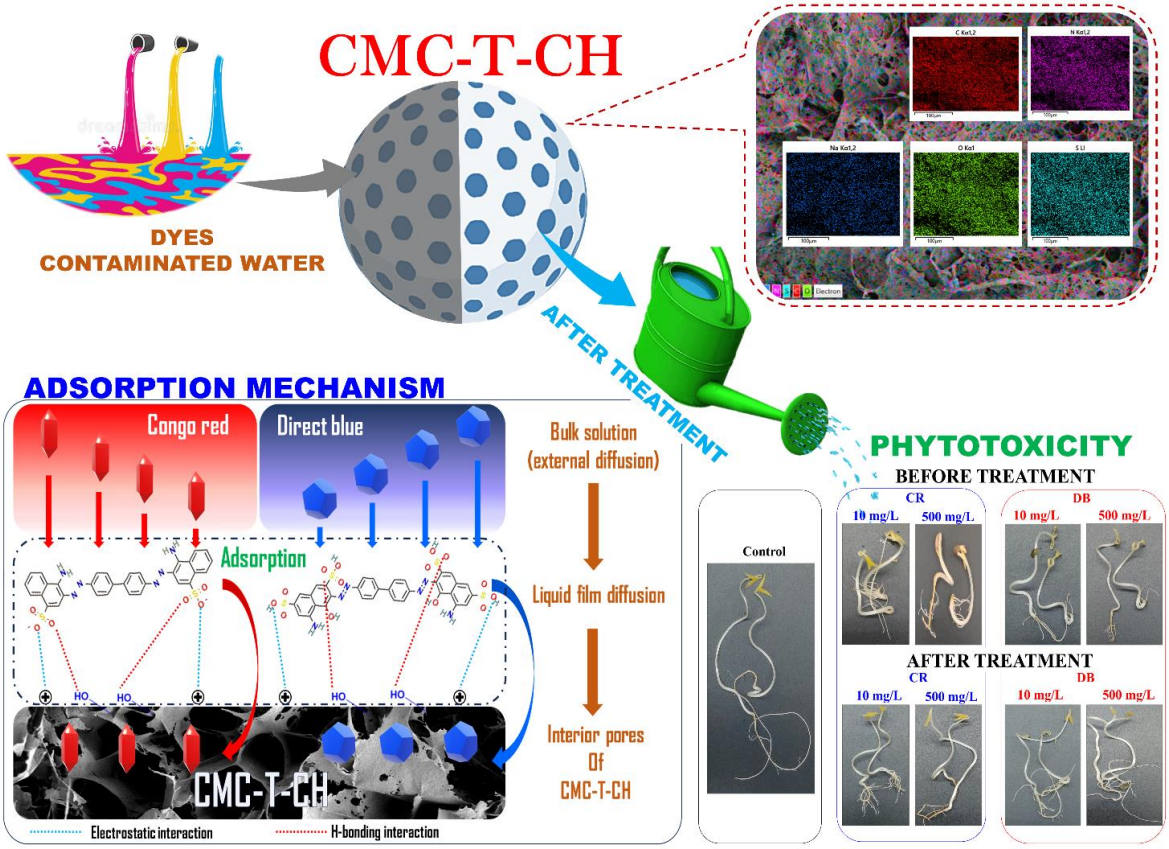

ABSTRACT

A novel adsorbent, CMC-T-CH, was fabricated by crosslinking of carboxymethyl cellulose (CMC) and chitosan (CH) with triethylenetetramine. The adsorbent's efficacy in removing the hazardous dyes, Direct blue (DB) and Congo red (CR), was investigated. Different physical, chemical, and biological methods have been employed to eliminate CR and DB dyes from aqueous solution, and adsorption has shown potential in eradicating these dyes effectively. Various characterization methods were employed to investigate the physicochemical characteristics of CMC-T-CH. The removal process was performed at optimized conditions of pH 6 for CR and pH 5 for DB at the temperature of 35°C, resulting in maximum removal efficiencies of 99% and 98.33% for CR and DB, respectively. Langmuir isotherm and pseudo-second-order kinetic mathematical models were utilised to analysed the interaction of adsorbate and adsorbent during the removal process. The maximum theoretical adsorptive capacities of 519.53 and 534.25 mg/g were achieved for CR and DB removal, respectively. The regeneration study revealed that the dye-loaded CMC-T-CH could be reused several times. The phytotoxicity assay showed that the germination of *Vigna mungo* seeds improved after the removal treatment, thus confirming the potential of CMC-T-CH in the elimination of CR and DB.

4.1. Introduction

Today, dyes are employed extensively in the textile, food, pharmaceuticals, plastics, personnel and care, and paper industries. These industries discharge coloured effluent-containing contaminants that affect the health of humans and other aquatic living beings (Khan and Malik 2014). Every year, over 100,000 commercial dyes and millions of dye products are manufactured (Forgacs, Cserháti, and Oros 2004). Around 10-12% of dyes are wasted in production, and about 20% of the dyes end up in industrial wastewater, contributing to water pollution (Elango, Rathika, and Elango 2017; Noroozi and Sorial 2013).

According to research studies (Chung 2016; Puvaneswari, Muthukrishnan, and Gunasekaran 2006), around 70% of globally manufactured dyes are anionic azo dyes. Among these dyes, Congo red (CR) and Direct blue (DB) are commonly used anionic azo dyes in many industrial sectors; for example, in pulp and paper, paint, textiles, cosmetics, and pharmaceuticals (Tang et al. 2014). According to a report published by the CPCB (Central Pollution Control Board) in India, a comprehensive assessment was conducted to identify and document hazardous chemicals used in the textile industry. This information can be found in Section 2.2 of the report (*Anon n.d.-a*). Among the listed pollutants, azo dyes are also included. Hence, the current study has chosen Congo Red (C.I. no. 22120) (*Anon n.d.-b*) and Direct Blue (C.I. no. 22610) (*Anon n.d.-c*) as model azo dyes. Direct discharge of untreated and unprocessed CR and DB wastewater into waterbodies has harmed the aquatic ecosystem and its inhabitants, causing drastic mutations in genes, innate toxicity, skin sensitization and irritation, sunlight blockage into aquatic flora, and many other disastrous consequences (Hernández-Zamora et al. 2016; Hernández-Zamora and Martínez-Jerónimo 2019). Synthetic dyes have also been categorized by the United States Environmental Protection Agency (USEPA) as potentially harmful and hazardous to ecosystems and living things (Kishor et al. 2021). These synthetic dyes are thermally, optically, and physiochemically stable due to the occurrence of azoic linkages among

aromatic rings, which makes them persistent and causes serious harm to the environment when they are allowed to persist for an extended period (Qurrat-Ul-Ain et al. 2020; Sarkar et al. 2017).

Different physical, chemical, and biological methods have eliminated dyes from industrial effluents. These methods include filtration, membrane filtration, nano-filtration, flocculation, coagulation, ion exchange, photocatalysis, etc. (Liang et al. 2021; Liu et al. 2022; Saravanan et al. 2020; Sarkar et al. 2017). Filtration is an economical and direct method to remove suspended solids particles, including large dye molecules (Ho et al., 2011). It cannot remove dissolved dyes, colloidal matter, and small particles. In order to ensure optimum performance, regular maintenance and replacement of filters are often required. Membrane filtration offers advantages in removing dyes, particles, and colloidal substances with increased removal efficiency (Zheng et al., 2017). However, crusting and membrane contamination are frequent problems that require frequent cleaning. Membrane filtration's operating and maintenance costs are higher than conventional filtration methods. Nanofiltration is a highly selective method with increased efficiency in the removal of small particles, including dyes, while at the same time retaining valuable components (Walha et al., 2007). It does, however, require increased training pressure and increased energy consumption. Also, the crusting of the membrane poses a problem and requires cleaning and regular maintenance. Flocculation and coagulation effectively remove suspended and colloidal particles, including dyes, and can be combined with other treatment methods to increase effectiveness (Adams et al., 2002). However, the addition of chemical substances such as coagulants or flocculants requires optimization of the dosage. Sludge generation and disposal are challenging in this method. Ionic exchange removes specific dyes through the ionic exchange mechanism, achieving great efficiency and selectivity (Han et al., 2020). However, the absorption capacity is limited. Therefore, periodic regeneration or replacement of the ionic exchange resin is necessary, and the operating and

maintenance costs associated with the ionic exchange are relatively high. Photocatalysis uses light to catalyze the degradation of pigments via oxidizing reactions, ensuring complete degradation (Kong et al., 2019). However, the light source requires appropriate catalysts. Photocatalysis is economically expensive and may involve hazardous catalysts or by-products. Adsorption has been used as an effective and economical technique to eradicate many inorganic and organic contaminants, and it can remove contaminants at very low concentrations. This is because the solid surface used for adsorption offers a large surface area for the contaminants to adhere to, which increases the chances of contact between the contaminants and the adsorbent material. Additionally, adsorbent materials can be tailored to target specific contaminants, making the process even more efficient (Cui et al. 2022; Kumar et al. 2022; Zhang, Sun, and Liu 2023). Agro-waste adsorbent (Kuncoro et al. 2018), animal waste adsorbent (Darmokoesoemo, Magdhalena, et al. 2016; Darmokoesoemo, Setianingsih, et al. 2016; Neolaka, Lawa, et al. 2023), Carbon-based materials (Neolaka, Riwu, et al. 2023; Patra et al. 2019; Patwa et al. 2022), resins (El-Sharkawy et al. 2015; Pandey, Shukla, and Singh 2017), natural minerals (Awasthi, Jadhao, and Kumari 2019; Ngulube et al. 2017), and other expensive materials are currently the most popular adsorbent materials. Unsatisfactory adsorption performance is the main problem with these adsorption materials. Thus, formulation of highly porous, recyclable adsorbent at a low cost is the need of the hour.

Researchers are interested in polysaccharides as they are naturally occurring, non-toxic, biodegradable, and affordable raw materials. Chitosan (CH) is a biodegradable and hydrophilic polymer that is non-toxic and has various functional groups, such as amino and hydroxyl, that give it excellent dye adsorption capacity (Ashrafizadeh et al. 2023). Carboxymethyl cellulose (CMC) is a biocompatible and biodegradable polymer that contains hydroxyl and carboxyl functional groups, making it an effective adsorbent for cationic contaminants (Rana et al. 2023). These two polymers have heteroatoms (carbon, oxygen, and nitrogen) in their

backbones, which can be used to formulate a novel adsorbent with excellent removal efficiency towards organic and inorganic dyes (Manzoor et al. 2019).

The novel aspect of this investigation is the fabrication of a CMC-T-CH adsorbent and its application in remediating dye-contaminated synthetic water (CR and DB). This study includes the characterization of the adsorbent's physicochemical properties, optimization of batch mode studies with various process parameters, investigation of the adsorbent-adsorbate interaction using mathematical models, and the conduct of phytotoxicity studies to assess the effectiveness of the adsorbent in removing CR and DB.

4.2. Material and Experiments

4.2.1. Reagents and Chemicals

The reagents, chemicals, and materials utilized for investigation were of the analytical grade. They were obtained from local vendors of SRL Pvt Ltd, Sigma Aldrich, and Himedia Laboratories Pvt Ltd. The Table 4.1 contains information about the materials list and their role.

Table 4.1: Detail list of chemicals, reagents, and salts.

Serial No.	*CHEMICAL/REAGENT/SALT*	*PURPOSE*
1.	Congo Red	Adsorbate
2.	Direct Blue 6	Adsorbate
3.	Chitosan	Adsorbent
4.	Carboxymethyl cellulose	Adsorbent
5.	Acetic acid	Dissolving agent
6.	0.1 M Sodium Hydroxide (NaOH)	Adjusting pH
7.	0.1 M Hydrochloric acid (HCl)	Adjusting pH

8.	Ferric chloride ($FeCl_3.6H_2O$)	Source of Ferric (Fe^{+3}) ions
9.	Lead Nitrate [$Pb(NO_3)_2$]	Source of lead (Pb^{+2}) ions
10.	Cobalt (II) Chloride ($CoCl_2$)	Source of cobalt (Co^{+2}) ions
11.	Sodium Sulphate (Na_2SO_4)	Source of sulphate (SO_4^{-2}) ions
12.	Sodium Nitrate ($NaNO_3$)	Source of nitrate (NO_3^{-1}) ions
13.	Sodium Chloride (NaCl)	Source of chloride (Cl^{-1}) ions
14.	1% Sodium Hypochlorite (NaClO)	Rinsing *Vigna mungo* seeds

4.2.2. Fabrication of adsorbent

The adsorbent fabrication was performed according to (Kong, Wang, and Lou 2020) with some modifications, and the process steps are illustrated in Figure 4.1. Initially, 2 grams of CMC were dispersed in 200 mL of distilled water on a magnetic stirrer at 60°C until the CMC powder was dissolved completely. Similarly, CH suspension was prepared by blending 2 grams of chitosan flakes with 2% (v/v) acetic acid solution (100 ml) at 60°C (Step 1). Next, CH solution was added into the CMC solution drop-wise, slowly, with the help of a syringe (Step 2). The CMC-CH mixture was placed in an incubator shaker at room temperature overnight. After the incubation period, the formed beads were thoroughly washed and stored at 25°C, and the beads were labelled as CMC-CH.

To stabilize the CMC-CH beads, the prepared CMC-CH beads were immersed into 1-5% (v/v) Triethylenetetramine (TETA) for a period of 24 h in an incubator shaker (Figure 4.1B). After completion of the process, the beads were washed multiple times with deionised water until the solution's pH was 7. The beads were labelled as CMC-T-CH and stored at 25°C for further use.

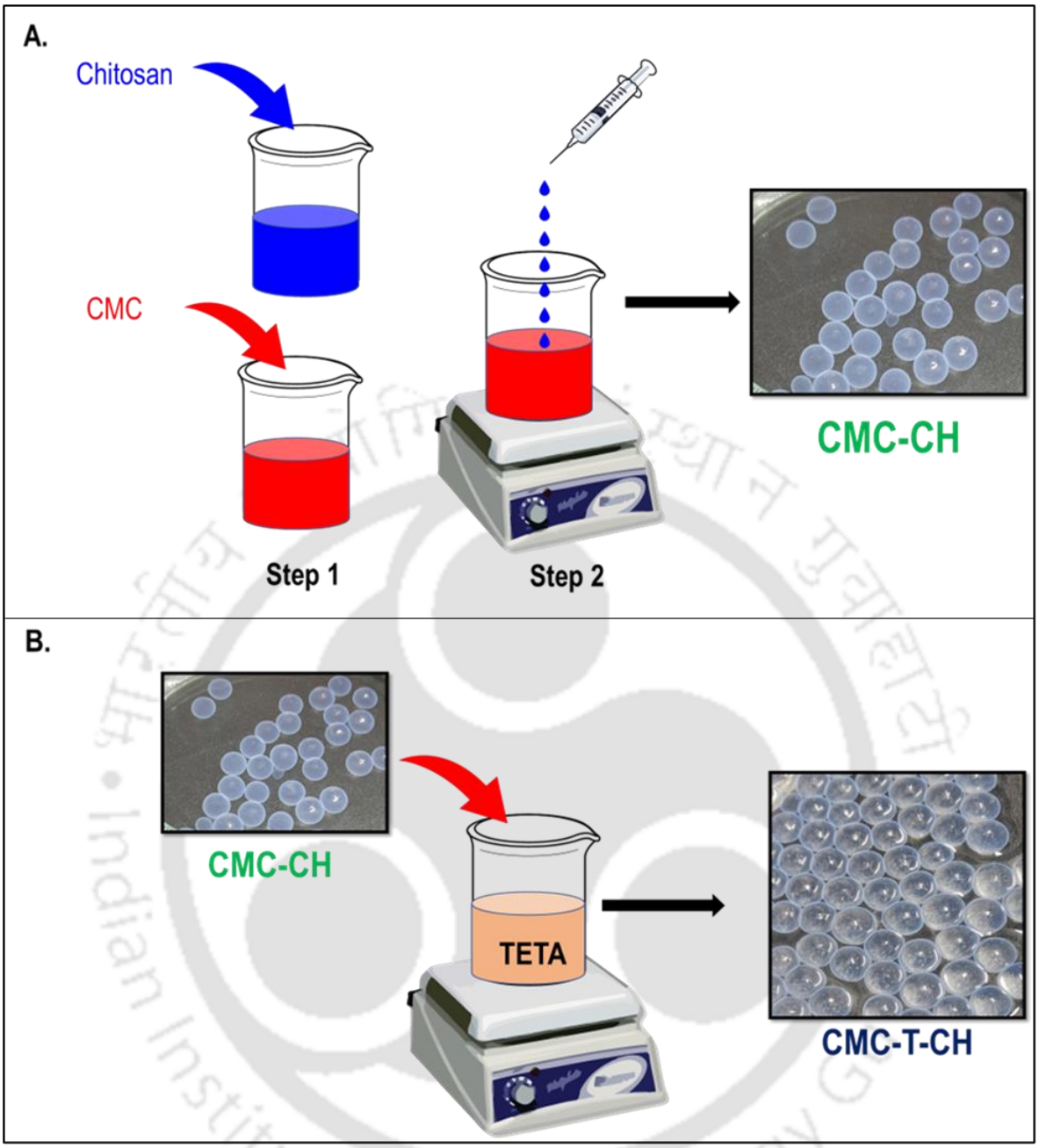

Figure 4.1: Schematic diagram of adsorbent preparation.

4.2.3. Characterization studies

The fabricated CMC-T-CH beads were lyophilized prior to characterization. The elemental composition and surface morphology of the CMC-T-CH beads were characterized with Energy dispersive X-ray spectroscopy (EDS) (Zeiss Sigma-300) and Field emission scanning electron microscopy (FESEM) (Zeiss, Gemini-300), respectively. Functional groups were investigated

using Fourier-transformed infrared spectroscopy (FTIR) (Nicolet iS10), and the thermal stability was investigated through Thermogravimetric Analyzer (TGA) (Netzsch, STA449F3A00). X-ray Powder Diffraction (XRD) (Rigaku Technologies, Japan, Smartlab) was used to determine the crystallinity of the beads.

4.2.4. Batch adsorption experiments

Congo Red and Direct Blue standard stock solutions (1000 mg/L) were initially made in distilled water. All the working solutions were prepared from these stock solutions, and all dilutions were made utilizing deionised water only. The batch adsorption analyses were conducted in an Erlenmeyer flask (100 mL) with a 20 ml working volume at 100 rpm in the shaker incubator. Various process influencing parameters, pH of the initial solution (~ pH 4 – 10), adsorbent dosage (10 – 50 mg) (dry weight), initial concentration (10, 50, 100, 200, and 500 mg/L) of CR and DB in the working solution, and temperature (25°C to 50°C) of the experiments, were investigated. The optimum process parameter values were investigated by keeping the other parameter constant except for the investigating one. The responses for the experiments mentioned above were the adsorption removal percentage and the adsorptive capacity of CR and DB. After the completion of each investigating parameter's experiments, the responses were recorded by the UV-Visible spectrophotometer. The adsorptive capacity (Q_t) (mg/g) and the removal efficiency (% R) were determined by the following mathematical equations:

$$Q_t = \frac{C_i - C_t}{w} * V \tag{4.1}$$

$$Removal\ (\%) = \frac{C_i - C_t}{C_i} \times 100 \tag{4.2}$$

Where 'Q_t' denotes to the adsorptive capacity of dye at time ‘t’ (mg/g); 'C_i' denotes to the initial CR and DB concentration in the solution (mg/L); 'C_t' stands for the CR and DB concentration

at a specific time ‘t’ (mg/L); 'w' denotes to the mass of biosorbent utilized (g) and 'V' refers to the volume of dye solution employed (L).

The regeneration ability of CMC-T-CH was investigated by dye adsorption-desorption cycles. The experiments were performed at the optimum process conditions, as calculated by the above-mentioned batch processes. The desorption experiment was performed by pouring the adsorbed beads into 0.1 M NaOH solution (100 mL). The flasks were subsequently put in the shaker incubator for 6 hours at 50 rpm. After incubation, the beads were rinsed with deionised water repeatedly to eliminate any residual desorbing agent (NaOH) from the beads. These adsorption-desorption experiments were investigated until the removal efficiency of CMC-T-CH was minimum.

A phytotoxicity assay was performed to show that the fabricated CMC-T-CH beads efficiently remediate dyes from water. *Vigna mungo* seeds were used as a model plant for this study. To prevent fungal and bacterial infections, the seeds were washed with a 1% (v/v) solution of sodium hypochlorite. They were subsequently cleaned in deionised water and allowed to dry at ambient temperature. They stored them in a sterile container for further experiments. The dried seeds (10 in number) were placed into the petri-dish containing 10 mL of untreated (control) and treated (sample) dyes solution. The blank sample was obtained by soaking the seeds in a petri dish with 10 mL of deionised water. The Petri dishes were kept for incubation at a dark place for seven days. After incubation, the length of the germinated seeds was measured as a means of assessing the response.

4.2.5. Adsorption interaction studies

The interaction between adsorbate (CR and DB) and adsorbent (CMC-T-CH) were studied with various isotherm and kinetics models over the equilibrated experimental data. The Section 1.5 covered the in-depth theory and associated mathematical equations.

4.3. Results and Discussions

4.3.1. Fabrication Mechanism

The proposed CMC-CH and CMC-T-CH fabrication mechanism has been illustrated in Figure 4.2. In CMC-CH beads, formation occurred by ionic interaction among the CMC and the CH moieties (Figure 4.2A) (Uyanga and Daoud 2021; Zhang et al. 2019). Additionally, the CMC-CH beads were unstable; they started disintegrating after a few hours. Whereas, in CMC-T-CH beads (Figure 4.2B), TETA act as a crosslinker that holds the two moieties together by various interactions (such as Schiff base formation, covalent bonds, amide bond, and intermolecular hydrogen bonding) (Chen et al. 2022; Zhang et al. 2019). Thus, the CMC-T-CH beads were more stable than the CMC-CH beads. Hence, CMC-T-CH beads were chosen for further investigations.

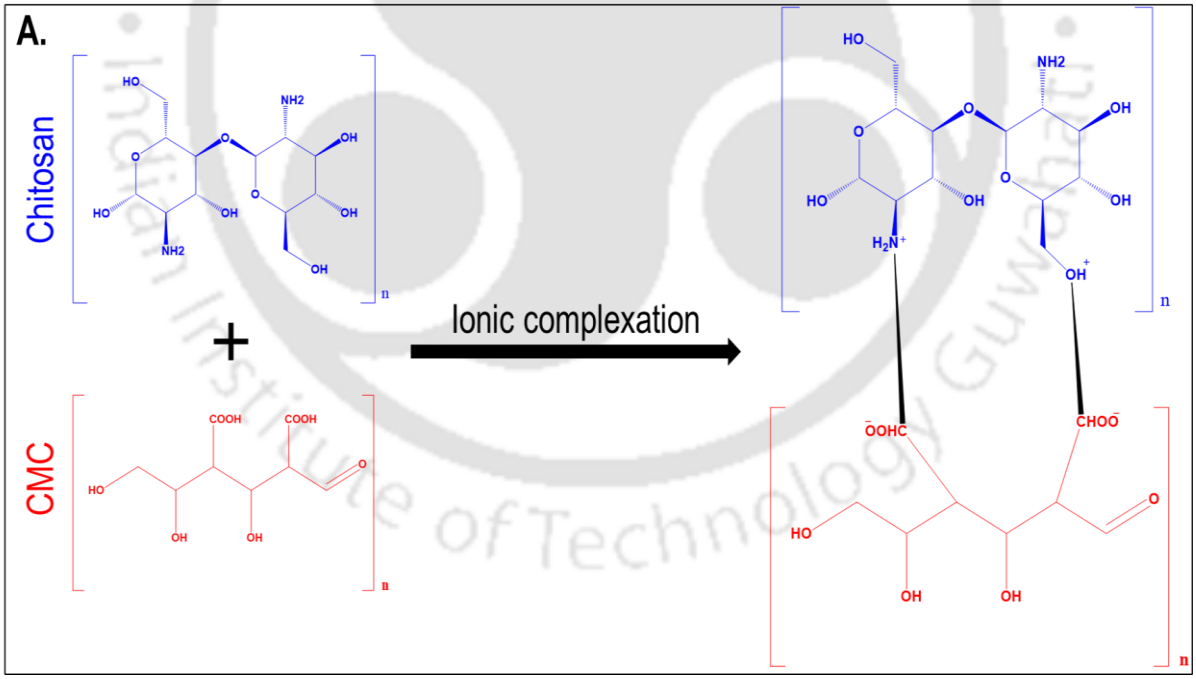

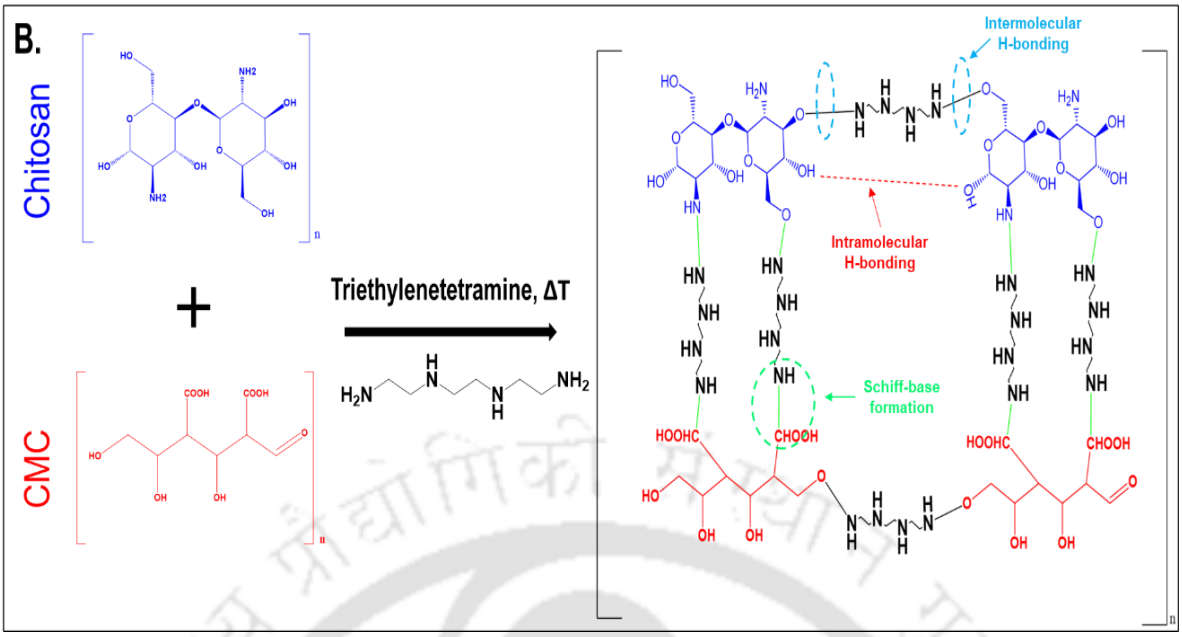

Figure 4.2: Fabrication reaction mechanism for the formation CMC-CH and CMC-T-CH.

4.3.2. Characterisation of CMC-T-CH adsorbent

Morphological characterization was characterized by FESEM. Figures 4.3A, 4.3C, and 4.3E showed digital photographs of Chitosan, CMC powder, and CMC-T-CH beads, respectively. The synthesized CMC-T-CH beads have an average diameter of 0.76 cm. The outer surface of the beads was smooth. Figures 4.3B, 4.3D, and 4.3F showed the FESEM images of chitosan, CMC powder, and cross-section of CMC-T-CH beads, respectively. Figures 4.3B and 4.3D showed smooth surfaces with minor irregularities on the surfaces, while the inner surface (cross-section) of CMC-T-CH beads has a fibrous structure with various pores. Thus, these pores facilitate the adsorption of the dyes.

By elemental composition analysis (Figure 4.3G, 4.3H, and 4.3I), it was revealed that the presence of nitrogen could be observed in the CMC-T-CH beads (Figure 4.3I) and in the CH (Figure 4.3G) that was not observed in the CMC (Figure 4.3H).

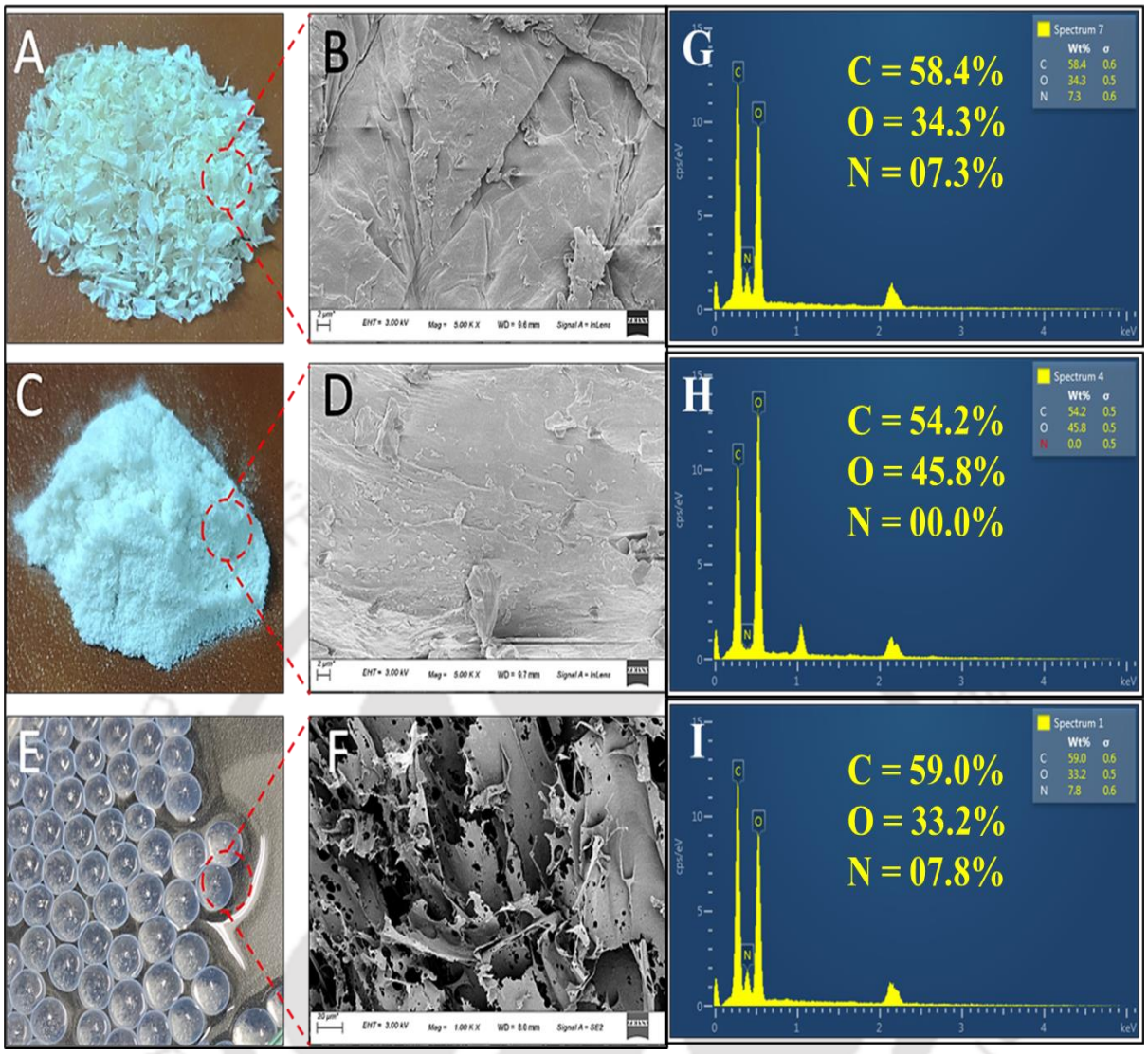

Figure 4.3: Digital images of Chitosan (A), CMC (C) and CMC-T-CH (E); FESEM images of Chitosan (B), CMC (D) and CMC-T-CH (F); and EDX spectrum of Chitosan (G), CMC (H) and CMC-T-CH (I).

The BET surface area analysis of chitosan (CH), carboxymethyl cellulose (CMC), and CMC-T-CH were conducted. The results are shown in the Table 4.2. The findings indicate that CMC-T-CH possesses a mesoporous structure characterized by pore diameters ranging from less than 5 nm to greater than 2 nm. These mesopores contribute to the enhanced adsorption capacity of CMC-T-CH as an adsorbent.

Table 4.2: Surface characterization of Carboxymethyl cellulose (CMC), Chitosan (CH), and CMC-T-CH.

PARAMETER	CMC	CH	CMC-T-CH
BET Surface area (m^2/g)	1.62	2.18	3.81
Total pore volume (cm^3/g)	0.05	0.07	0.19
Average pore size (nm)	2.17	2.38	3.01

The FTIR of CH, CMC, and CMC-T-CH were conducted in the range of 4000-400 cm^{-1} and the spectral plot is shown in Figure 4.4A. The obtained results were cross-checked and compared against the Infrared Spectroscopy Absorption Table to ensure their accuracy and reliability (*Anon n.d.-d*).

In the CH spectra, a prominent, broad peak in the 3300-3500 cm^{-1} range is attributed to the stretching vibrations of hydroxyl (-OH) (Naat et al. 2021). Peaks in the 2800-3000 cm^{-1} region indicate the stretching vibrations of aliphatic C-H bonds. Another peak around 1650-1655 cm^{-1} represents the amide I band, which signifies the bending vibrations of N-H groups. Peaks within the range of 1030-1150 cm^{-1} indicate the stretching vibrations of C-O and C-N bonds within the sugar ring.

Similarly, in the CMC spectra, a broad peak around 3300-3500 cm^{-1} is observed, indicating the stretching vibrations of hydroxyl (-OH) groups. Peaks in the region of 2800-3000 cm^{-1} represent the stretching vibrations of aliphatic C-H bonds. A peak at approximately 1598 cm^{-1} corresponds to the carboxylate group (COO-) stretching vibrations. Peaks around 1410-1430

cm^{-1} and 1310-1330 cm^{-1} indicate the bending vibrations of the carboxylate group. Peaks within the range of 1030-1150 cm^{-1} signify the stretching vibrations of C-O and C-O-C bonds in the sugar ring.

In the CMC-T-CH, in addition to the characteristic peaks of chitosan and CMC mentioned above, a stretching vibration of N-H groups, in the range of 3200-3400 cm^{-1}, and stretching vibrations of C-N bonds, in the range of 800-1200 cm^{-1} were observed. Table 4.3 summarizes the FTIR peaks along with their descriptions.

Table 4.3: FTIR peaks of CH, CMC, and CMC-T-CH.

COMPONENT	PEAK POSITION (cm^{-1})	DESCRIPTION
CHITOSAN (CH)	3300-3500	Stretching vibrations of -OH and -NH2 groups
	2800-3000	Stretching vibrations of aliphatic C-H bonds
	1655	Amide I band, bending vibrations of N-H groups
	1030-1150	stretching vibrations of C-O and C-N bonds
	3300-3500	Stretching vibrations of -OH
CARBOXYMETHYL CELLULOSE (CMC)	2800-3000	Stretching vibrations of aliphatic C-H bonds
	1598	Carboxylate group (COO-) stretching vibrations
	1410-1430	Bending vibrations of carboxylate group
	1310-1330	Bending vibrations of carboxylate group
	1030-1150	stretching vibrations of C-O and C-N bonds
CMC-T-CH	3200-3400	N-H stretching vibrations (TETA-related)
	800-1200	C-N stretching vibrations (TETA-related)

The crystallographic structures of the prepared CMC-T-CH, CH, and CMC were analysed by XRD. Figure 4.4B illustrates the plot of CH, CMC, and CMC-T-CH. In the CH diffractogram, two characteristic peaks (9.80° and 20.04°) were observed that correspond to cellulose II (Kumar et al. 2022). In the CMC diffractogram, a distinct peak at 20.04° could be seen. Moreover, the peaks at 9.80° and 20.04° were also observed in the CMC-T-CH. Finally, the XRD analysis suggested that the fabricated CMC-T-CH has an amorphous structure.

The thermal stability of CMC-T-CH was analysed by the TGA. Figure 4.4C depicts the TGA plot for CMC-T-CH. The thermal degradation of the adsorbent occurred in three stages. The First stage (I) showed a slight weight loss of 5.6% in the range of 20-250°C due to the dehydration of water content of the sample. The second stage (II) showed major weight loss of 43.8% up to 350°C due to thermal degradation of the CMC-T-CH polymeric chain. In the last stage (III), the residual material of the adsorbent would decompose.

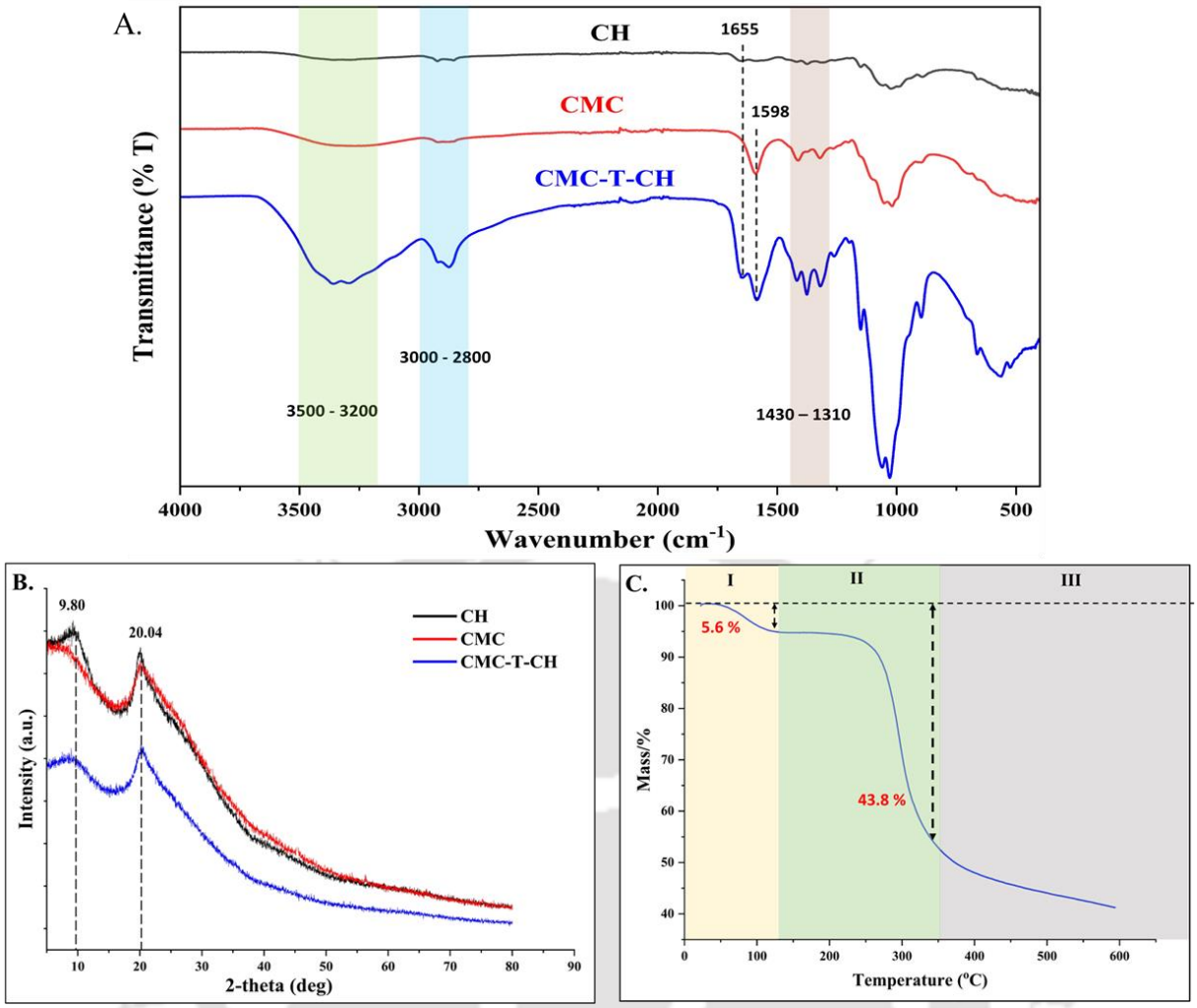

Figure 4.4: (A) FTIR spectrum of CH, CMC, and CMC-T-CH, (B) XRD diffractogram of CH, CMC, and CMC-T-CH; and (C) TGA plot of CMC-T-CH.

4.3.3. Impact of batch process parameters

4.3.3.1. Influence of point of zero charge (pH_{PZC}) of CMC-T-CH and initial pH of the CR and DB solution

The pH_{PZC} is the pH of the solution at which the CMC-T-CH's net surface charge would be zero (Bakatula et al. 2018). If the solution's pH< pH_{PZC}, the net surface charge of CMC-T-CH would be positive, and if the solution's pH> pH_{PZC}, it would be negative. The pH_{PZC} of the CMC-T-CH was investigated and found to be ~ 6.1 (Figure 4.5A).

The pH of the DB and CR solution is essential in the interaction between dyes (CR and DB) and CMC-T-CH. The pH study analysis of the CR and DB removal has been shown in Figure 4.5B (pH ranging from ~ 4.0 to ~ 10.0). At lower pH (pH<4), the CMC-T-CH beads were unstable as chitosan dissolved in the acidic medium; hence, the pH study was performed from 4.0 to 10.0. The CR adsorptive removal efficiency increased from pH 4 to pH 6, and then it started declining. In the case of DB, the removal efficiency increased till pH 5, and then the efficiency decreased. The CR and DB were in anionic form when the solution's pH<6.1 and the CMC-T-CH surface was positively charged; hence the superior interaction between the dye's molecules and CMC-T-CH would be electrostatic interaction. The EDS mapping analysis result showed the occurrence of sulphur in the mapping of both CR (Figure 4.5E) and DB (Figure 4.5F) after adsorption, as sulphur is a key component (Figure 4.5C and 4.5D) for both dyes, suggesting that the CR and DB successfully removed from the solution. The optimum initial pH of the solution in removing CR and DB were 6 and 5, respectively (Figure 4.5B).

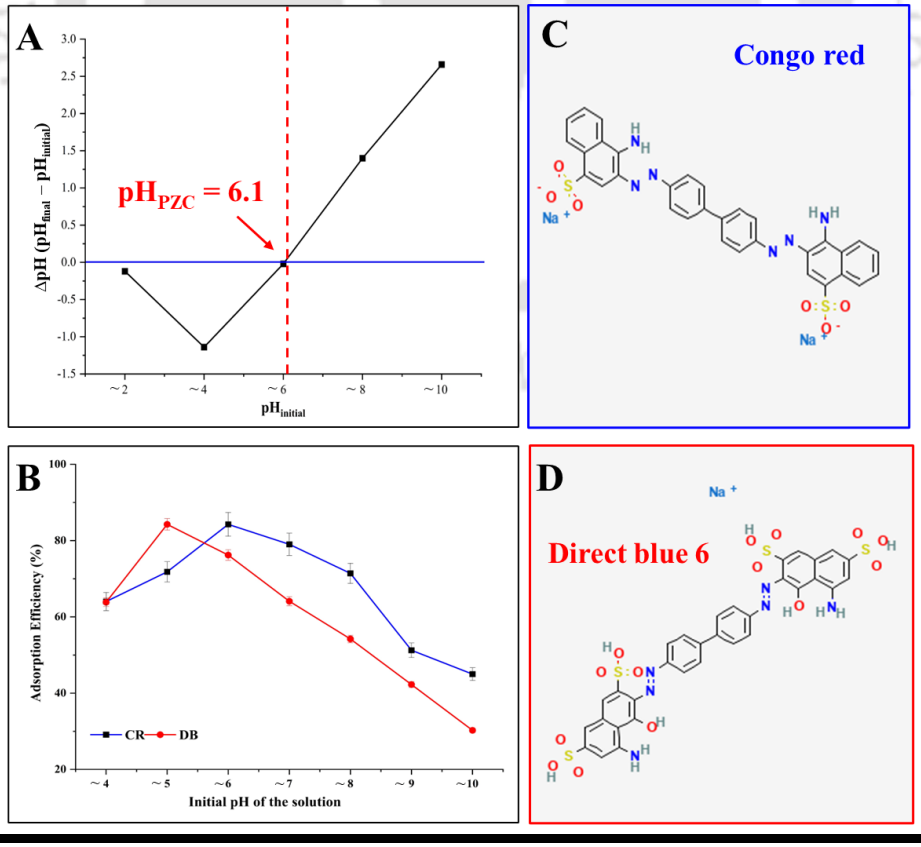

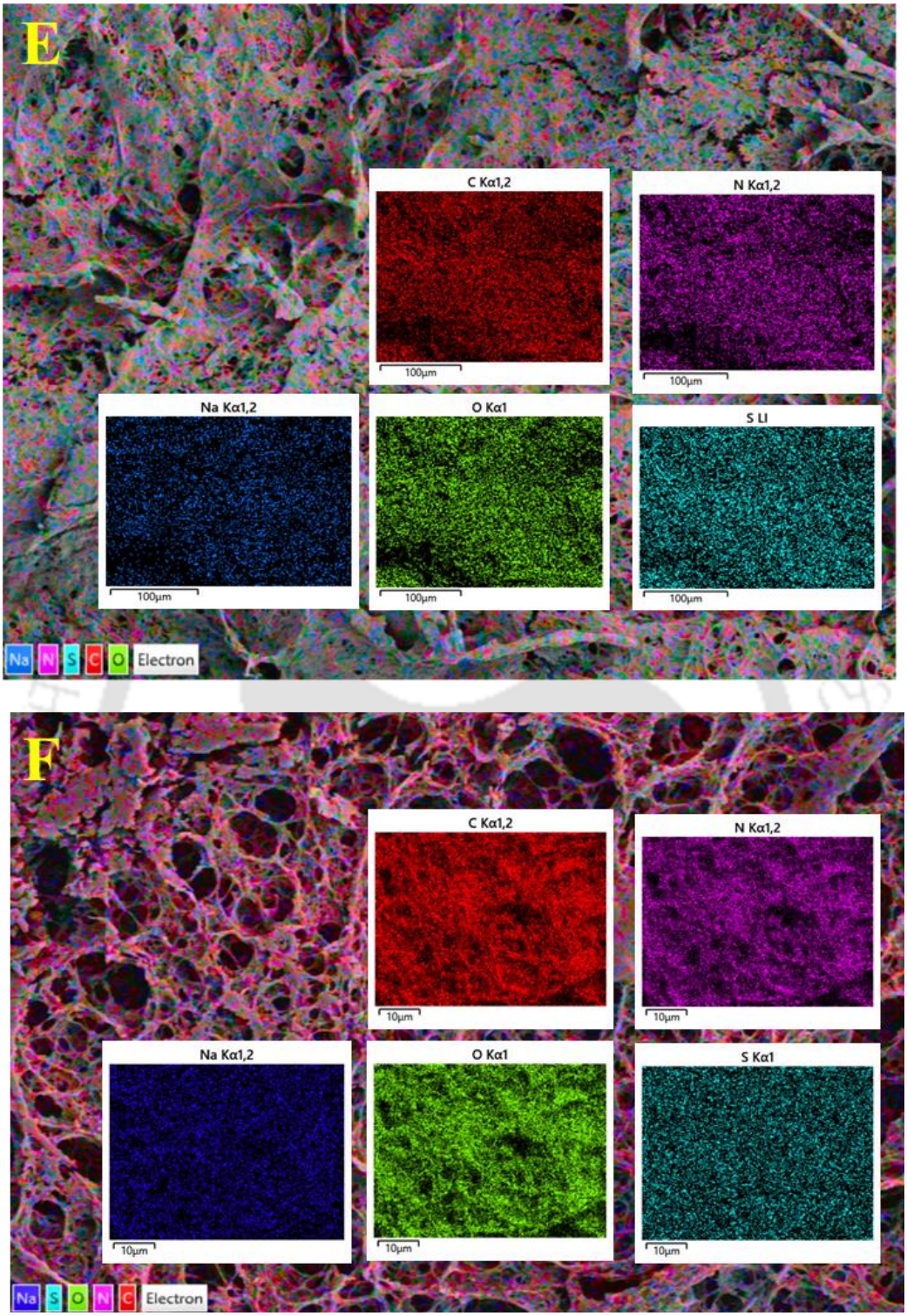

Figure 4.5: (A) pH_{PZC} plot of CMC-T-CH; (B) Effect of initial pH of DB and CR solution; (C) Chemical structure of Congo red; (D) Chemical structure of Direct blue 6; (E) EDS mapping of CMC-T-CH after CR adsorption; (F) EDS mapping of CMC-T-CH after DB adsorption.

4.3.3.2. Effect of CMC-T-CH dosage

The influence of CMC-T-CH dosage on the adsorption of CR and DB was investigated by varying the dosage of CMC-T-CH dry weight from 10 to 50 mg (0.5 to 2.5 mg/mL). The experiment was conducted at a 30°C with an initial CR and DB concentration of 100 mg/L with a working volume of 20 mL and pH values of 6.0 and 5.0 for CR and DB, respectively. The results indicate that the optimal dosage of CMC-T-CH was 20 mg, which achieved a removal efficiency of approximately 99% (as shown in Figure 4.6). Increasing the quantity of the adsorbent resulted in an increase in the removal efficiency, which can be associated with the greater availability of free active sites. However, at a certain point, the adsorption capacity reached equilibrium because of the fixed quantity of dye species, which resulted in the adsorption of all DB and CR on the CMC-T-CH surface.

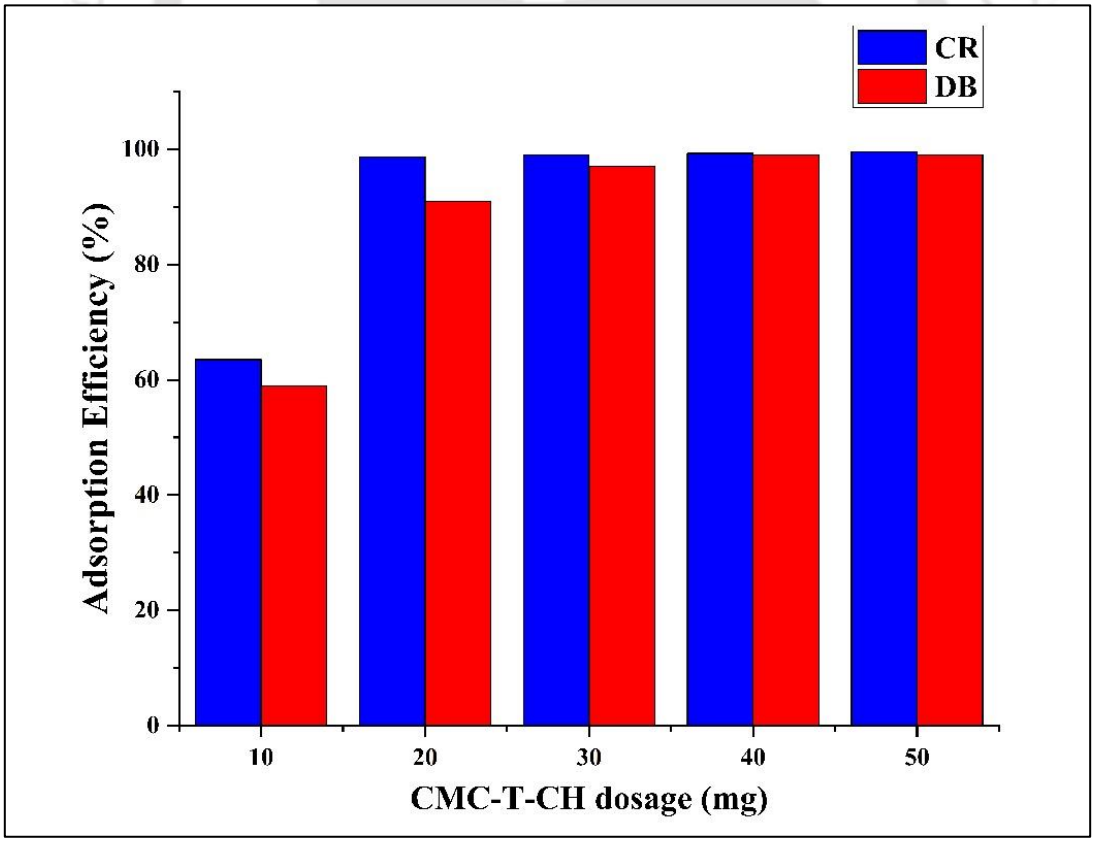

Figure 4.6: Effect of CMC-T-CH dosage.

4.3.3.3. Impact of initial CR and DB concentration of the experimental solution

The impact of initial CR and DB concentration on the adsorption capacity and removal efficiency by CMC-T-CH adsorbent was investigated. The experiments were performed at a temperature of 30°C with a fixed CMC-T-CH dosage of 20 mg for a 24-hour incubation period. The dye concentrations ranged from 10 mg/L to 500 mg/L, and pH values of 6.0 and 5.0 were used for CR and DB, respectively. The investigation's outcome revealed that CR and DB's adsorptive capacity increases with an increasing initial CR and DR concentration (Figures 4.7 and 4.8). However, adsorptive removal efficiency decreases with an increasing initial CR and DB concentrations which can be associated with the limited number of active sites that are accessible due to the fixed dosage of CMC-T-CH. The adsorptive capacity of the CMC-T-CH increases because the active sites on the CMC-T-CH surface get saturated with dye species. However, adsorption efficiency decreases as the number of available active sites decreases. As a result of an increase in the CR and DB initial concentrations, the quantity of unoccupied active sites on the CMC-T-CH decreases, decreasing the CMC-T-CH's adsorption efficiency.

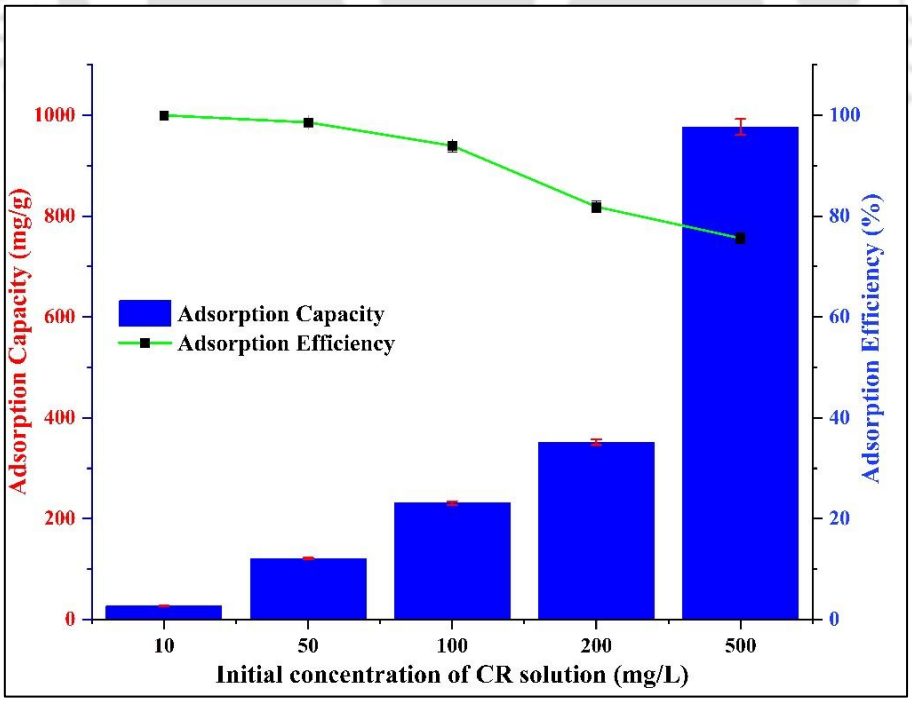

Figure 4.7: Effect of Initial concentration of CR solution.

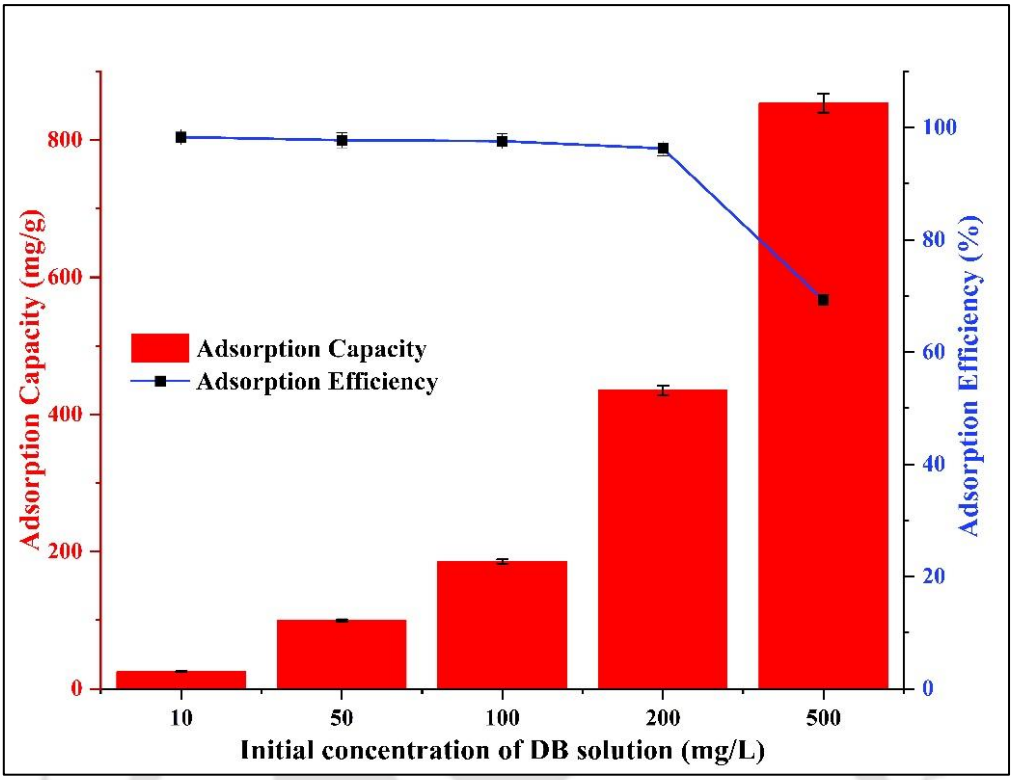

Figure 4.8: Effect of Initial concentration of DB solution.

4.3.3.4. Impact of experimental temperatures and interaction thermodynamics analysis

The impact of experimental temperature on the removal of DB and CR by CMC-T-CH adsorbent was investigated under optimized conditions at various temperatures ranging from 25°C to 50°C with varying initial dye concentrations. The findings are presented in Table 4.4 and 4.5, which display the calculated values of ΔG° (Change in Gibb's free energy), ΔH° (change in enthalpy), and ΔS° (change in entropy) through mathematical equations. The negative values of ΔG° indicate that the reaction between the dye molecules and CMC-T-CH adsorbent was random and thermochemically feasible. The negative values of ΔH° revealed that the adsorption process was exothermic, meaning that heat was liberated during the process. The positive values of ΔS° indicate that CR and DB molecules were randomly adsorbed on the CMC-T-CH surface. The thermodynamic analysis suggests that the CR and DB dyes removal by CMC-T-CH is feasible and spontaneous at different experimental temperatures.

Table 4.4: Thermodynamics Parameters (ΔG°, ΔH°, and ΔS°) for adsorption of CR by CMC-T-CH.

C_i (mg/L)	Temp. (^{0}C)	ΔG^0 kJ/mol	ΔH^0 kJ/mol	ΔS^0 J/mol
10	25	-21.84	-25.26	173.76
	30	-29.44		
	35	-33.41		
	40	-22.73		
	45	-28.20		
	50	-23.72		
50	25	-23.54	-7.55	114.50
	30	-25.70		
	35	-26.26		
	40	-28.25		
	45	-27.21		
	50	-22.75		
100	25	-27.84	-8.50	112.36
	30	-24.66		
	35	-25.54		
	40	-21.27		
	45	-25.54		
	50	-25.50		
200	25	-24.47	-13.169	116.24
	30	-24.10		
	35	-21.64		
	40	-26.24		
	45	-21.13		
	50	-23.96		
500	25	-17.43	-7.24	89.52
	30	-18.64		
	35	-22.64		
	40	-24.15		
	45	-18.28		
	50	-21.72		

Table 4.5: Thermodynamics Parameters (ΔG°, ΔH°, and ΔS°) for adsorption of DB by CMC-T-CH.

C_i (mg/L)	Temp. (^{0}C)	ΔG^0 kJ/mol	ΔH^0 kJ/mol	ΔS^0 J/mol
10	25	-25.34	-14.58	130.74
	30	-23.89		
	35	-31.34		
	40	-20.50		
	45	-20.16		
	50	-33.72		
50	25	-29.14	-16.23	32.76
	30	-25.92		
	35	-22.22		
	40	-26.06		
	45	-24.16		
	50	-29.85		
100	25	-26.19	-2.43	77.36
	30	-27.13		
	35	-23.64		
	40	-26.81		
	45	-25.41		
	50	-28.30		
200	25	-20.86	-32.96	182.60
	30	-22.33		
	35	-25.12		
	40	-23.24		
	45	-24.05		
	50	-25.51		
500	25	-19.48	-11.04	103.69
	30	-20.71		
	35	-21.61		
	40	-21.01		
	45	-20.71		
	50	-22.31		

4.3.4. Adsorption interaction analysis

4.3.4.1. Isotherm analysis

The interactions of the adsorptive removal of CR and DB by CMC-T-CH were investigated by isotherm modelling. The adsorption isotherm experiments were investigated at various initial CR and DB concentrations; solution pH for CR was 6 and for DB was 5, shaking speed of 100 rpm at the temperature of 35°C. The Langmuir model assumes that each adsorption site can only support one adsorbate of the same energy and suggest that a uniform monolayer adsorption process occurred (del Bubba, Arias, and Brix 2003; Xu, Ji, et al. 2020). According to the Freundlich model, CR and DB adsorption occurred in a multi-layered manner (Appel 1973; Xu, Jian, et al. 2020). The Temkin model explains how the interaction between the adsorbate (DB and CR) and the adsorbent (CMC-T-CH) influences the heat of adsorption (Kalavathy et al. 2005). Sips isotherm, which combines the Langmuir and Freundlich expressions, was developed to forecast heterogeneous adsorption systems (Foo and Hameed 2010). The analysed isotherms data are presented in Table 4.6. The Langmuir isotherm displayed a good regression fit with the experimental values over Freundlich isotherms, suggesting that the adsorption of dyes by the CMC-T-CH was monolayered and the surface of the CMC-T-CH was homogenous. The Langmuir isotherm calculated the theoretical maximum adsorptive capacity and was observed to be 519.53 and 534.25 mg/g for CR and DB adsorption, respectively. The Temkin isotherm also fit well, supporting the heat associated with CR and DB adsorption. The Sips isotherm also shows an excellent fit to the experimental values. The Sips constant (m) is equal to unity, suggesting that the adsorption occurred in a monolayered manner, verifying the occurrence of the Langmuir isotherm. The non-linear isotherm plots of CR and DB are illustrated in Figures 4.9A and 4.9B. Table 4.7 shows the comparative analysis of the maximum adsorption capacities of previously reported adsorbents for the removal of CR and DB, and it shows that CMC-T-CH exhibits a notably high adsorption capacity for CR and DB removal.

Table 4.6: Adsorption isotherm models along with their parameters.

ISOTHERMS	*ISOTHERM CONSTANTS*	*CR*	*DB*
FREUNDLICH	K_F	25.97	13.86
	1/n	1.80	1.59
	R^2	0.99	0.95
LANGMUIR	Q_L	519.53	534.25
	K_L	0.02	0.01
	R^2	0.99	0.97
TEMKIN	A	0.37	0.18
	B	93.29	91.72
	R^2	0.97	0.92
SIPS	K_S	0.02	0.025
	Q_S	581.27	354.22
	m	0.68	1.24
	R^2	0.99	0.93

Table 4.7: Comparison of adsorption capacity by previously reported adsorbent towards CR and DB removal.

Adsorbent	*Maximum adsorption capacity (mg/g)*	*Reference*
Congo red		
Chitosan/Rectorite/Cellulose composite hydrogels	380	(Tu et al. 2017)
Chitosan/carboxymethylcellulose polyelectrolyte complexes adsorbent	70.86	(Ferreira et al. 2023)
Reusable kaolin impregnated aminated chitosan composite beads	104	(Abou Alsoaud et al. 2022)
Carboxymethyl chitosan hybrid montmorillonite composite	81.77	(Zhang et al. 2020)
Fe3O4@PDA/CMC aerogel	92.35	(Lei et al. 2021)
EDTA-functionalized magnetic chitosan oligosaccharide and	432.34	(Lian et al. 2020)

carboxymethyl cellulose nanocomposite		
CMC-T-CH	**519.53**	**This study**
Direct blue		
Zinc oxide nanoparticles (ZnO-NPs)	370.37	(Eleryan et al. 2023)
Nanocomposites of chitosan-multi-walled carbon nanotubes (ch-MWCNTs)	29.32	(Abbasi and Habibi 2016)
Magnetic nanocomposite of Chitosan/SiO2/CNTs (MNCSC)	61.35	(Abbasi 2017)
Porous chitosan (MCh)	163.934	(Patra et al. 2021)
Perovskite lanthanum aluminate (PLA)	71.4	(Manjunatha et al. 2019)
CMC-T-CH	**534.25**	**This study**

4.3.4.2. Adsorption kinetics analysis

The adsorption kinetics models responses of CR and DB adsorption by CMC-T-CH were examined through the data generated by the experimental equilibrated data, and the generated values of various kinetic models are summarized in Table 4.8. Figures 4.9C and 4.9D illustrate the plot of CR and DB obtained after analysing the kinetic models. The outcomes of the models verified that the pseudo-second-order kinetics best fit over the other kinetics adsorption models, indicating that chemisorption occurred between the adsorbent (CMC-T-CH) and the adsorbate (CR and DB). Additionally, the experimental adsorptive capacity (Q_e) values correlated to the theoretical adsorptive capacity (Q_t) values, indicating the validity of the results.

Table 4.8: Adsorption kinetics models and their parameters.

C_i (mg/l)	Q_e Expt. (mg/g)	Pseudo-First Order			Pseudo-Second Order			Intra-Particle Diffusion		
		K_1 (1/min)	Q_e (mg/g)	R^2	K_2 (1/min)	Q_e (mg/g)	R^2	K_{id} (mg/g $min^{1/2}$)	C (mg/g)	R^2
CR										
10	43.15	0.072	40.72	0.92	0.003	42.74	0.97	1.11	70.73	0.59
50	217.80	0.009	206.93	0.98	$3.98x10^{-5}$	214.58	0.99	9.26	15.06	0.94
100	293.15	0.009	271.52	0.98	$2.78 x10^{-5}$	301.27	0.99	12.29	15.07	0.95
200	348.37	0.010	337.12	0.96	$3.39 x10^{-5}$	362.59	0.99	11.60	19.65	0.89
500	463.01	0.009	364.79	0.88	$9.85 x10^{-6}$	491.32	0.98	15.84	38.58	0.95
DB										
10	46.43	0.021	32.50	0.70	3.12	37.61	0.81	3.32	37.46	0.83
50	239.28	0.006	155.53	0.65	$1.64 x10^{-5}$	244.85	0.96	12.09	12.04	0.97
100	292.85	0.005	216.71	0.74	$7.89 x10^{-6}$	289.92	0.99	16.47	$1.60 x10^{-10}$	0.98
200	435.71	0.004	257.07	0.59	$4.09 x10^{-6}$	431.35	0.99	17.97	$2.52 x10^{-12}$	0.95
500	760.91	0.003	570.69	0.75	$1.43 x10^{-6}$	753.30	0.99	28.30	$6.75 x10^{-10}$	0.95

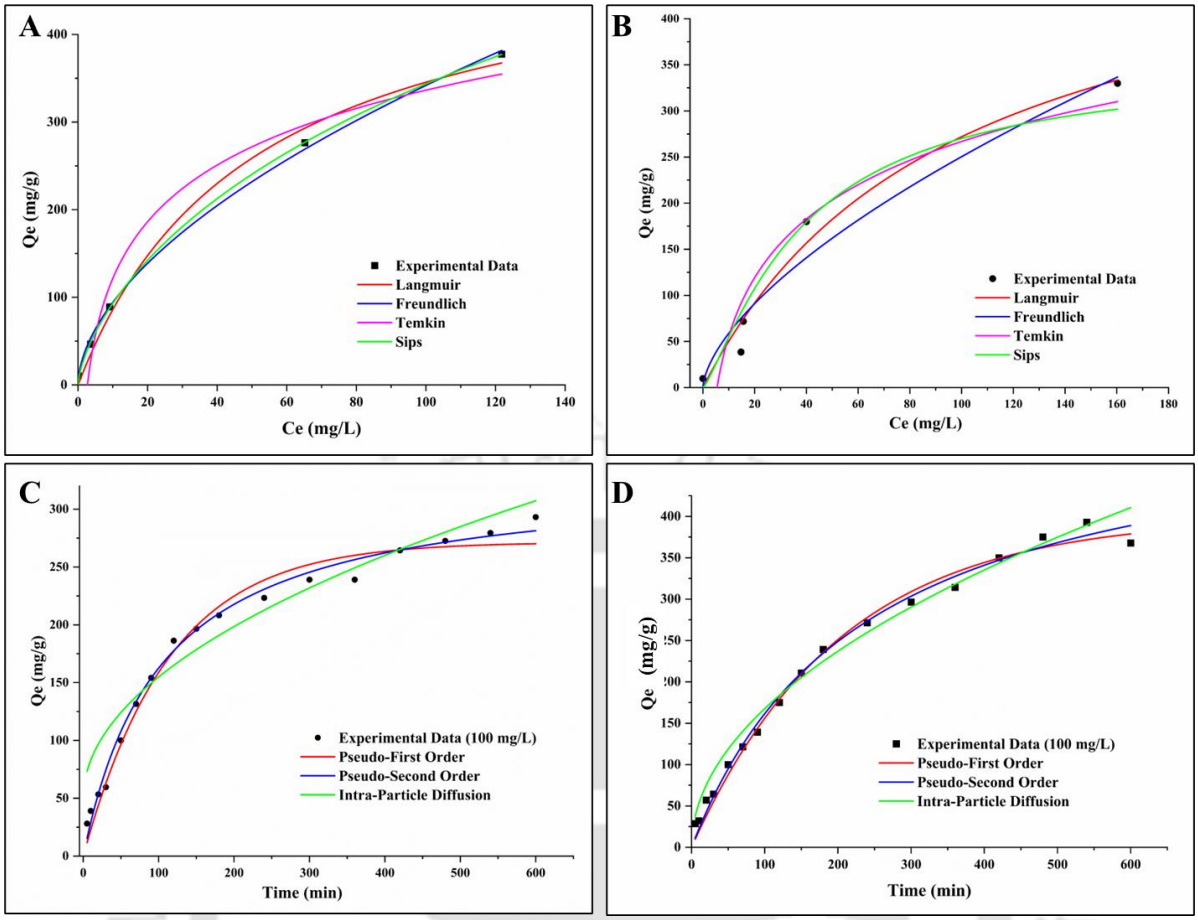

Figure 4.9: (A) Non-linear isotherm modelling plot of CR; (B) Non-linear isotherm modelling plot of DB; (C) Non-linear kinetics modelling plot of CR; Non-linear kinetics modelling plot of DB.

4.3.5. Effect of various ion species

The impact of various ions on the efficiency of CMC-T-CH in removing CR and DB was analysed, and the outcomes are illustrated in Figure 4.10. The results indicated that the removal efficiency of CMC-T-CH for CR and DB was not significantly affected by cationic species such as Fe^{3+}, Pb^{2+}, and Co^{2+}. In contrast, anionic species such as SO_4^{2-}, Cl^-, and NO_3^- were found to have a negative impact on CR and DB removal efficiency. This observation was attributed to the competition between the ionic moieties and the dye molecules for binding to the active sites onto the surface of CMC-T-CH. The occurrence of excessive amounts of SO_4^{2-}

, Cl^-, and NO_3^- could potentially hinder the performance of CMC-T-CH in removing CR and DB. Thus, it is essential to consider the ion effect when using CMC-T-CH to remove CR and DB in wastewater treatment processes.

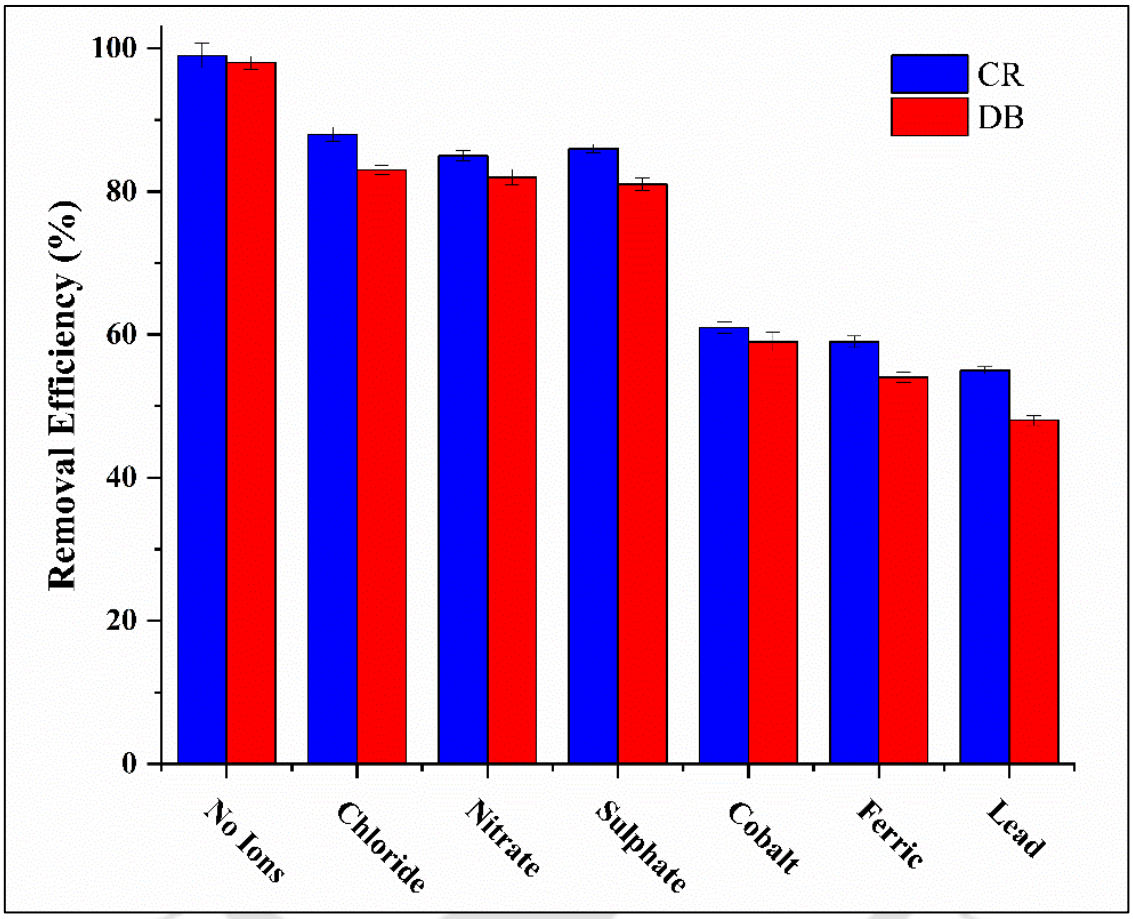

Figure 4.10: Effect of various ion species.

4.3.6. Regeneration ability of CMC-T-CH

One of the crucial aspects of the adsorption process is the reusability and regeneration of spent adsorbent (Unugul and Nigiz 2020). Reusability will result in lower adsorbent costs, higher adsorption efficiency, and lower operating costs. In the present study, the desorption of spent CMC-T-CH was performed by a mild alkali solution (0.1M NaOH), and its regeneration and reusability ability were investigated. Figure 4.11 shows the outcomes of the study. The

adsorption efficiency of CMC-T-CH for the removal of DB and CR after the first adsorption-desorption cycle was 84 and 81 % (approximately), respectively. The regeneration efficiency gradually decreased for both dyes from the first to sixth cycles. This suggested that electrostatic attraction, as well as ion exchange, control the adsorption process. Under base treatment, complete regeneration of spent CMC-T-CH was not possible, resulting in the loss of adsorption capacity. The regeneration ability of CMC-T-CH was efficient up to four cycles of adsorption-desorption.

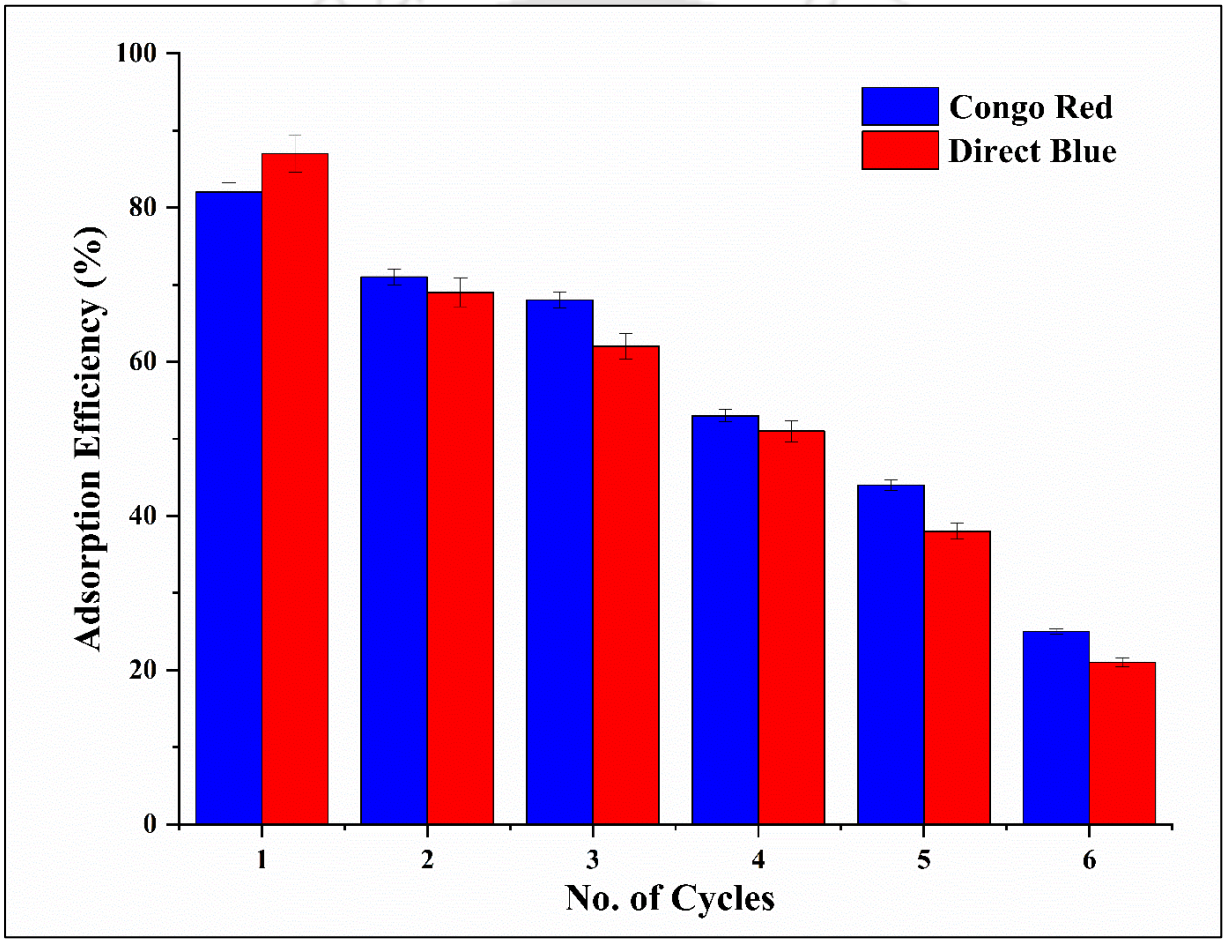

Figure 4.11: Regeneration study plot of CMC-T-CH.

4.3.7. Possible adsorption mechanism for the CR and DB removal by CMC-T-CH

Based on the obtained results, the possible adsorption mechanism of CR and DB onto CMC-T-CH could be described (Figure 4.12) as follows:

(i) The transport of CR and DB molecules from the bulk solution to the external surface of CMC-T-CH occurs primarily through a process known as liquid film diffusion.

(ii) The adsorption of CR and DB onto the surface of CMC-T-CH is attributed to two main factors (a) Electrostatic interactions: These interactions arise between the positively charged surface molecules of CMC-T-CH and the negatively charged sulfonate groups of CR and DB., and (b) Hydrogen bonding: Hydrogen bonding takes place between the surface hydrogen atoms of the adsorbent and the oxygen molecules of CR and DB.

(iii) Following adsorption onto the surface, CR and DB molecules exhibit migration into the pores of CMC-T-CH.

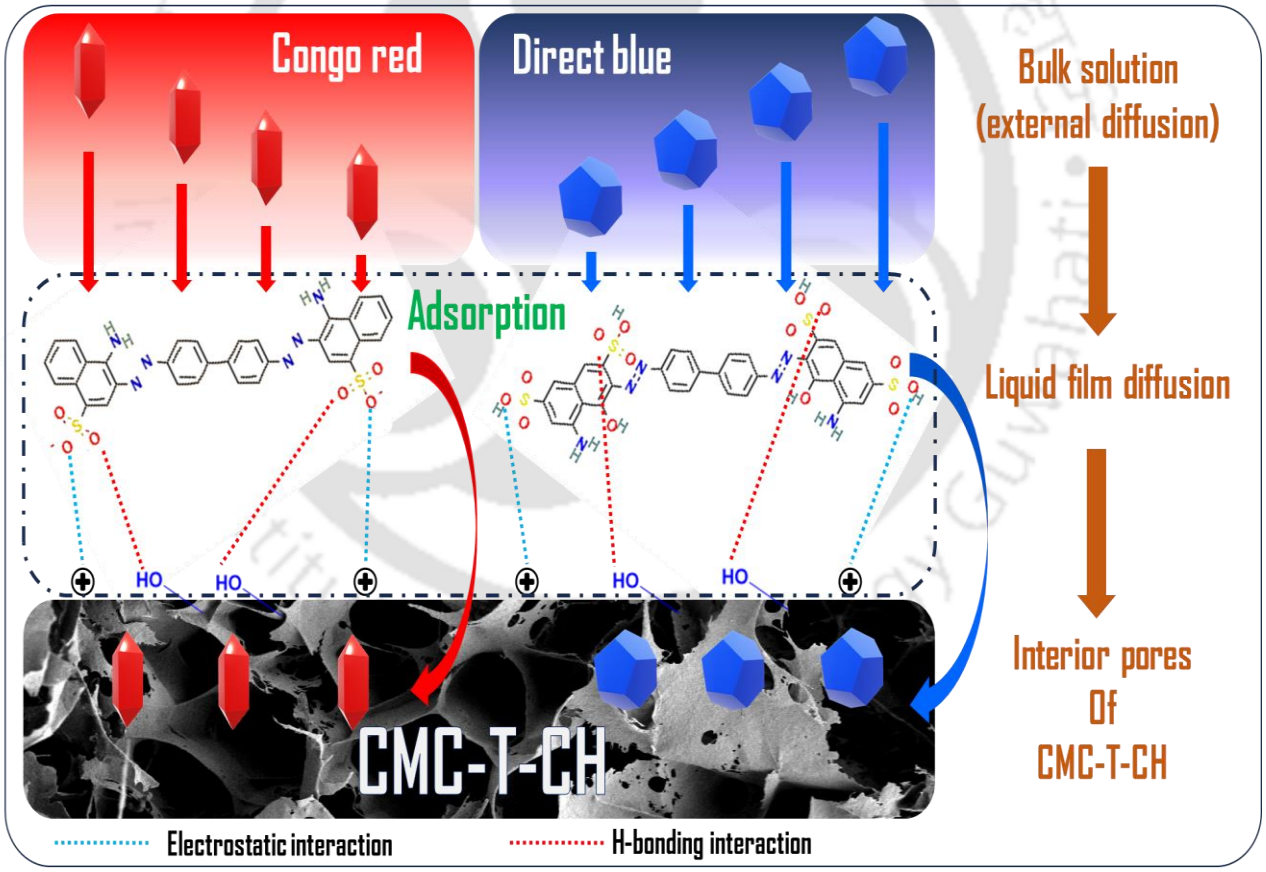

Figure 4.12: Possible adsorption mechanism of CR and DB adsorption by CMC-T-CH.

4.3.8. Phytotoxicity analysis

The phytotoxicity assessment of the fabricated CMC-T-CH was performed to validate the adsorbent efficiency in removing CR and DB from water. The toxicity test was performed on *Vigna mungo* seeds by germinating them in the solution obtained before and after adsorption. The experimental outcomes have been illustrated in Figure 4.13. The seeds that were germinated in the water (control) grew up to 27 cm in mean root length (approximately). The seeds grown in the Congo red and Direct blue dyes before and after the adsorption process showed a reduction in mean root length compared to the control. The root mean length of the seeds germinated in the 10 and 500 mg/L of Congo red dye before treatment were 11.2 and 4.2 cm, respectively, and after treatment, they were 19.2 and 12.4 cm, respectively (Figure 4.13B). For Direct blue (10 and 500 mg/L), the root mean length before treatment was 10.1 and 3.8 cm, respectively, and after the adsorption treatment, the length was increased to 17.6 and 11.6 cm, respectively (Figure 4.13C). The phytotoxicity analysis revealed an improvement in seed root length growth after the adsorption process. Thus, the fabricated CMC-T-CH adsorbent successfully remediates the dyes (congo red and direct blue) from the aqueous solution.

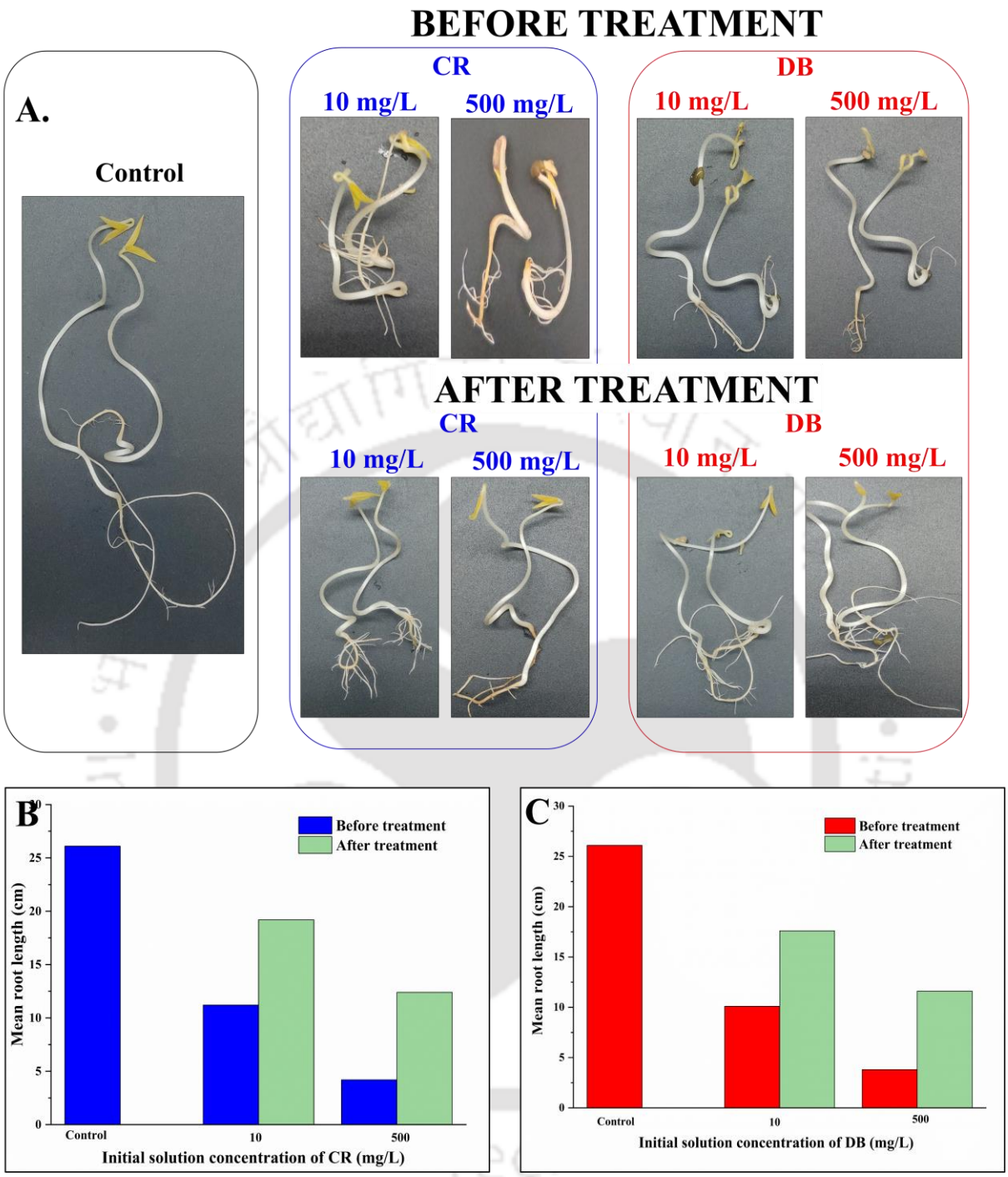

Figure 4.13: (A) Phytotoxic assessment of CMC-T-CH removing CR and DB by utilizing seeds of *Vigna mungo*; (B) Seed germination root length comparison for CR before and after adsorption treatment; and (C) Seed germination root length comparison for DB before and after adsorption treatment.

4.4. Conclusion

In the current study, a novel CMC-T-CH adsorbent was fabricated from the two bio-polymers, carboxymethyl cellulose (CMC) and chitosan (CH), to eliminate the hazardous contaminant, Congo red, and Direct blue dyes. Triethylenetetramine (TETA) was used as a linking agent that provides stability to the synthesized beads and more amine groups to the adsorbent, which increase the affinity towards anionic contaminants. The synthesized CMC-T-CH exhibited enhanced physicochemical properties, including a fibrous structure with multiple pores, which contributed to its efficient removal of CR and DB. The adsorption process parameters were optimized to remove the dyes efficiently. The interaction of adsorbate and adsorbent was also studied by various mathematical isotherm and kinetics models confirming that the removal process was chemisorption (pseudo-second-order kinetics) by forming a monolayer of adsorbed dyes over the CMC-T-CH (Langmuir isotherm). The CMC-T-CH could regenerate up to four cycles of adsorption-desorption by treating the spent adsorbent with a mild NaOH solution. The efficacy of CMC-T-CH in successfully removing congo red and direct blue was confirmed by phytotoxicity analysis, where the plant growth improved after the treatment (adsorption). Overall, CMC-T-CH has shown excellent adsorption efficiency toward CR and DB and can potentially treat natural dyeing wastewater and other pollutants.

Chapter 5

Continuous Adsorption for Direct Blue dye removal by CMC-T-CH and multi-contaminant treatment from real-time samples

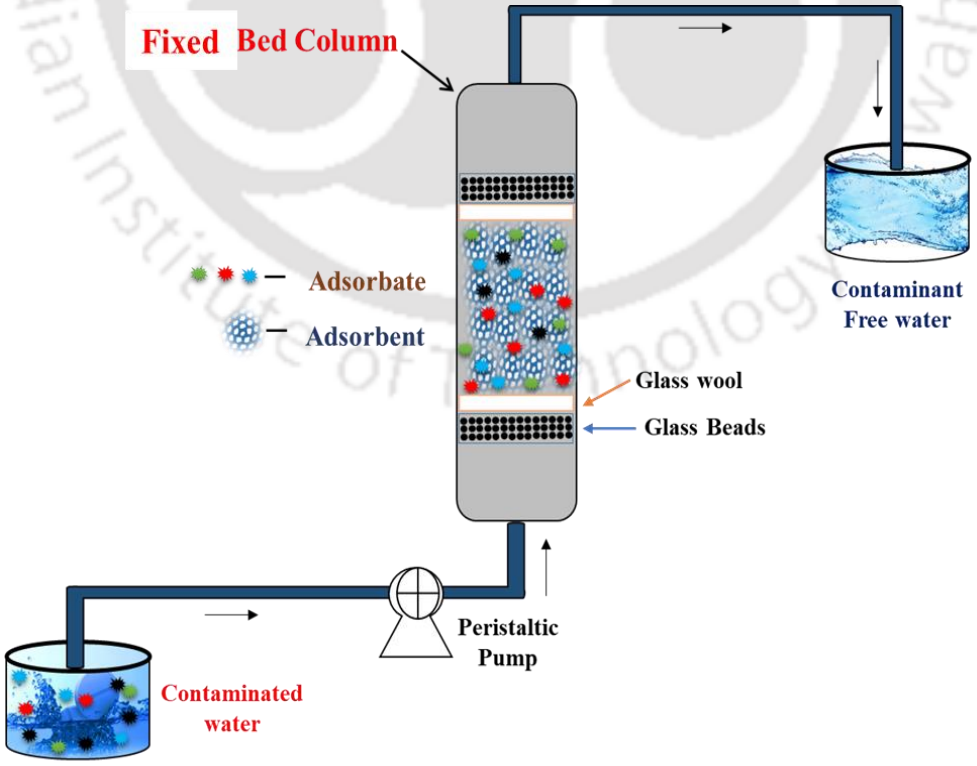

ABSTRACT

This study investigated the effectiveness of a continuous packed bed adsorption process for removing Direct Blue dye from water using a biosorbent of chitosan and carboxymethylcellulose (CMC-T-CH). The experiments involved varying the CMC-T-CH bed height (~1 to ~3 cm), Direct Blue inlet concentration (~1 to ~50 mg/L), and inlet flow rate (~0.5 to ~3 ml/min) to evaluate column performance. The highest column capacity achieved was 4.0 mg of Direct Blue per gram CMC-T-CH, with a flow rate of 1 ml/min, an inlet concentration of 10 mg/L, and a bed height of 3 cm. The breakthrough curves were analyzed using three mathematical models: Adams-Bohart, Thomas, and Yoon-Nelson. Among them, the Thomas and Yoon-Nelson models provided a good fit for the experimental data under different conditions. Furthermore, the study analyzed three real-time wastewater samples, demonstrating the effectiveness of this column system.

5.1. Introduction

The demand for synthetic dyes has risen significantly in today's fast-paced society, leading to a significant increase in production to meet the needs of various textile products. One commonly used dye, Direct Blue 6, is utilized in multiple industries, including textile, paper, leather, paint, and cosmetics (Tang et al., 2014). However, the environmental impact of these dyes is a growing concern. The presence of Direct Blue 6 in water bodies poses a significant threat to the ecosystem by reducing light penetration and hindering photosynthesis, ultimately resulting in eutrophication (Sarkar et al., 2017). Furthermore, these dyes possess carcinogenic, malignant, and genotoxic properties that can lead to skin irritation, allergies, DNA mutations, and the proliferation of tumor cells in both humans and animals (Hernández-Zamora & Martínez-Jerónimo, 2019). These dangers highlight the urgent need for a more sustainable and environmentally-friendly alternative. It is crucial that we act towards a safer future by choosing eco-friendly options that prioritize the well-being of our planet and personal health.

About 350-380 cubic meters of water is produced for every tonne of textile manufacturing (Forgacs et al., 2004). This highlights the urgent need to separate dyes from industrial wastewater to prevent health risks and environmental pollution. Various techniques have been studied to remove dyes, including chemical, biological, and physicochemical methods (Saravanan et al., 2020; Sarkar et al., 2017). Among these, adsorption is the most effective and economical, using adsorbents like carbon, ion exchange resin, biomass adsorbent, and carbon nanotubes (Kumar et al., 2022; Patra et al., 2021). However, due to their high processing costs, researchers are seeking alternative and more efficient adsorbents that are also economical.

Polysaccharides like chitosan (CH) and carboxymethyl cellulose (CMC) have gained attention due to their natural origin, non-toxicity, biodegradability, and affordability. Chitosan exhibits excellent dye adsorption capacity due to its amino and hydroxyl groups (Ashrafizadeh et al.,

2023), while carboxymethyl cellulose's hydroxyl and carboxyl groups make it effective for cationic contaminants (Rana et al., 2023). Combining these polymers can create a novel adsorbent with superior dye removal efficiency (Manzoor et al., 2019).

Column studies are essential for designing continuous adsorption systems. These studies help determine model parameters necessary for large-scale wastewater treatment. Packed-bed columns offer advantages like operational simplicity, high yield, and easy scalability. This research aims to evaluate the dynamic behavior of an adsorbent column, focusing on breakthrough curves under varying experimental conditions such as inlet flow rate, pH, and bed depth. Kinetic modeling using the Adams–Bohart, Thomas, and Yoon Nelson models was employed to determine the design parameters for dye adsorption in the column.

5.2.Material and Experiments

5.2.1. Reagents and Chemicals

The reagents, chemicals, and materials utilized for investigation were of the analytical grade. They were obtained from local vendors of SRL Pvt Ltd, Sigma Aldrich, and Himedia Laboratories Pvt Ltd. The Table 5.1 contains information about the materials list and their role.

Table 5.1: Detail list of chemicals, reagents, and salts.

Serial No.	*CHEMICAL/REAGENT/SALT*	*PURPOSE*
1.	Direct Blue 6	Adsorbate
2.	Chitosan	Adsorbent
3.	Carboxymethyl cellulose	Adsorbent
4.	Acetic acid	Dissolving agent
5.	0.1 M Sodium Hydroxide (NaOH)	Adjusting pH
6.	0.1 M Hydrochloric acid (HCl)	Adjusting pH

5.2.2. Fabrication of adsorbent

The detailed preparation protocol has been described in the Section 4.2.2. Initially, 2 grams of CMC were dispersed in 200 mL of distilled water on a magnetic stirrer at 60°C until the CMC powder was dissolved completely. Similarly, CH suspension was prepared by blending 2 grams of chitosan flakes with 2% (v/v) acetic acid solution (100 ml) at 60°C (Step 1). Next, CH solution was added into the CMC solution drop-wise, slowly, with the help of a syringe (Step 2). The CMC-CH mixture was placed in an incubator shaker at room temperature overnight. After the incubation period, the formed beads were thoroughly washed and stored at 25°C, and the beads were labelled as CMC-CH.

To stabilize the CMC-CH beads, the prepared CMC-CH beads were immersed into 1-5% (v/v) Triethylenetetramine (TETA) for a period of 24 h in an incubator shaker (Figure 4.1B). After completion of the process, the beads were washed multiple times with deionised water until the solution's pH was 7. The beads were labelled as CMC-T-CH and stored at 25°C for further use.

5.2.3. Continuous Adsorption Experiments

The Continuous column studies were performed to estimate the capacity of the CMC-T-CH to eliminate Direct Blue (DB) under various conditions in continuous mode. For conducting continuous column studies, glass column of diameter 15 mm with thickness ~1 mm and height 60 mm was used. Peristaltic pump (PP-20-EX, Miclins, India) was used to pump the DB solution into the column. The flow was kept upward to prevent channelling. Various parameters influencing the adsorption of DB such as bed height, initial DB concentration and flow rate were studied. The effect of bed height was studied by considering bed height 1 cm, 2 cm, and 3 cm. The influence of flow rate was investigated by using flow rate 0.5 mL/min, 1 mL/min and 3 mL/min. The effect of initial DB concentration was examined by using 1 mg/L, 10 mg/L

and 50 mg/L DB dye. Various column adsorption parameters and their equations were given in Appendix A4.

5.2.4. Collection of wastewater samples for Real-time application

Wastewater samples were gathered in real-time from three distinct locations using standard protocols for wastewater sampling. The coordinates for each spot are as follows: Spot 1 - 26°18’42.3"N, 91°67’70.8"E; Spot 2 - 26°18’13.6"N, 91°42'41.0"E; and Spot 3 - 26°13'26.5"N, 91°42'55.5"E (Figure 5.1).

Figure 5.1: Sampling sites for wastewater collection.

These collected wastewater samples underwent analysis for various physico-chemical parameters, including biochemical oxygen demand (BOD, in mg/L), chemical oxygen demand (COD, in mg/L), total dissolved solids (TDS, in mg/L), pH levels, conductivity (measured in µs/cm), turbidity (measured in NTU), and concentrations of dye (Direct Blue 6) and pharmaceutical contaminants (Ciprofloxacin and Diclofenac) (measured in mg/L), both before and after the adsorption process. The protocol for continuous adsorption studies for real-time samples would be same as mentioned in Section 5.2.3.

5.3. Results and Discussions

5.3.1. Analysis of Column Performance under Varied Operating Conditions

The performance of the column under different operating conditions was evaluated to understand the dynamics of a breakthrough curve study. Key parameters such as bed height, flow rate, and initial inlet concentration were investigated to assess their impact on the breakthrough curve shape and overall column performance.

The experimental setup involved conducting breakthrough curve studies using a packed-bed column Figure 5.2. Various combinations of bed heights (1.0 cm, 2.0 cm, and 3.0 cm), flow rates (0.5 mL/min, 1.0 mL/min, and 3.0 mL/min), and initial inlet concentrations of Direct Blue 6 dye (1.0 mg/L, 10.0 mg/L, and 50.0 mg/L) were employed. The experimental parameters such as total time, t_{total} (min), total adsorption capacity, q_{total} (mg), total DB adsorbed, m_{total} (mg), effective volume, V_{eff} (mL) and removal efficiency, R (%) are tabulated in the Table 5.2.

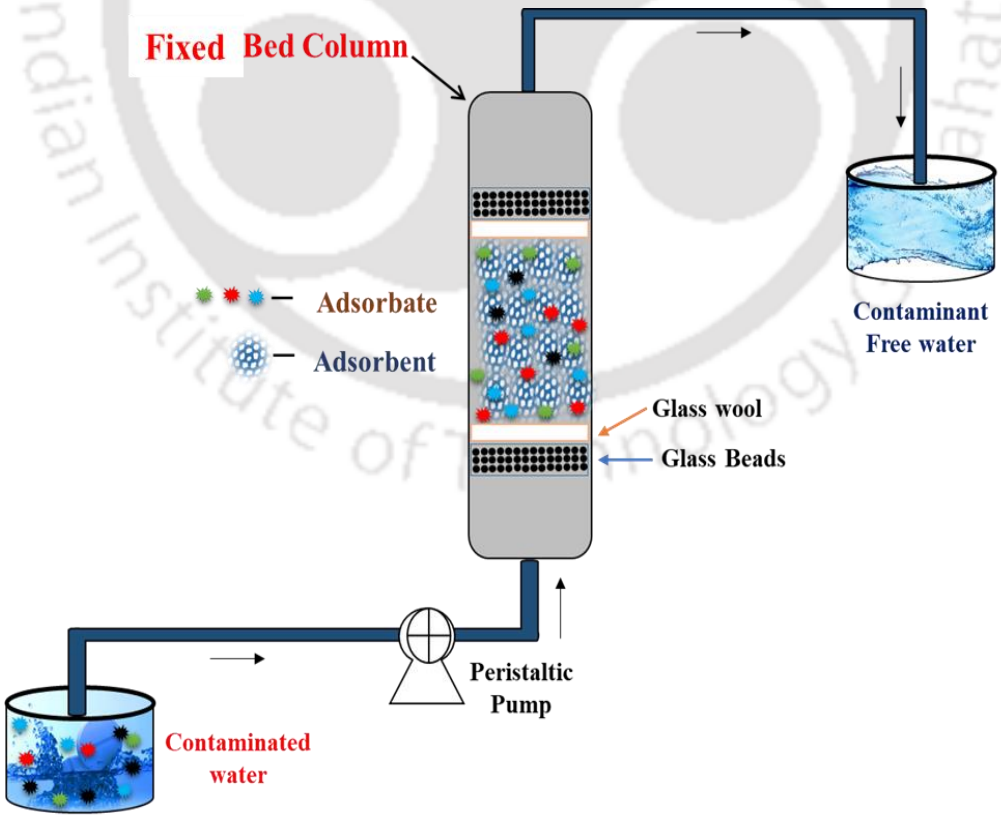

Figure 5.2: Schematic diagram of Laboratory Continuous Packed-bed adsorption column.

Table 5.2: Various column parameters of DB biosorption onto CMC-T-CH adsorbent.

Z	F	C_o	t_{total}	m_{total}	Q_{total}	$q_{e\ (exp.)}$	V_{eff}	R
cm	mL/min	mg/L	min	mg	mg	mg/g	ml	%
2.00	0.50	1.00	180.00	0.09	0.03	0.07	90.00	30.00
2.00	0.50	10.00	300.00	1.50	0.75	1.88	150.00	50.00
2.00	0.50	50.00	3000.00	75.00	5.93	14.81	1500.00	7.90
2.00	0.50	10.00	300.00	1.50	0.75	1.88	150.00	50.00
2.00	1.00	10.00	240.00	2.40	0.50	1.25	240.00	20.83
2.00	3.00	10.00	300.00	9.00	0.60	1.50	900.00	6.67
1.00	1.00	10.00	360.00	3.60	0.90	4.50	360.00	25.00
2.00	1.00	10.00	240.00	2.40	0.50	1.25	240.00	20.83
3.00	**1.00**	**10.00**	**210.00**	**2.10**	**1.60**	**4.00**	**210.00**	**76.19**

5.3.1.1. Impact of bed height on breakthrough curves

The results depicted in Figure 5.3 offer an in-depth analysis of the impact of varying bed depths, specifically 1, 2, and 3 cm, on the breakthrough curves. By maintaining a constant influent concentration of 10 mg L^{-1} and flow rate of 1 ml min^{-1}, it is evident that each curve's shape and slope transform with the bed depth. The breakthrough time increases in proportion to the adsorbent's bed height, signifying that a higher bed depth enhances the adsorbent's efficacy.

Figure 5.3 further reveals that an increase in the bed height from 1 to 3 cm leads to a decrease in the slope of the breakthrough curve, thereby creating a rapid mass transfer zone.

Moreover, the breakthrough curve does not conform to the typical "S" shape profile found in optimal adsorption systems. This is because the DB dye possesses a large molecular diameter and complex structure, unlike adsorbates with small molecular diameters and simple structures that generate the "S" shape profile (Walker & Weatherley, 1997).

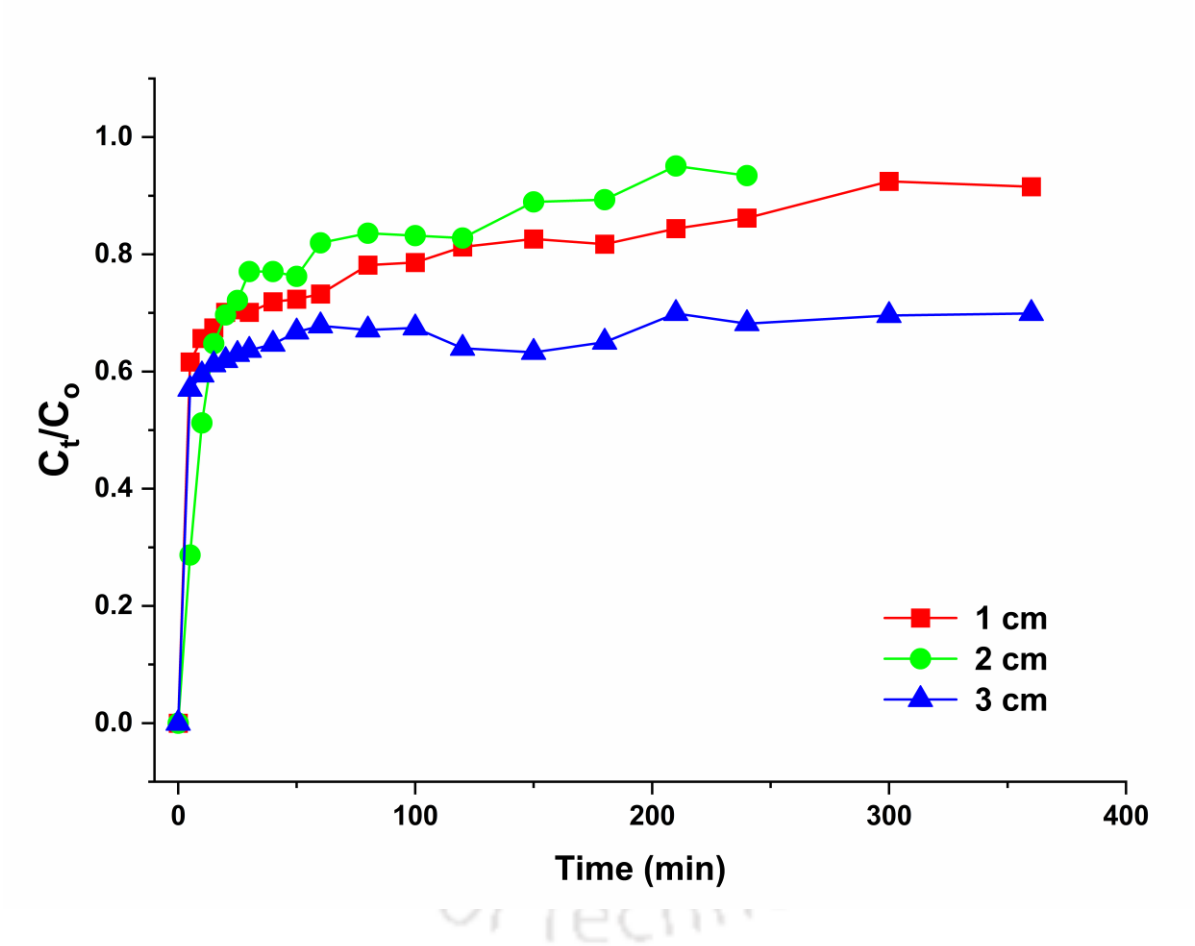

Figure 5.3: Breakthrough curves of DB removal using CMC-T-CH packed in columns of different bed heights.

According to Table 5.2, lowering the bed height results in a decrease in both the removal percentage and the total weight of DB adsorbed by CMC-T-CH in the column. Conversely, a taller bed leads to more DB being adsorbed due to the increased surface area of the adsorbent,

providing more sites for adsorption. Similarly, the removal percentage drops as the bed depth decreases, likely because there is less adsorbent available. These findings align with previous studies (Ahmad & Hameed, 2010; López-Cervantes et al., 2018).

5.3.1.2. Impact of flow rate on breakthrough curves

To study the impact of flow rate (0.5, 1.0, and, 3 ml min^{-1}) on breakthrough curves, we kept the bed height at 2 cm and the initial DB concentration at 10 mg L^{-1} constant. The results, presented in Figure 5.4 and Table 5.2, show that breakthrough generally happened more quickly with higher flow rates. Breakthrough time increased as the flow rate decreased because at a slower inlet DB rate, CMC-T-CH had more time to interact with the dye, leading to greater removal of DB in the column.

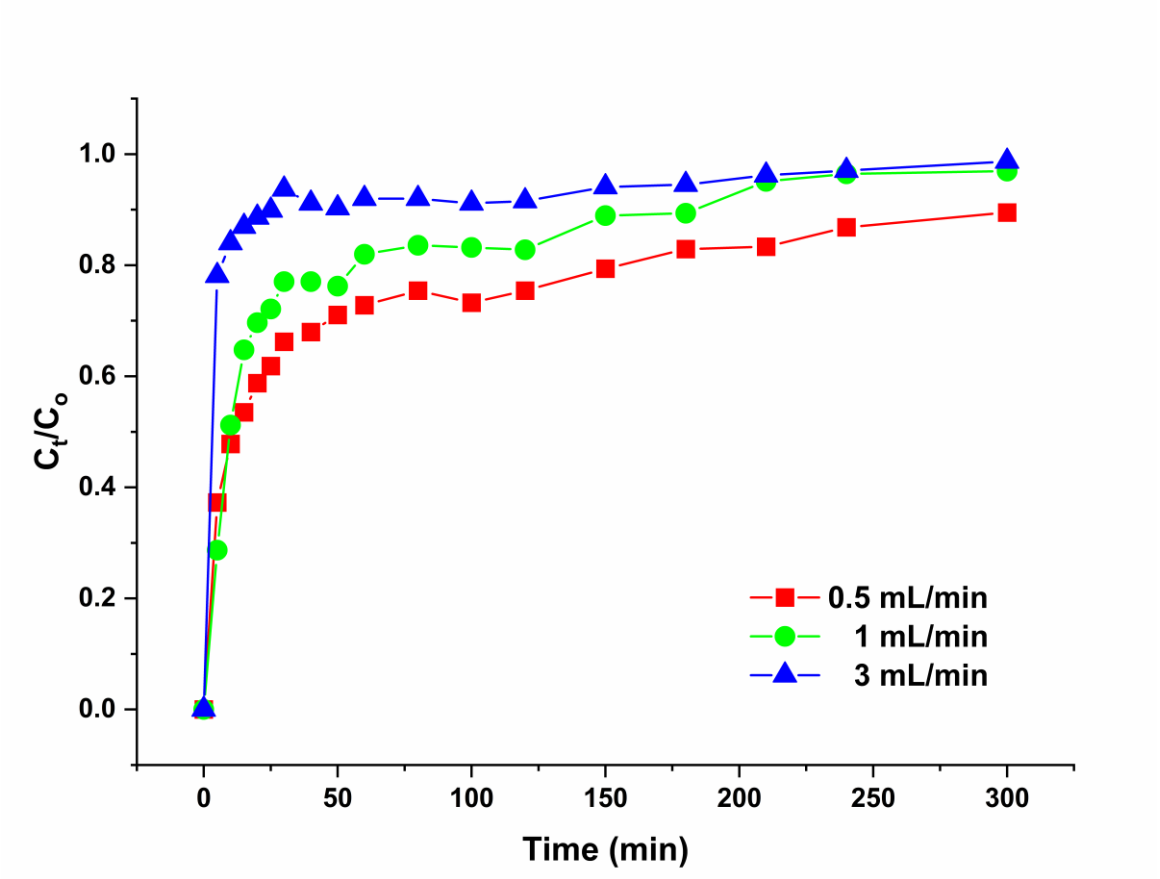

Figure 5.4: Breakthrough curves of DB removal using CMC-T-CH packed in columns of different flow rates.

The changes in the breakthrough curve's slope and adsorption capacity can be explained by mass transfer principles. At higher flow rates, the mass transfer rate increases, meaning more dye is adsorbed per unit bed height with increasing flow rate, resulting in quicker saturation. This phenomenon aligns with findings from Ahmad & Hameed, 2010; López-Cervantes et al., 2018.

5.3.1.3. Impact of initial inlet DB concentration on breakthrough curves

The impact of DB inlet concentration (1.0, 10.0, and 50 mg L^{-1}) onto DB removal by CMC-T-CH was investigated by maintaining a bed height of 2 cm and a flow rate of 1 ml min^{-1}. The results are presented in Figure 5.5 and Table 5.2. As the initial concentration increased, the breakthrough times decreased. Lower initial concentrations resulted in more scattered breakthrough curves and slower breakthrough. However, the values of q_{total} and $q_{e\ (exp.)}$ increased with rising inlet dye concentration, while the % removal decreased when the DB concentration increased from 1 to 50 mg L^{-1}. This is because a low influent concentration leads to slow transport of the DB dye to the surface of the CMC-T-CH adsorbent, indicating a reduced diffusion coefficient and mass transfer driving force (López-Cervantes et al., 2018).

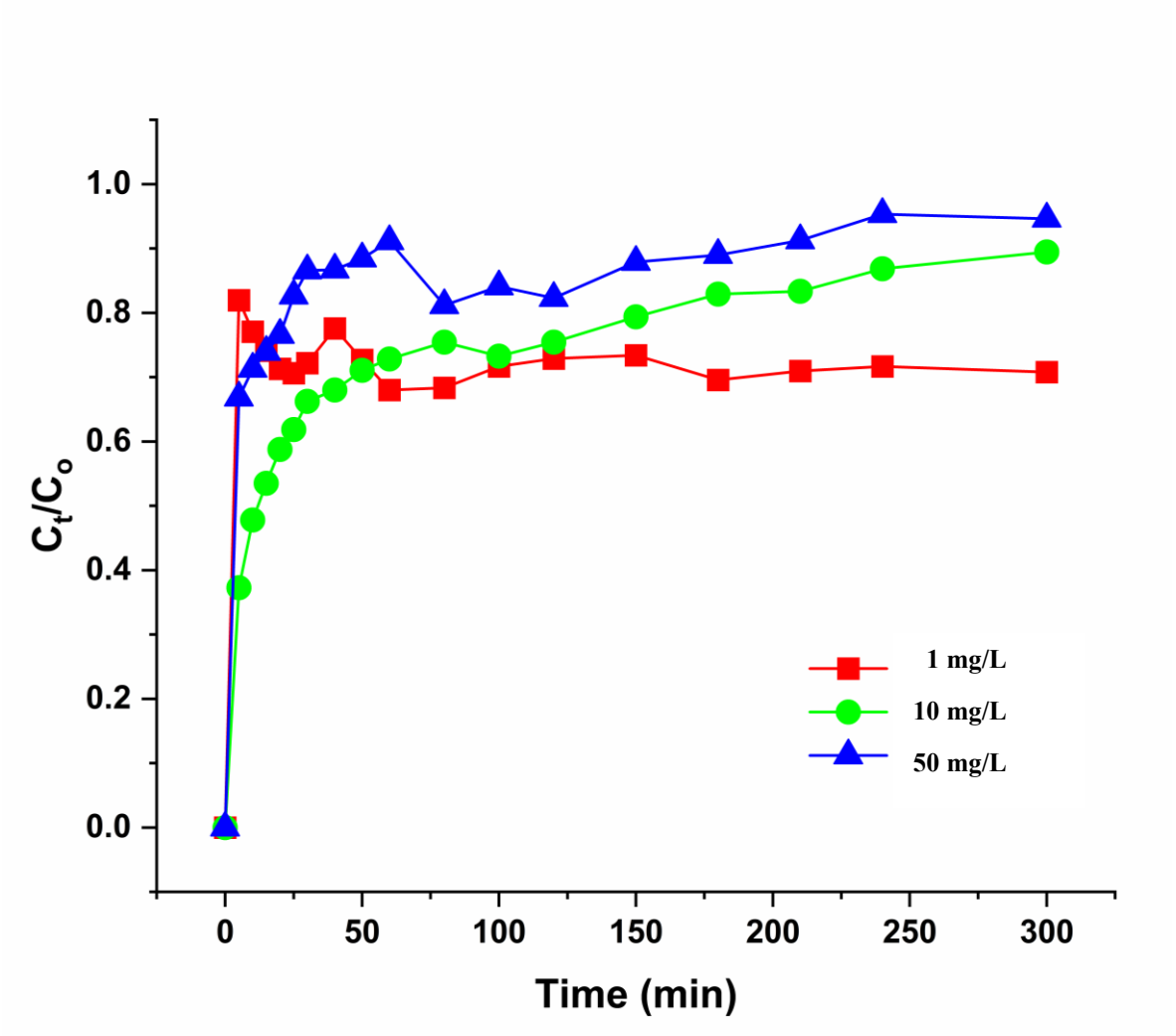

Figure 5.5: Breakthrough curves of DB removal using CMC-T-CH packed in columns of different inlet DB concentrations.

5.3.2. Breakthrough curve and modelling

The Thomas model was employed in its linearized form to estimate the parameters k_{TH} and q_o. Table 5.3 presents the estimated Thomas parameters and the regression coefficients (R^2). The results in Table 5.3 indicate that as influent DB concentration and bed depth increase, q_o values also increase while k_{TH} values decrease. Conversely, both q_o and k_{TH} values increase with higher flow rates. Despite the Thomas model offering good adjustments for adsorption conditions, it does not correlate well in predicting breakthrough curves. This discrepancy is evident in the differences between experimental and model-calculated adsorption capacity

values. The main limitation of the Thomas model lies in its derivation from second-order kinetics, assuming biosorption is not limited by chemical reactions but by mass transfer at the interface. This limitation can introduce errors when modeling biosorption processes under specific conditions (Aksu & Gönen, 2004; López-Cervantes et al., 2018).

The Adams-Bohart adsorption model was utilized to analyze the initial segment of the breakthrough curve from experimental data. Table 5.3 presents the calculated values of k_{AB} and N_{AB} obtained through linear regression analysis on all breakthrough curves. The value of k_{AB} and N_{AB} increase across different flow rates, while they decrease with increasing bed depth. Moreover, k_{AB} decreases and N_{AB} increases with higher initial DB concentrations.

The Adams-Bohart model, rooted in surface reaction theory, posits that equilibrium is not instant, linking adsorption rate to both adsorbate concentration and the remaining capacity of the adsorbent. It is applicable in low concentration regions and when mass transfer limits the adsorption rate (Karimi et al., 2012). Consequently, the Adams-Bohart model is not suitable for predicting experimental data under the tested conditions and with this dye.

The Yoon-Nelson model adopts a two-phase flow approach, treating the fluid and particles as distinct phases. It employs equations that describe the behavior of these phases, considering their interactions. Parameters such as the rate constant (k_{YN}) and τ (time for 50% breakthrough) were derived from the Yoon-Nelson plot across varying concentrations, bed heights, and flow rates, detailed in Tables 5.3. The values of k_{YN} were observed to rise with increasing concentrations and flow rates but no significance change observed with increase in the bed heights. The good fit of experimental data with the Thomas and Yoon-Nelson model suggests that these two models could be used to show the behaviour of adsorbent and adsorbate in a continuous adsorption system.

Table 5.3.: Parameters of different models for BF adsorption in packed bed at various conditions.

Column parameters			Thomas Model			Adams-Bohart Model			Yoon-Nelson Model		
Z	**F**	**C_o**	**q_o**	**k_{TH}**	**R^2**	**N_{AB}**	**k_{AB}**	**R^2**	**k_{YN}**	**τ**	**R^2**
cm	mL/min	mg/L	mg/g	mL/mg min		mg/L	mL/mg min		1/min	min	
2.00	0.50	1.00	0.81	1.36	0.71	0.25	2.1E-04	0.76	1.19	3.74	0.78
2.00	0.50	10.00	0.05	1.14	0.61	0.65	8.0E-05	0.52	0.12	7.64	0.61
2.00	0.50	50.00	2.13	0.10	0.56	1.30	4.0E-05	0.61	0.05	16.89	0.56
2.00	0.50	10.00	1.25	0.05	0.61	721.65	2.0E-04	0.61	0.01	17.64	0.61
2.00	1.00	10.00	3.42	0.15	0.74	1172.67	2.1E-04	0.42	0.07	14.38	0.74
2.00	3.00	10.00	5.22	1.24	0.85	4379.41	4.8E-05	0.60	1.12	3.87	0.85
1.00	1.00	10.00	3.49	0.15	0.45	3837.04	1.0E-04	0.87	0.01	21.64	0.45
2.00	1.00	10.00	6.85	0.03	0.71	1042.02	2.5E-04	0.41	0.02	44.38	0.71
3.00	1.00	10.00	7.45	0.02	0.77	4078.82	3.9E-05	0.53	0.01	77.09	0.77

5.3.3. Application of Adsorbent on Real-Time wastewater samples

The analysis of physico-chemical parameters in real-time wastewater, both before and after the adsorption process, offers crucial insights into the efficacy of the synthesized adsorbents during adsorption. These studies were conducted in a glass column of diameter 15 mm with thickness ~1 mm and height 60 mm. Peristaltic pump (PP-20-EX, Miclins, India) was used to pump the solution into the column. The flow was kept upward to prevent channelling. The protocol for continuous adsorption studies for real-time samples would be same as mentioned in Section 5.2.3.

Initially, the collected wastewater displayed elevated levels of pollutants, as indicated by several parameters reflecting organic and inorganic contaminants and overall water quality. Post-adsorption, a notable decrease in parameters such as BOD, COD, TDS, pH, conductivity, and turbidity was observed, signifying the successful removal of pollutants by the adsorbents. A detailed comparison of these physico-chemical parameters before and after the adsorption process is presented in Table 5.4.

The pH of the wastewater prior to the adsorption process ranged from 5.72 to 8.01, within the acceptable limits set by both the World Health Organization (WHO) (WHO, 2006) and the Central Pollution Control Board (CPCB) (*CPCB | Central Pollution Control Board*, n.d.). The adsorption method successfully neutralized the pH, showing its ability to counteract acidity or alkalinity in the wastewater. Initially, the BOD levels were notably high, ranging from 4.7 to 186.1 mg/L. Following adsorption, a significant reduction in BOD was observed, with values ranging from 1.1 to 83.19 mg/L. Particularly, spot 3 exhibited a considerably lower BOD level compared to other spots, indicating efficient removal of organic pollutants and the adsorbent's effectiveness in mitigating biodegradable organic matter.

Similarly, COD levels, initially ranging from 40.0 to 317.0 mg/L, experienced a substantial decrease post-adsorption, with values ranging from 7.9 to 49.0 mg/L, indicating effective removal of both biodegradable and non-biodegradable organic pollutants. Conductivity levels, initially between 121.7 and 470.1 µs/cm, also saw a considerable decrease after adsorption, suggesting the removal of dissolved salts and ions. Initially, the concentrations of Ciprofloxacin and Diclofenac varied, with some spots exceeding permissible limits. However, after adsorption, these values decreased significantly, reaching negligible levels.

These outcomes demonstrate that adsorption of pollutants by synthesized adsorbents effectively improved the physico-chemical parameters of the wastewater, aligning it more closely with environmental standards. This underscores the potential of the adsorbent (CMC-T-CH) for use in wastewater treatment processes.

Table 5.4: Physico-chemical parameters of real-time wastewater before and after adsorption process.

Indicators	WHO Effluent Standard	CPCB Effluent Standard	Spot 1 26°18'42.3"N 91°67'70.8"E		Spot 2 26°18'13.6"N 91°42'41.0"E		Spot 3 26°13'26.5"N 91°42'55.5"E	
			BA	AA	BA	AA	BA	AA
BOD (mg/L)	nil/ 5.0-7.0	30	186.1	83.16	42.1	10.3	4.7	1.1
COD (mg/L)	nil/ 40	250	317	49.0	129.5	18.3	40	7.9
TDS (mg/L)	1000/ nil	nil	234.3	89.6	171.3	91.8	68.7	17.3
pH	6.0-8.5/ 6.0-9.5	5.5-9.0	5.72	7.34	7.06	6.5	8.01	7.2
Conductivity (µs/cm)	nil/ 1000	nil	470.1	186.2	398.9	129.2	121.7	33.9
Turbidity (NTU)	5	nil	33.64	5.42	26.42	4.9	4.18	1.12

Ciprofloxacin	**100 ng/L**	**NA**	220 ng/L	130.62 ng/L	0	0	78 ng/L	24 ng/L
Diclofenac	**100 ng/L**	**NA**	95 ng/L	29.68 ng/L	0	0	53 ng/L	17 ng/L
BA- Before Adsorption; AA- After Adsorption								

5.4. **Conclusion**

This study used CMC-T-CH adsorbent to remove Direct Blue dye, a harmful contaminant, in a continuous adsorption column. The results of the column experiments led to several conclusions. Firstly, CMC-T-CH proved an effective adsorbent for removing DB from solutions. The adsorption process was found to be dependent on various factors such as bed depth, influent DB concentration, and flow rate. When the bed height was reduced, the removal percentage and total DB adsorbed by CMC-T-CH in the column decreased. However, under specific conditions (flow rate of 1 ml/min, initial concentration of 10 mg/l, and 3 cm bed height), the maximum removal (76.19%) was achieved. Lastly, the breakthrough curves' behavior aligned well with the Thomas model, indicating that internal and external diffusion were not the governing factors in the column's adsorption process. The study also analyzed three real-time wastewater samples, demonstrating this column system's effectiveness.

Chapter 6

Summary

And

Conclusions

6.1. Overall Summary

Chapter 1 provides a detailed introduction to the global issue of deteriorating water quality. It emphasizes the increasing presence of emerging contaminants and their potential impact on human health and the environment. The chapter also highlights the urgent need to address these challenges and introduces the central theme of the thesis, which focuses on using bio-based engineered adsorbents to eliminate these contaminants. The chapter further explores various theoretical aspects of modeling studies. Lastly, it briefly introduces the specific problem statements and outlines the thesis structure.

In Chapter 2, Magnetic activated carbon (MAAC) was synthesized using a simple co-precipitation method with activated carbon to efficiently remove the emerging antibiotic contaminant Ciprofloxacin (CIP). Surface characterization of MAAC confirmed its porous nature and improved magnetic properties. Several process parameters, such as pH, temperature, initial concentration of CIP, and MAAC dosage, influenced the adsorption efficiency of CIP by MAAC. The Langmuir isotherm and pseudo-second-order kinetics indicated the formation of a monolayer of CIP on MAAC under optimal conditions, with chemisorption playing a role in the sorbate-sorbent interaction. Thermodynamically, the adsorption process was spontaneous, endothermic, and favored disorderliness, enhancing adsorption. The presence of co-existing metal ions reduced adsorption efficiency, while anionic salts had a minor impact. Recyclability tests showed a decrease in MAAC's adsorption capacity for CIP over consecutive cycles (up to 5 cycles) and a loss of magnetic properties. Phytotoxicity tests demonstrated MAAC's ability to adsorb CIP effectively, allowing for the successful germination of Vigna mungo seeds.

In Chapter 3, The ACCB adsorbent, a combination of commercial activated carbon and chitosan, was developed to remove the pharmaceutical pollutant Diclofenac from water. The adsorbent’s porous surface and improved properties were confirmed through various tests. The

adsorption process was influenced by pH, temperature, initial Diclofenac concentration, and ACCB dosage. Under optimal conditions, the adsorption followed Freundlich isotherm and pseudo-second-order kinetics, indicating multilayer adsorption via chemisorption. The maximum adsorption capacity was 99.29 mg/g. The process was spontaneous, endothermic, and increased disorder, facilitating adsorption. However, the adsorption capacity decreased after multiple cycles. Seed toxicity tests showed better germination in the post-treated solution, suggesting the adsorbent's effectiveness.

In Chapter 4, a novel adsorbent CMC-T-CH was developed from two bio-polymers, carboxymethyl cellulose (CMC) and chitosan (CH), to remove hazardous contaminants, Congo red and Direct blue dyes. Triethylenetetramine (TETA) was used as a stabilizing agent, providing more amine groups to the adsorbent, thereby increasing its affinity towards anionic contaminants. With its enhanced physicochemical properties and fibrous structure with multiple pores, the CMC-T-CH efficiently removed the dyes. The adsorption process was optimized and confirmed to be chemisorption, forming a monolayer of adsorbed dyes on the CMC-T-CH. The adsorbent could be regenerated for up to four cycles by treating it with a mild NaOH solution. Phytotoxicity analysis confirmed the effectiveness of CMC-T-CH in removing the dyes, as plant growth improved after treatment. Overall, CMC-T-CH demonstrated excellent adsorption efficiency towards Congo red and Direct blue and could potentially treat natural dyeing wastewater and other pollutants.

In Chapter 5, CMC-T-CH adsorbent in a continuous column to remove the Direct Blue dye. The effectiveness of the adsorbent was confirmed, with the adsorption process influenced by factors such as bed depth, dye concentration, and flow rate. A decrease in bed height led to a reduction in dye removal and total adsorption. Optimal conditions (flow rate of 1 ml/min, initial concentration of 10 mg/l, and bed height of 3 cm) resulted in maximum removal of 76.19%.

The behavior of the breakthrough curves aligned with the Thomas model, suggesting that diffusion was not the primary factor in the adsorption process. The system's effectiveness was further demonstrated by analyzing real-time wastewater samples.

The comparison table of various bio-based engineered adsorbents, the model pollutants used in the entire thesis work, and their various adsorption parameters were tabulated in Table 6.1.

6.2. Significance of the Thesis Work

- This research will make a significant contribution to the field of sustainable engineering.
- The bio-based engineered adsorbents synthesized in this study could be an effective alternative to activated carbon filters in water purification systems.
- The synthesized magnetic adsorbents offer several advantages, including selectivity, regenerating ability, and ease of separation from water systems post-adsorption.

6.3. Future Perspectives

- There is potential for integrating the adsorption capabilities of bio-based engineered adsorbents with other water treatment technologies.
- Future work could expand toxicological evaluations to include long-term and cumulative effects on various model organisms.
- There is a need to transition from laboratory-scale studies to practical applications.
- Regulatory frameworks should be developed to incorporate bio-based engineered adsorbents into water quality standards.

Table 6.1. Adsorption parameters of various bio-based engineered adsorbents and the model pollutants used in the entire thesis work.

Biosorbent	Pollutant	pH	Biosorbent Dosage (g/L)	Initial Concentration (mg/L)	Temp. °C	Isotherm	Kinetics	Reusability (Cycles)	Adsorption Capacity (mg/g)	Removal %
MAAC	Ciprofloxacin	6	2	100	40	Langmuir	PSO	5	81.97	78.35
ACCB	Diclofenac	6	1.5	200	40	Freundlich	PSO	4	99.29	97.10
CMC-T-CH	Congo red	6	1	500	35	Langmuir	PSO	5	**519.53**	99.00
	Direct blue	5	1	500	35	Langmuir	PSO	5	**534.25**	98.33

Bibliography

References

Abbasi, M. (2017). Synthesis and characterization of magnetic nanocomposite of chitosan/SiO2/carbon nanotubes and its application for dyes removal. *Journal of Cleaner Production*, *145*, 105–113. https://doi.org/10.1016/J.JCLEPRO.2017.01.046

Abbasi, M., & Habibi, M. M. (2016). Optimization and characterization of Direct Blue 71 removal using nanocomposite of Chitosan-MWCNTs: Central composite design modeling. *Journal of the Taiwan Institute of Chemical Engineers*, *62*, 112–121. https://doi.org/10.1016/J.JTICE.2016.01.019

Abou Alsoaud, M. M., Taher, M. A., Hamed, A. M., Elnouby, M. S., & Omer, A. M. (2022). Reusable kaolin impregnated aminated chitosan composite beads for efficient removal of Congo red dye: isotherms, kinetics and thermodynamics studies. *Scientific Reports 2022 12:1*, *12*(1), 1–19. https://doi.org/10.1038/s41598-022-17305-w

Adams, C., Wang, Y., Loftin, K., & Meyer, M. (2002). Removal of Antibiotics from Surface and Distilled Water in Conventional Water Treatment Processes. *Journal of Environmental Engineering*, *128*(3). https://doi.org/10.1061/(asce)0733-9372(2002)128:3(253)

Afzal, M. Z., Sun, X. F., Liu, J., Song, C., Wang, S. G., & Javed, A. (2018). Enhancement of ciprofloxacin sorption on chitosan/biochar hydrogel beads. *Science of The Total Environment*, *639*, 560–569. https://doi.org/10.1016/J.SCITOTENV.2018.05.129

Agarwal, A., Prajapati, R., Singh, O. P., Raza, S. K., & Thakur, L. K. (2015). Pesticide residue in water—a challenging task in India. *Environmental Monitoring and Assessment*, *187*(2), 1–21. https://doi.org/10.1007/S10661-015-4287-Y/TABLES/4

Agarwal, H. C., Kaushik, C. P., & Pillai, M. K. K. (1987). Organochlorine insecticide residues in the rain water in Delhi, India. *Water, Air, and Soil Pollution*, *32*(3–4), 293–302. https://doi.org/10.1007/bf00225115

Agrawal, A., Pandey, R. S., & Sharma, B. (2010). Water pollution with special reference to pesticide contamination in India. *Journal of Water Resource and Protection*, *2*(05), 432–448. https://doi.org/10.4236/jwarp.2010.25050

Ahmad, A. A., & Hameed, B. H. (2010). Fixed-bed adsorption of reactive azo dye onto granular activated carbon prepared from waste. *Journal of Hazardous Materials*, *175*(1–3), 298–303. https://doi.org/10.1016/J.JHAZMAT.2009.10.003

Aksu, Z., & Gönen, F. (2004). Biosorption of phenol by immobilized activated sludge in a continuous packed bed: prediction of breakthrough curves. *Process Biochemistry*, *39*(5), 599–613. https://doi.org/10.1016/S0032-9592(03)00132-8

Aleem, A., & Malik, A. (2005). Genotoxicity of the Yamuna river water at Okhla (Delhi), India. *Ecotoxicology and Environmental Safety*, *61*(3), 404–412. https://doi.org/10.1016/j.ecoenv.2004.09.001

Alnajrani, M. N., & Alsager, O. A. (2020). Removal of Antibiotics from Water by Polymer of Intrinsic Microporosity: Isotherms, Kinetics, Thermodynamics, and Adsorption Mechanism. *Scientific Reports 2020 10:1*, *10*(1), 1–14. https://doi.org/10.1038/s41598-020-57616-4

Al-Tohamy, R., Ali, S. S., Li, F., Okasha, K. M., Mahmoud, Y. A. G., Elsamahy, T., Jiao, H., Fu, Y., & Sun, J. (2022). A critical review on the treatment of dye-containing wastewater: Ecotoxicological and health concerns of textile dyes and possible remediation approaches for environmental safety. *Ecotoxicology and Environmental Safety*, *231*, 113160. https://doi.org/10.1016/J.ECOENV.2021.113160

Antoniou, M. G., Zhao, C., O'Shea, K. E., Zhang, G., Dionysiou, D. D., Zhao, C., Han, C., Nadagouda, M. N., Choi, H., Fotiou, T., Triantis, T. M., & Hiskia, A. (2016). CHAPTER 1 Photocatalytic Degradation of Organic Contaminants in Water: Process Optimization and Degradation Pathways. *RSC Energy and Environment Series*, *2016-January*(15), 1–34. https://doi.org/10.1039/9781782627104-00001

Anumol, T., Vijayanandan, A., Park, M., Philip, L., & Snyder, S. A. (2016). Occurrence and fate of emerging trace organic chemicals in wastewater plants in Chennai, India. *Environment International*, *92*, 33–42. https://doi.org/10.1016/j.envint.2016.03.022

Appel, J. (1973a). Freundlich's adsorption isotherm. *Surface Science*, *39*(1), 237–244. https://doi.org/10.1016/0039-6028(73)90105-2

Appel, J. (1973b). Freundlich's adsorption isotherm. *Surface Science*, *39*(1), 237–244. https://doi.org/10.1016/0039-6028(73)90105-2

Arman, N. Z., Salmiati, S., Aris, A., Salim, M. R., Nazifa, T. H., Muhamad, M. S., Marpongahtun, M., Ayed, L. Ben, Golomazou, E., Karanis, P., Scheid, P., Tzoraki, O., Lass, A., Shahid Iqbal, M., & My, A. A.). (2021). A Review on Emerging Pollutants in the Water Environment: Existences, Health Effects and Treatment Processes. *Water 2021, Vol. 13, Page 3258*, *13*(22), 3258. https://doi.org/10.3390/W13223258

Arslan, H., Eskikaya, O., Bilici, Z., Dizge, N., & Balakrishnan, D. (2022). Comparison of Cr(VI) adsorption and photocatalytic reduction efficiency using leonardite powder. *Chemosphere*, *300*, 134492. https://doi.org/10.1016/J.CHEMOSPHERE.2022.134492

Ashrafizadeh, M., Hushmandi, K., Mirzaei, S., Bokaie, S., Bigham, A., Makvandi, P., Rabiee, N., Thakur, V. K., Kumar, A. P., Sharifi, E., Varma, R. S., Aref, A. R., Wojnilowicz, M., Zarrabi, A., Karimi-Maleh, H., Voelcker, N. H., Mostafavi, E., & Orive, G. (2023). Chitosan-based nanoscale systems for doxorubicin delivery: Exploring biomedical application in cancer therapy. In *Bioengineering and Translational Medicine* (Vol. 8, Issue 1). https://doi.org/10.1002/btm2.10325

Awasthi, A., Jadhao, P., & Kumari, K. (2019). Clay nano-adsorbent: structures, applications and mechanism for water treatment. *SN Applied Sciences*, *1*(9), 1–21. https://doi.org/10.1007/S42452-019-0858-9/FIGURES/8

Aydin, S., Aydin, M. E., Beduk, F., & Ulvi, A. (2019). Removal of antibiotics from aqueous solution by using magnetic Fe3O4/red mud-nanoparticles. *Science of The Total Environment*, *670*, 539–546. https://doi.org/10.1016/J.SCITOTENV.2019.03.205

Bai, L., Liu, Y., Ding, A., Ren, N., Li, G., & Liang, H. (2019). Fabrication and characterization of thin-film composite (TFC) nanofiltration membranes incorporated with cellulose nanocrystals (CNCs) for enhanced desalination performance and dye removal. *Chemical Engineering Journal*, *358*, 1519–1528. https://doi.org/10.1016/J.CEJ.2018.10.147

Bakatula, E. N., Richard, D., Neculita, C. M., & Zagury, G. J. (2018). Determination of point of zero charge of natural organic materials. *Environmental Science and Pollution Research*, *25*(8), 7823–7833. https://doi.org/10.1007/S11356-017-1115-7/FIGURES/4

Bakore, N., John, P. J., & Bhatnagar, P. (2004). Organochlorine pesticide residues in wheat and drinking water samples from Jaipur, Rajasthan, India. *Environmental Monitoring and Assessment*, *98*(1–3), 381–389. https://doi.org/10.1023/b:emas.0000038197.76047.83

Besha, A. T., Gebreyohannes, A. Y., Tufa, R. A., Bekele, D. N., Curcio, E., & Giorno, L. (2017). Removal of emerging micropollutants by activated sludge process and membrane bioreactors and the effects of micropollutants on membrane fouling: A review. *Journal of Environmental Chemical Engineering*, *5*(3), 2395–2414. https://doi.org/10.1016/J.JECE.2017.04.027

Bexfield, L. M., Toccalino, P. L., Belitz, K., Foreman, W. T., & Furlong, E. T. (2019). Hormones and Pharmaceuticals in Groundwater Used As a Source of Drinking Water Across the United States. *Environmental Science and Technology*, *53*(6), 2950–2960. https://doi.org/10.1021/ACS.EST.8B05592/SUPPL_FILE/ES8B05592_SI_002.XLSX

Central Pollution Control Board-New Delhi Charter for Water Recycling & Pollution Prevention in Textile Industries in Ganga River Basin Save Water for Next Generation. (n.d.).

Chen, X., Song, Z., Yuan, B., Li, X., Li, S., Thang Nguyen, T., Guo, M., & Guo, Z. (2022). Fluorescent carbon dots crosslinked cellulose Nanofibril/Chitosan interpenetrating hydrogel system for sensitive detection and efficient adsorption of Cu (II) and Cr (VI). *Chemical Engineering Journal*, *430*, 133154. https://doi.org/10.1016/J.CEJ.2021.133154

Chung, K. T. (2016). Azo dyes and human health: A review. *Journal of Environmental Science and Health - Part C Environmental Carcinogenesis and Ecotoxicology Reviews*, *34*(4). https://doi.org/10.1080/10590501.2016.1236602

Congo red (C.I. 22120) indicator Reag. Ph Eur 573-58-0. (n.d.). Retrieved June 25, 2023, from https://www.sigmaaldrich.com/IN/en/product/mm/101340

Contaminants of Emerging Concern including Pharmaceuticals and Personal Care Products | US EPA. (n.d.). Retrieved March 17, 2022, from https://www.epa.gov/wqc/contaminants-emerging-concern-including-pharmaceuticals-and-personal-care-products

Corazzari, I., Nisticò, R., Turci, F., Faga, M. G., Franzoso, F., Tabasso, S., & Magnacca, G. (2015). Advanced physico-chemical characterization of chitosan by means of TGA coupled on-line with FTIR and GCMS: Thermal degradation and water adsorption capacity. *Polymer Degradation and Stability*, *112*, 1–9. https://doi.org/10.1016/J.POLYMDEGRADSTAB.2014.12.006

Cui, L., Liu, W., Liu, H., Qin, Q., Wu, S., He, S., Pang, X., Zhu, C., & Shen, P. (2019). PH-Triggered Charge-Reversal Mesoporous Silica Nanoparticles Stabilized by Chitosan Oligosaccharide/Carboxymethyl Chitosan Hybrids for Effective Intracellular Delivery of Doxorubicin. *ACS Applied Bio Materials*, *2*(5), 1907–1919. https://doi.org/10.1021/ACSABM.8B00830/ASSET/IMAGES/LARGE/MT-2018-00830B_0009.JPEG

Cui, Y., Ding, J., Lin, J., Li, Q., & Ding, L. (2022). Cellulose-incorporated imprinted materials with amphiphilic crosslinking structure for selective adsorption of bisphenol A. *Industrial Crops and Products*, *187*, 115308. https://doi.org/10.1016/J.INDCROP.2022.115308

Danalıoğlu, S. T., Bayazit, Ş. S., Kerkez Kuyumcu, Ö., & Salam, M. A. (2017). Efficient removal of antibiotics by a novel magnetic adsorbent: Magnetic activated carbon/chitosan (MACC) nanocomposite. *Journal of Molecular Liquids*, *240*, 589–596. https://doi.org/10.1016/J.MOLLIQ.2017.05.131

Darmokoesoemo, H., Magdhalena, Putranto, T. W. L. C., & Kusuma, H. S. (2016). Telescope snail (Telescopium sp) and mangrove crab (Scylla sp) as adsorbent for the removal of Pb2+ from aqueous solutions. *Rasayan Journal of Chemistry*, *9*(4).

Darmokoesoemo, H., Setianingsih, F. R., Putranto, T. W. L. C., & Kusuma, H. S. (2016). Horn snail (Telescopium sp) and mud crab (Scylla sp) shells powder as low cost adsorbents for removal of Cu2+ from synthetic wastewater. *Rasayan Journal of Chemistry*, *9*(4).

de Souza, R. M., Seibert, D., Quesada, H. B., de Jesus Bassetti, F., Fagundes-Klen, M. R., & Bergamasco, R. (2020). Occurrence, impacts and general aspects of pesticides in surface water: A review. *Process Safety and Environmental Protection*, *135*, 22–37. https://doi.org/10.1016/J.PSEP.2019.12.035

Del Bubba, M., Arias, C. A., & Brix, H. (2003). Phosphorus adsorption maximum of sands for use as media in subsurface flow constructed reed beds as measured by the Langmuir isotherm. *Water Research*, *37*(14), 3390–3400. https://doi.org/10.1016/S0043-1354(03)00231-8

Dey, S., Bano, F., & Malik, A. (2019). Pharmaceuticals and personal care product (PPCP) contamination—a global discharge inventory. *Pharmaceuticals and Personal Care Products: Waste Management and Treatment Technology Emerging Contaminants and Micro Pollutants*, 1–26. https://doi.org/10.1016/B978-0-12-816189-0.00001-9

DIRECT BLUE 6 (C.I. 22610) AldrichCPR | Sigma-Aldrich. (n.d.). Retrieved June 25, 2023, from https://www.sigmaaldrich.com/IN/en/product/aldrich/s468509

Dutta Gupta, S., Mukherjee, A., Bhattacharya, J., & Bhattacharya, A. (2018). *An Overview of Agricultural Pollutants and Organic Contaminants in Groundwater of India*. 247–255. https://doi.org/10.1007/978-981-10-3889-1_15

Dutta, S., Gupta, B., Srivastava, S. K., & Gupta, A. K. (2021). Recent advances on the removal of dyes from wastewater using various adsorbents: a critical review. *Materials Advances*, *2*(14), 4497–4531. https://doi.org/10.1039/D1MA00354B

Elango, G., Rathika, G., & Elango, S. (2017). Physico-Chemical Parameters of Textile Dyeing Effluent and Its Impacts with Casestudy. *International Journal of Research in Chemistry and Environment*, *7*(1).

Eleryan, A., Aigbe, U. O., Ukhurebor, K. E., Onyancha, R. B., Hassaan, M. A., Elkatory, M. R., Ragab, S., Osibote, O. A., Kusuma, H. S., & El Nemr, A. (2023). Adsorption of direct blue 106 dye using zinc oxide nanoparticles prepared via green synthesis technique. *Environmental Science and Pollution Research*, *30*(26), 69666–69682. https://doi.org/10.1007/S11356-023-26954-X/TABLES/8

El-Sharkawy, I. I., Uddin, K., Miyazaki, T., Baran Saha, B., Koyama, S., Kil, H. S., Yoon, S. H., & Miyawaki, J. (2015). Adsorption of ethanol onto phenol resin based adsorbents for developing next generation cooling systems. *International Journal of Heat and Mass Transfer*, *81*, 171–178. https://doi.org/10.1016/J.IJHEATMASSTRANSFER.2014.10.012

Emerging Contaminants. (n.d.). Retrieved March 17, 2022, from https://www.wqa.org/Whats-in-Your-Water/Emerging-Contaminants

Ertugay, N., & Acar, F. N. (2017). Removal of COD and color from Direct Blue 71 azo dye wastewater by Fenton's oxidation: Kinetic study. *Arabian Journal of Chemistry*, *10*, S1158–S1163. https://doi.org/10.1016/J.ARABJC.2013.02.009

Ferreira, D. C. M., dos Santos, T. C., Coimbra, J. S. dos R., & de Oliveira, E. B. (2023). Chitosan/carboxymethylcellulose polyelectrolyte complexes (PECs) are an effective material for dye and heavy metal adsorption from water. *Carbohydrate Polymers*, *315*, 120977. https://doi.org/10.1016/J.CARBPOL.2023.120977

Flagship UN report extolls win-win water partnerships to avert global crisis | UN News. (n.d.). Retrieved April 23, 2024, from https://news.un.org/en/story/2023/03/1134862

Foo, K. Y., & Hameed, B. H. (2010). Insights into the modeling of adsorption isotherm systems. *Chemical Engineering Journal*, *156*(1), 2–10. https://doi.org/10.1016/J.CEJ.2009.09.013

Forgacs, E., Cserháti, T., & Oros, G. (2004). Removal of synthetic dyes from wastewaters: A review. In *Environment International* (Vol. 30, Issue 7). https://doi.org/10.1016/j.envint.2004.02.001

Han, S., Zang, Y., Gao, Y., Yue, Q., Zhang, P., Kong, W., Jin, B., Xu, X., & Gao, B. (2020). Co-monomer polymer anion exchange resin for removing Cr(VI) contaminants: Adsorption kinetics, mechanism and performance. *Science of the Total Environment*, *709*. https://doi.org/10.1016/j.scitotenv.2019.136002

Hassan, A., Khan, A., & Barros, R. (2023). Pharmaceuticals in Water: Risks to Aquatic Life and Remediation Strategies. *Hydrobiology 2023, Vol. 2, Pages 395-409*, *2*(2), 395–409. https://doi.org/10.3390/HYDROBIOLOGY2020026

He, S., Li, Y., Weng, L., Wang, J., He, J., Liu, Y., Zhang, K., Wu, Q., Zhang, Y., & Zhang, Z. (2018). Competitive adsorption of Cd2+, Pb2+ and Ni2+ onto Fe3+-modified argillaceous limestone: Influence of pH, ionic strength and natural organic matters. *Science of The Total Environment*, *637–638*, 69–78. https://doi.org/10.1016/J.SCITOTENV.2018.04.300

Helmecke, M., Fries, E., & Schulte, C. (2020). Regulating water reuse for agricultural irrigation: risks related to organic micro-contaminants. *Environmental Sciences Europe*, *32*(1), 1–10. https://doi.org/10.1186/S12302-019-0283-0/FIGURES/1

Hernández-Zamora, M., & Martínez-Jerónimo, F. (2019). Exposure to the azo dye Direct blue 15 produces toxic effects on microalgae, cladocerans, and zebrafish embryos. *Ecotoxicology*, *28*(8). https://doi.org/10.1007/s10646-019-02087-1

Hernández-Zamora, M., Martínez-Jerónimo, F., Cristiani-Urbina, E., & Cañizares-Villanueva, R. O. (2016). Congo red dye affects survival and reproduction in the cladoceran

Ceriodaphnia dubia. Effects of direct and dietary exposure. *Ecotoxicology*, *25*(10). https://doi.org/10.1007/s10646-016-1731-x

Ho, L., Grasset, C., Hoefel, D., Dixon, M. B., Leusch, F. D. L., Newcombe, G., Saint, C. P., & Brookes, J. D. (2011). Assessing granular media filtration for the removal of chemical contaminants from wastewater. *Water Research*, *45*(11). https://doi.org/10.1016/j.watres.2011.04.005

Hoyett, Z., & Hoyett, Z. (2017). Pharmaceuticals and Personal Care Products: Risks, Challenges, and Solutions. *Risk Assessment*. https://doi.org/10.5772/INTECHOPEN.70799

Idohou, E. A., Fatombi, J. K., Osseni, S. A., Agani, I., Neumeyer, D., Verelst, M., Mauricot, R., & Aminou, T. (2020). Preparation of activated carbon/chitosan/Carica papaya seeds composite for efficient adsorption of cationic dye from aqueous solution. *Surfaces and Interfaces*, *21*, 100741. https://doi.org/10.1016/J.SURFIN.2020.100741

Imminent risk of a global water crisis, warns the UN World Water Development Report 2023 | UNESCO. (n.d.). Retrieved April 23, 2024, from https://www.unesco.org/en/articles/imminent-risk-global-water-crisis-warns-un-world-water-development-report-2023

Infrared Spectroscopy Absorption Table. (n.d.). Retrieved June 24, 2023, from https://chem.libretexts.org/Ancillary_Materials/Reference/Reference_Tables/Spectroscopic_Reference_Tables/Infrared_Spectroscopy_Absorption_Table

Isik, Z., Saleh, M., M'barek, I., Yabalak, E., Dizge, N., & Deepanraj, B. (2022). Investigation of the adsorption performance of cationic and anionic dyes using hydrochared waste human hair. *Biomass Conversion and Biorefinery*, *1*, 1–14. https://doi.org/10.1007/S13399-022-02582-2/FIGURES/11

Juliano, C., & Magrini, G. A. (2017). Cosmetic Ingredients as Emerging Pollutants of Environmental and Health Concern. A Mini-Review. *Cosmetics 2017, Vol. 4, Page 11*, *4*(2), 11. https://doi.org/10.3390/COSMETICS4020011

Kalavathy, M. H., Karthikeyan, T., Rajgopal, S., & Miranda, L. R. (2005). Kinetic and isotherm studies of Cu(II) adsorption onto H3PO4-activated rubber wood sawdust. *Journal of Colloid and Interface Science*, *292*(2), 354–362. https://doi.org/10.1016/J.JCIS.2005.05.087

Kapoor, R. T., Danish, M., Singh, R. S., Rafatullah, M., & Abdul, A. K. (2021). Exploiting microbial biomass in treating azo dyes contaminated wastewater: Mechanism of degradation and factors affecting microbial efficiency. *Journal of Water Process Engineering*, *43*, 102255. https://doi.org/10.1016/J.JWPE.2021.102255

Karimi, M., Shojaei, A., Nematollahzadeh, A., & Abdekhodaie, M. J. (2012). Column study of Cr (VI) adsorption onto modified silica–polyacrylamide microspheres composite. *Chemical Engineering Journal*, *210*, 280–288. https://doi.org/10.1016/J.CEJ.2012.08.046

Kaveeshwar, A. R., Ponnusamy, S. K., Revellame, E. D., Gang, D. D., Zappi, M. E., & Subramaniam, R. (2018). Pecan shell based activated carbon for removal of iron(II) from fracking wastewater: Adsorption kinetics, isotherm and thermodynamic studies. *Process*

Safety and Environmental Protection, *114*, 107–122. https://doi.org/10.1016/J.PSEP.2017.12.007

Khan, S., & Malik, A. (2014). Environmental and health effects of textile industry wastewater. In *Environmental Deterioration and Human Health: Natural and Anthropogenic Determinants* (Vol. 9789400778900). https://doi.org/10.1007/978-94-007-7890-0_4

Kim, Y. S., & Kim, J. H. (2019). Isotherm, kinetic and thermodynamic studies on the adsorption of paclitaxel onto Sylopute. *The Journal of Chemical Thermodynamics*, *130*, 104–113. https://doi.org/10.1016/J.JCT.2018.10.005

Kishor, R., Purchase, D., Saratale, G. D., Saratale, R. G., Ferreira, L. F. R., Bilal, M., Chandra, R., & Bharagava, R. N. (2021). Ecotoxicological and health concerns of persistent coloring pollutants of textile industry wastewater and treatment approaches for environmental safety. *Journal of Environmental Chemical Engineering*, *9*(2). https://doi.org/10.1016/j.jece.2020.105012

Kohli, H. P., Gupta, S., & Chakraborty, M. (2019). Separation of Diclofenac using pseudo-emulsion hollow fiber membrane: Optimization by Box-Behnken response surface design. *Journal of Water Process Engineering*, *32*, 100880. https://doi.org/10.1016/J.JWPE.2019.100880

Kong, J., Yang, T., Rui, Z., & Ji, H. (2019). Perovskite-based photocatalysts for organic contaminants removal: Current status and future perspectives. *Catalysis Today*, *327*. https://doi.org/10.1016/j.cattod.2018.06.045

Kong, Q., Wang, X., & Lou, T. (2020). Preparation of millimeter-sized chitosan/carboxymethyl cellulose hollow capsule and its dye adsorption properties. *Carbohydrate Polymers*, *244*, 116481. https://doi.org/10.1016/J.CARBPOL.2020.116481

Kumar, A., Patra, C., Kumar, S., & Narayanasamy, S. (2022a). Effect of magnetization on the adsorptive removal of an emerging contaminant ciprofloxacin by magnetic acid activated carbon. *Environmental Research*, *206*. https://doi.org/10.1016/j.envres.2021.112604

Kumar, A., Patra, C., Kumar, S., & Narayanasamy, S. (2022b). Effect of magnetization on the adsorptive removal of an emerging contaminant ciprofloxacin by magnetic acid activated carbon. *Environmental Research*, *206*, 112604. https://doi.org/10.1016/J.ENVRES.2021.112604

Kumar, A., Patra, C., Rajendran, H. K., & Narayanasamy, S. (2022). Activated carbon-chitosan based adsorbent for the efficient removal of the emerging contaminant diclofenac: Synthesis, characterization and phytotoxicity studies. *Chemosphere*, *307*, 135806. https://doi.org/10.1016/J.CHEMOSPHERE.2022.135806

Kumar, A., Singh, S., Rajulapati, V., & Goyal, A. (2020). Evaluation of pre-treatment methods for Lantana camara stem for enhanced enzymatic saccharification. *3 Biotech*, *10*(2). https://doi.org/10.1007/s13205-019-2029-5

Kumar, S., Narayanasamy, S., & Venkatesh, R. P. (2018). Removal of Cr(VI) from synthetic solutions using water caltrop shell as a low-cost biosorbent. *Https://Doi.Org/10.1080/01496395.2018.1560333*, *54*(17), 2783–2799. https://doi.org/10.1080/01496395.2018.1560333

Kumari, B., Madan, V. K., & Kathpal, T. S. (2007). Pesticide residues in rain water from Hisar, India. *Environmental Monitoring and Assessment*, *133*(1–3), 467–471. https://doi.org/10.1007/s10661-006-9601-2

Kumari, M., Mohapatra, D., & Bhushan, M. (2022). *Emerging Contaminants: Sources, Effects, and Treatment by New Adsorption Methods*. 97–121. https://doi.org/10.1007/978-981-19-1847-6_5

Kuncoro, E. P., Isnadina, D. R. M., Darmokoesoemo, H., Fauziah, O. R., & Kusuma, H. S. (2018). Characterization, kinetic, and isotherm data for adsorption of Pb2+ from aqueous solution by adsorbent from mixture of bagasse-bentonite. *Data in Brief*, *16*. https://doi.org/10.1016/j.dib.2017.11.098

Kuncoro, E. P., Soedarti, T., Putranto, T. W. C., Darmokoesoemo, H., Abadi, N. R., & Kusuma, H. S. (2018). Characterization of a mixture of algae waste-bentonite used as adsorbent for the removal of Pb2+ from aqueous solution. *Data in Brief*, *16*. https://doi.org/10.1016/j.dib.2017.12.030

Lehutso, R. F., Daso, A. P., & Okonkwo, J. O. (2017). Occurrence and environmental levels of triclosan and triclocarban in selected wastewater treatment plants in Gauteng Province, South Africa. *Emerging Contaminants*, *3*(3), 107–114. https://doi.org/10.1016/J.EMCON.2017.07.001

Lei, C., Wen, F., Chen, J., Chen, W., Huang, Y., & Wang, B. (2021). Mussel-inspired synthesis of magnetic carboxymethyl chitosan aerogel for removal cationic and anionic dyes from aqueous solution. *Polymer*, *213*, 123316. https://doi.org/10.1016/J.POLYMER.2020.123316

Li, Z., Yahyaoui, S., Bouzid, M., Erto, A., & Dotto, G. L. (2021). Interpretation of diclofenac adsorption onto ZnFe2O4/chitosan magnetic composite via BET modified model by using statistical physics formalism. *Journal of Molecular Liquids*, *327*, 114858. https://doi.org/10.1016/J.MOLLIQ.2020.114858

Lian, Z., Li, Y., Xian, H., Ouyang, X. kun, Lu, Y., Peng, X., & Hu, D. (2020). EDTA-functionalized magnetic chitosan oligosaccharide and carboxymethyl cellulose nanocomposite: Synthesis, characterization, and Pb(II) adsorption performance. *International Journal of Biological Macromolecules*, *165*, 591–600. https://doi.org/10.1016/J.IJBIOMAC.2020.09.156

Liang, H., Liu, R., An, X., Hu, C., Zhang, X., & Liu, H. (2021). Bimetal-organic frameworks with coordinatively unsaturated metal sites for highly efficient Fenton-like catalysis. *Chemical Engineering Journal*, *414*, 128669. https://doi.org/10.1016/J.CEJ.2021.128669

Liu, J., He, X., Zhong, H., Lei, P., Zhang, J., Xu, Y., & Wei, Y. (2022). Removal of methylmercury and its potential relationship to microbiota in sludge anaerobic digestion under thermal hydrolysis. *Bioresource Technology*, *347*, 126394. https://doi.org/10.1016/J.BIORTECH.2021.126394

Liu, Q., Yang, B., Zhang, L., & Huang, R. (2015). Adsorption of an anionic azo dye by cross-linked chitosan/bentonite composite. *International Journal of Biological Macromolecules*, *72*, 1129–1135. https://doi.org/10.1016/J.IJBIOMAC.2014.10.008

López-Cervantes, J., Sánchez-Machado, D. I., Sánchez-Duarte, R. G., & Correa-Murrieta, M. A. (2018). Study of a fixed-bed column in the adsorption of an azo dye from an aqueous medium using a chitosan–glutaraldehyde biosorbent. *Adsorption Science and Technology*, *36*(1–2), 215–232. https://doi.org/10.1177/0263617416688021/ASSET/IMAGES/LARGE/10.1177_0263617416688021-FIG8.JPEG

Lu, Y., Wang, Z., Ouyang, X. kun, Ji, C., Liu, Y., Huang, F., & Yang, L. Y. (2020). Fabrication of cross-linked chitosan beads grafted by polyethylenimine for efficient adsorption of diclofenac sodium from water. *International Journal of Biological Macromolecules*, *145*, 1180–1188. https://doi.org/10.1016/J.IJBIOMAC.2019.10.044

Luo, W., Hai, F. I., Price, W. E., Guo, W., Ngo, H. H., Yamamoto, K., & Nghiem, L. D. (2014). High retention membrane bioreactors: Challenges and opportunities. *Bioresource Technology*, *167*, 539–546. https://doi.org/10.1016/J.BIORTECH.2014.06.016

Maheshwari, K., Agrawal, M., & Gupta, A. B. (2021). *Dye Pollution in Water and Wastewater*. 1–25. https://doi.org/10.1007/978-981-16-2892-4_1

Malik, A., Ojha, P., & Singh, K. P. (2009). Levels and distribution of persistent organochlorine pesticide residues in water and sediments of Gomti river (India)—a tributary of the Ganges River. *Environmental Monitoring and Assessment*, *148*(1–4), 421–435. https://doi.org/10.1007/s10661-008-0172-2

Manjunatha, C. R., Nagabhushana, B. M., Raghu, M. S., Pratibha, S., Dhananjaya, N., & Narayana, A. (2019). Perovskite lanthanum aluminate nanoparticles applications in antimicrobial activity, adsorptive removal of Direct Blue 53 dye and fluoride. *Materials Science and Engineering: C*, *101*, 674–685. https://doi.org/10.1016/J.MSEC.2019.04.013

Manzoor, K., Ahmad, M., Ahmad, S., & Ikram, S. (2019). Synthesis, Characterization, Kinetics, and Thermodynamics of EDTA-Modified Chitosan-Carboxymethyl Cellulose as Cu(II) Ion Adsorbent. *ACS Omega*, *4*(17), 17425–17437. https://doi.org/10.1021/ACSOMEGA.9B02214/ASSET/IMAGES/LARGE/AO9B02214_0006.JPEG

Meek, R. W., Vyas, H., & Piddock, L. J. V. (2015). Nonmedical Uses of Antibiotics: Time to Restrict Their Use? *PLOS Biology*, *13*(10), e1002266. https://doi.org/10.1371/JOURNAL.PBIO.1002266

Mishra, V., Sharma, U., Rawat, D., Benson, D., Singh, M., & Sharma, R. S. (2020). Fast-changing life-styles and ecotoxicity of hair dyes drive the emergence of hidden toxicants threatening environmental sustainability in Asia. *Environmental Research*, *184*, 109253. https://doi.org/10.1016/J.ENVRES.2020.109253

Moussout, H., Ahlafi, H., Aazza, M., & Bourakhouadar, M. (2016). Kinetics and mechanism of the thermal degradation of biopolymers chitin and chitosan using thermogravimetric analysis. *Polymer Degradation and Stability*, *130*, 1–9. https://doi.org/10.1016/J.POLYMDEGRADSTAB.2016.05.016

Naat, J. N., Neolaka, Y. A. B., Lapailaka, T., Rachmat Triandi, T., Sabarudin, A., Darmokoesoemo, H., & Kusuma, H. S. (2021). Adsorption of Cu(II) and Pb(II) using

silica@mercapto (hs@m) hybrid adsorbent synthesized from silica of Takari sand: Optimization of parameters and kinetics. *Rasayan Journal of Chemistry*, *14*(1). https://doi.org/10.31788/RJC.2021.1415803

Naseem, K., Farooqi, Z. H., Begum, R., & Irfan, A. (2018). Removal of Congo red dye from aqueous medium by its catalytic reduction using sodium borohydride in the presence of various inorganic nano-catalysts: A review. *Journal of Cleaner Production*, *187*, 296–307. https://doi.org/10.1016/J.JCLEPRO.2018.03.209

Neolaka, Y. A. B., Lawa, Y., Naat, J., Lalang, A. C., Widyaningrum, B. A., Ngasu, G. F., Niga, K. A., Darmokoesoemo, H., Iqbal, M., & Kusuma, H. S. (2023). Adsorption of methyl red from aqueous solution using Bali cow bones (Bos javanicus domesticus) hydrochar powder. *Results in Engineering*, *17*. https://doi.org/10.1016/j.rineng.2022.100824

Neolaka, Y. A. B., Riwu, A. A. P., Aigbe, U. O., Ukhurebor, K. E., Onyancha, R. B., Darmokoesoemo, H., & Kusuma, H. S. (2023). Potential of activated carbon from various sources as a low-cost adsorbent to remove heavy metals and synthetic dyes. *Results in Chemistry*, *5*. https://doi.org/10.1016/j.rechem.2022.100711

Ngulube, T., Gumbo, J. R., Masindi, V., & Maity, A. (2017). An update on synthetic dyes adsorption onto clay based minerals: A state-of-art review. *Journal of Environmental Management*, *191*, 35–57. https://doi.org/10.1016/J.JENVMAN.2016.12.031

Nguyen, M.-L. ;, Nakhjiri, A. T. ;, Kamal, M. ;, Mohamed, A. ;, Algarni, M. ;, Yu, S. T. ;, Wang, F.-M. ;, Su, C.-H., Nguyen, M.-L., Taghvaie Nakhjiri, A., Kamal, M., Mohamed, A., Algarni, M., Yu, S. T., Wang, F.-M., & Su, C.-H. (2022). State-of-the-Art Review on the Application of Membrane Bioreactors for Molecular Micro-Contaminant Removal from Aquatic Environment. *Membranes 2022, Vol. 12, Page 429*, *12*(4), 429. https://doi.org/10.3390/MEMBRANES12040429

Noroozi, B., & Sorial, G. A. (2013). Applicable models for multi-component adsorption of dyes: A review. *Journal of Environmental Sciences (China)*, *25*(3). https://doi.org/10.1016/S1001-0742(12)60194-6

Pandey, N., Shukla, S. K., & Singh, N. B. (2017). Water purification by polymer nanocomposites: an overview. *Https://Doi.Org/10.1080/20550324.2017.1329983*, *3*(2), 47–66. https://doi.org/10.1080/20550324.2017.1329983

Parlakidis, P., Rodriguez, M. S., Gikas, G. D., Alexoudis, C., Perez-Rojas, G., Perez-Villanueva, M., Carrera, A. P., Fernández-Cirelli, A., & Vryzas, Z. (2022). Occurrence of Banned and Currently Used Herbicides, in Groundwater of Northern Greece: A Human Health Risk Assessment Approach. *International Journal of Environmental Research and Public Health*, *19*(14), 8877. https://doi.org/10.3390/IJERPH19148877/S1

Patra, C., Gupta, R., Bedadeep, D., & Narayanasamy, S. (2020). Surface treated acid-activated carbon for adsorption of anionic azo dyes from single and binary adsorptive systems: A detail insight. *Environmental Pollution*, *266*, 115102. https://doi.org/10.1016/J.ENVPOL.2020.115102

Patra, C., Medisetti, R. M. N., Pakshirajan, K., & Narayanasamy, S. (2019a). Assessment of raw, acid-modified and chelated biomass for sequestration of hexavalent chromium from aqueous solution using Sterculia villosa Roxb. shells. *Environmental Science and*

Pollution Research, *26*(23), 23625–23637. https://doi.org/10.1007/S11356-019-05582-4/TABLES/5

Patra, C., Medisetti, R. M. N., Pakshirajan, K., & Narayanasamy, S. (2019b). Assessment of raw, acid-modified and chelated biomass for sequestration of hexavalent chromium from aqueous solution using Sterculia villosa Roxb. shells. *Environmental Science and Pollution Research*, *26*(23), 23625–23637. https://doi.org/10.1007/S11356-019-05582-4/TABLES/5

Patra, C., Medisetti, R. M. N., Pakshirajan, K., & Narayanasamy, S. (2019c). Assessment of raw, acid-modified and chelated biomass for sequestration of hexavalent chromium from aqueous solution using Sterculia villosa Roxb. shells. *Environmental Science and Pollution Research*, *26*(23), 23625–23637. https://doi.org/10.1007/S11356-019-05582-4/TABLES/5

Patra, C., Suganya, E., Sivaprakasam, S., Krishnamoorthy, G., & Narayanasamy, S. (2021a). A detailed insight on fabricated porous chitosan in eliminating synthetic anionic dyes from single and multi-adsorptive systems with related studies. *Chemosphere*, *281*, 130706. https://doi.org/10.1016/J.CHEMOSPHERE.2021.130706

Patra, C., Suganya, E., Sivaprakasam, S., Krishnamoorthy, G., & Narayanasamy, S. (2021b). A detailed insight on fabricated porous chitosan in eliminating synthetic anionic dyes from single and multi-adsorptive systems with related studies. *Chemosphere*, *281*, 130706. https://doi.org/10.1016/J.CHEMOSPHERE.2021.130706

Pattanaik, L., Padhi, S. K., Hariprasad, P., & Naik, S. N. (2020). Life cycle cost analysis of natural indigo dye production from Indigofera tinctoria L. plant biomass: a case study of India. *Clean Technologies and Environmental Policy*, *22*(8), 1639–1654. https://doi.org/10.1007/S10098-020-01914-Y/FIGURES/7

Patwa, D., Muigai, H. H., Ravi, K., Sreedeep, S., & Kalita, P. (2022). A Novel Application of Biochar Produced from Invasive Weeds and Industrial Waste in Thermal Backfill for Crude Oil Industries. *Waste and Biomass Valorization*, *13*(6), 3025–3042. https://doi.org/10.1007/S12649-022-01694-0/TABLES/4

Peng, J., Wang, X., & Lou, T. (2020). Preparation of chitosan/gelatin composite foam with ternary solvents of dioxane/acetic acid/water and its water absorption capacity. *Polymer Bulletin*, *77*(10), 5227–5244. https://doi.org/10.1007/S00289-019-03016-2/TABLES/2

Pereira, M. B. B., França, D. B., Araújo, R. C., Silva Filho, E. C., Rigaud, B., Fonseca, M. G., & Jaber, M. (2020). Amino hydroxyapatite/chitosan hybrids reticulated with glutaraldehyde at different pH values and their use for diclofenac removal. *Carbohydrate Polymers*, *236*, 116036. https://doi.org/10.1016/J.CARBPOL.2020.116036

PK Mutiyar, A. M. (2012). Status of organochlorine pesticides in Ganga river basin: anthropogenic or glacial. *Drink Water Engineering Science Discuss*, *5*, 1–30. https://doi.org/10.5194/dwesd-5-1-2012

PK Mutiyar, A. M. A. P. (2011). Status of organochlorine pesticides in the drinking water well-field located in the Delhi region of the flood plains of river Yamuna. *Drink Water Engineering Science Discuss*, *4*, 85–115. https://doi.org/10.5194/dwesd-4-85-2011

Pradhan, S. S., Gowda, G. B., Adak, T., Guru-Pirasanna-Pandi, G., Patil, N. B., Annamalai, M., Rath, P. C., Pradhan, S. S., Gowda, G. B., Adak, T., Guru-Pirasanna-Pandi, G., Patil, N. B., Annamalai, M., & Rath, P. C. (2022). Pesticides Occurrence in Water Sources and Decontamination Techniques. *Pesticides - Updates on Toxicity, Efficacy and Risk Assessment*. https://doi.org/10.5772/INTECHOPEN.103812

Pramanik, S., Kumar, M., & Qureshi, A. (2021). Mercury in skin-care products in India and consumer exposure risks. *Regulatory Toxicology and Pharmacology*, *121*, 104870. https://doi.org/10.1016/J.YRTPH.2021.104870

Priya, A. K., Gnanasekaran, L., Rajendran, S., Qin, J., & Vasseghian, Y. (2022). Occurrences and removal of pharmaceutical and personal care products from aquatic systems using advanced treatment- A review. *Environmental Research*, *204*, 112298. https://doi.org/10.1016/J.ENVRES.2021.112298

PubChem, Diclofenac . (n.d.). Retrieved March 17, 2022, from https://pubchem.ncbi.nlm.nih.gov/compound/3033

Puvaneswari, N., Muthukrishnan, J., & Gunasekaran, P. (2006). Toxicity assessment and microbial degradation of azo dyes. In *Indian Journal of Experimental Biology* (Vol. 44, Issue 8).

Qurrat-Ul-Ain, Khurshid, S., Gul, Z., Khatoon, J., Shah, M. R., Hamid, I., Khan, I. A. T., & Aslam, F. (2020). Anionic azo dyes removal from water using amine-functionalized cobalt–iron oxide nanoparticles: a comparative time-dependent study and structural optimization towards the removal mechanism. *RSC Advances*, *10*(2), 1021–1041. https://doi.org/10.1039/C9RA07686G

Rajendran, R. B., Imagawa, T., Tao, H., & Ramesh, R. (2005). Distribution of PCBs HCHs and DDTs, and their ecotoxicological implications in Bay of Bangal, India. *Environment International*, *31*(4), 503–512. https://doi.org/10.1016/j.envint.2004.10.009

Rana, A. K., Mostafavi, E., Alsanie, W. F., Siwal, S. S., & Thakur, V. K. (2023). Cellulose-based materials for air purification: A review. *Industrial Crops and Products*, *194*, 116331. https://doi.org/10.1016/J.INDCROP.2023.116331

Renita, A. A., Vardhan, K. H., Kumar, P. S., Ngueagni, P. T., Abilarasu, A., Nath, S., Kumari, P., & Saravanan, R. (2021). Effective removal of malachite green dye from aqueous solution in hybrid system utilizing agricultural waste as particle electrodes. *Chemosphere*, *273*, 129634. https://doi.org/10.1016/J.CHEMOSPHERE.2021.129634

Rizzo, L., Malato, S., Antakyali, D., Beretsou, V. G., Đolić, M. B., Gernjak, W., Heath, E., Ivancev-Tumbas, I., Karaolia, P., Lado Ribeiro, A. R., Mascolo, G., McArdell, C. S., Schaar, H., Silva, A. M. T., & Fatta-Kassinos, D. (2019). Consolidated vs new advanced treatment methods for the removal of contaminants of emerging concern from urban wastewater. *Science of The Total Environment*, *655*, 986–1008. https://doi.org/10.1016/J.SCITOTENV.2018.11.265

Salimi, M., Esrafili, A., Gholami, M., Jonidi Jafari, A., Rezaei Kalantary, R., Farzadkia, M., Kermani, M., & Sobhi, H. R. (2017). Contaminants of emerging concern: a review of new approach in AOP technologies. *Environmental Monitoring and Assessment 2017 189:8*, *189*(8), 1–22. https://doi.org/10.1007/S10661-017-6097-X

Sankararamakrishnan, N., Kumar Sharma, A., & Sanghi, R. (2005). Organochlorine and organophosphorus pesticide residues in ground water and surface waters of Kanpur, Uttar Pradesh, India. *Environment International*, *31*(1), 113–120. https://doi.org/10.1016/j.envint.2004.08.001

Saravanan, A., Jeevanantham, S., Senthil Kumar, P., Varjani, S., Yaashikaa, P. R., & Karishma, S. (2020). Enhanced Zn(II) ion adsorption on surface modified mixed biomass – Borassus flabellifer and Aspergillus tamarii: Equilibrium, kinetics and thermodynamics study. *Industrial Crops and Products*, *153*, 112613. https://doi.org/10.1016/J.INDCROP.2020.112613

Sarkar, S., Banerjee, A., Halder, U., Biswas, R., & Bandopadhyay, R. (2017). Degradation of Synthetic Azo Dyes of Textile Industry: a Sustainable Approach Using Microbial Enzymes. *Water Conservation Science and Engineering 2017 2:4*, *2*(4), 121–131. https://doi.org/10.1007/S41101-017-0031-5

Sathishkumar, K., AlSalhi, M. S., Sanganyado, E., Devanesan, S., Arulprakash, A., & Rajasekar, A. (2019). Sequential electrochemical oxidation and bio-treatment of the azo dye congo red and textile effluent. *Journal of Photochemistry and Photobiology B: Biology*, *200*, 111655. https://doi.org/10.1016/J.JPHOTOBIOL.2019.111655

Sathishkumar, P., Meena, R. A. A., Palanisami, T., Ashokkumar, V., Palvannan, T., & Gu, F. L. (2020). Occurrence, interactive effects and ecological risk of diclofenac in environmental compartments and biota - a review. *Science of The Total Environment*, *698*, 134057. https://doi.org/10.1016/J.SCITOTENV.2019.134057

Shah, A. I., Din Dar, M. U., Bhat, R. A., Singh, J. P., Singh, K., & Bhat, S. A. (2020). Prospectives and challenges of wastewater treatment technologies to combat contaminants of emerging concerns. *Ecological Engineering*, *152*, 105882. https://doi.org/10.1016/J.ECOLENG.2020.105882

Shahnaz, T., Vishnu Priyan, V., Pandian, S., & Narayanasamy, S. (2021). Use of Nanocellulose extracted from grass for adsorption abatement of Ciprofloxacin and Diclofenac removal with phyto, and fish toxicity studies. *Environmental Pollution*, *268*, 115494. https://doi.org/10.1016/J.ENVPOL.2020.115494

Shirani, Z., Song, H., & Bhatnagar, A. (2020). Efficient removal of diclofenac and cephalexin from aqueous solution using Anthriscus sylvestris-derived activated biochar. *Science of The Total Environment*, *745*, 140789. https://doi.org/10.1016/J.SCITOTENV.2020.140789

Soares, S. F., Fernandes, T., Sacramento, M., Trindade, T., & Daniel-da-Silva, A. L. (2019). Magnetic quaternary chitosan hybrid nanoparticles for the efficient uptake of diclofenac from water. *Carbohydrate Polymers*, *203*, 35–44. https://doi.org/10.1016/J.CARBPOL.2018.09.030

Somsesta, N., Sricharoenchaikul, V., & Aht-Ong, D. (2020). Adsorption removal of methylene blue onto activated carbon/cellulose biocomposite films: Equilibrium and kinetic studies. *Materials Chemistry and Physics*, *240*, 122221. https://doi.org/10.1016/J.MATCHEMPHYS.2019.122221

Sonwani, R. K., Swain, G., Giri, B. S., Singh, R. S., & Rai, B. N. (2020). Biodegradation of Congo red dye in a moving bed biofilm reactor: Performance evaluation and kinetic modeling. *Bioresource Technology*, *302*, 122811. https://doi.org/10.1016/J.BIORTECH.2020.122811

Spiliotopoulou, A., Antoniou, M. G., & Andersen, H. R. (2021). Natural fluorescence emission–an indirect measurement of applied ozone dosages to remove pharmaceuticals in biologically treated wastewater. *Environmental Technology (United Kingdom)*, *42*(4), 584–596. https://doi.org/10.1080/09593330.2019.1639827/SUPPL_FILE/TENT_A_1639827_SM1233.DOCX

Sreeramareddygari, M., Mannekote Shivanna, J., Somasundrum, M., Soontarapa, K., & Surareungchai, W. (2021). Polythiocyanuric acid-functionalized MoS2 nanosheet-based high flux membranes for removal of toxic heavy metal ions and congo red. *Chemical Engineering Journal*, *425*, 130592. https://doi.org/10.1016/J.CEJ.2021.130592

Taha, S. M., Amer, M. E., Elmarsafy, A. E., & Elkady, M. Y. (2014). Adsorption of 15 different pesticides on untreated and phosphoric acid treated biochar and charcoal from water. *Journal of Environmental Chemical Engineering*, *2*(4), 2013–2025. https://doi.org/10.1016/J.JECE.2014.09.001

Tang, Y., Shao, Y., Chen, N., & Yao, K. F. (2014). Rapid decomposition of Direct Blue 6 in neutral solution by Fe–B amorphous alloys. *RSC Advances*, *5*(8), 6215–6221. https://doi.org/10.1039/C4RA10000J

Tchounwou, B., Luo, X., Cao, Z., Femi Bakare, B., & Adeyinka, G. C. (2022). Occurrence and Fate of Triclosan and Triclocarban in Selected Wastewater Systems across Durban Metropolis, KwaZulu-Natal, South Africa. *International Journal of Environmental Research and Public Health 2022, Vol. 19, Page 6769*, *19*(11), 6769. https://doi.org/10.3390/IJERPH19116769

Tu, H., Yu, Y., Chen, J., Shi, X., Zhou, J., Deng, H., & Du, Y. (2017). Highly cost-effective and high-strength hydrogels as dye adsorbents from natural polymers: chitosan and cellulose. *Polymer Chemistry*, *8*(19), 2913–2921. https://doi.org/10.1039/C7PY00223H

UN World Water Development Report 2023 | UN-Water. (n.d.). Retrieved April 23, 2024, from https://www.unwater.org/publications/un-world-water-development-report-2023

Unugul, T., & Nigiz, F. U. (2020). Preparation and Characterization an Active Carbon Adsorbent from Waste Mandarin Peel and Determination of Adsorption Behavior on Removal of Synthetic Dye Solutions. *Water, Air, and Soil Pollution*, *231*(11), 1–14. https://doi.org/10.1007/S11270-020-04903-5/TABLES/5

Uyanga, K. A., & Daoud, W. A. (2021). Carboxymethyl cellulose-chitosan composite hydrogel: Modelling and experimental study of the effect of composition on microstructure and swelling response. *International Journal of Biological Macromolecules*, *181*, 1010–1022. https://doi.org/10.1016/J.IJBIOMAC.2021.04.117

Velusamy, K., Periyasamy, S., Kumar, P. S., Jayaraj, T., Krishnasamy, R., Sindhu, J., Sneka, D., Subhashini, B., & Vo, D. V. N. (2021). Analysis on the removal of emerging contaminant

from aqueous solution using biochar derived from soap nut seeds. *Environmental Pollution*, *287*, 117632. https://doi.org/10.1016/J.ENVPOL.2021.117632

Vishnu Priyan, V., Kumar, N., Rajendran, H. K., Ray, J., & Narayanasamy, S. (2022). Sequestration and toxicological assessment of emerging contaminants with polypyrrole modified carboxymethyl cellulose (CMC/PPY): Case of ibuprofen pharmaceutical drug. *International Journal of Biological Macromolecules*, *221*, 547–557. https://doi.org/10.1016/J.IJBIOMAC.2022.09.046

Walha, K., Amar, R. Ben, Firdaous, L., Quéméneur, F., & Jaouen, P. (2007). Brackish groundwater treatment by nanofiltration, reverse osmosis and electrodialysis in Tunisia: performance and cost comparison. *Desalination*, *207*(1–3). https://doi.org/10.1016/j.desal.2006.03.583

Walker, G. M., & Weatherley, L. R. (1997). Adsorption of acid dyes on to granular activated carbon in fixed beds. *Water Research*, *31*(8), 2093–2101. https://doi.org/10.1016/S0043-1354(97)00039-0

Wang, J., & Bai, Z. (2017). Fe-based catalysts for heterogeneous catalytic ozonation of emerging contaminants in water and wastewater. *Chemical Engineering Journal*, *312*, 79–98. https://doi.org/10.1016/J.CEJ.2016.11.118

WHO. (2006). Guidelines for the Safe Use of Wastewater, Excreta and Greywater, Volume 1: Policy and Regulatory Aspects. World Health Organization.

Wu, J., Yang, J., Feng, P., Huang, G., Xu, C., & Lin, B. (2020). High-efficiency removal of dyes from wastewater by fully recycling litchi peel biochar. *Chemosphere*, *246*, 125734. https://doi.org/10.1016/J.CHEMOSPHERE.2019.125734

Xu, T., Zhao, W., Guo, X., Zhang, H., Hu, S., Huang, Z., & Yin, D. (2020). Characteristics of antibiotics and antibiotic resistance genes in Qingcaosha Reservoir in Yangtze River Delta, China. *Environmental Sciences Europe*, *32*(1), 1–11. https://doi.org/10.1186/S12302-020-00357-Y/FIGURES/5

Yabalak, E., Mahmood Al-Nuaimy, M. N., Saleh, M., Isik, Z., Dizge, N., & Balakrishnan, D. (2022). Catalytic efficiency of raw and hydrolyzed eggshell in the oxidation of crystal violet and dye bathing wastewater by thermally activated peroxide oxidation method. *Environmental Research*, *212*, 113210. https://doi.org/10.1016/J.ENVRES.2022.113210

Yu, F., Li, Y., Han, S., & Ma, J. (2016). Adsorptive removal of antibiotics from aqueous solution using carbon materials. *Chemosphere*, *153*, 365–385. https://doi.org/10.1016/J.CHEMOSPHERE.2016.03.083

Zhang, H., Ma, J., Wang, F., Chu, Y., Yang, L., & Xia, M. (2020). Mechanism of carboxymethyl chitosan hybrid montmorillonite and adsorption of Pb(II) and Congo red by CMC-MMT organic-inorganic hybrid composite. *International Journal of Biological Macromolecules*, *149*, 1161–1169. https://doi.org/10.1016/J.IJBIOMAC.2020.01.201

Zhang, Q., Sun, Y., & Liu, Y. (2023). Green synthesis of chitosan–phytic acid polymers and nanoparticles. *Industrial Crops and Products*, *199*, 116747. https://doi.org/10.1016/J.INDCROP.2023.116747

Zhang, W., Wang, H., Hu, X., Feng, H., Xiong, W., Guo, W., Zhou, J., Mosa, A., & Peng, Y. (2019). Multicavity triethylenetetramine-chitosan/alginate composite beads for enhanced

Cr(VI) removal. *Journal of Cleaner Production*, *231*, 733–745. https://doi.org/10.1016/J.JCLEPRO.2019.05.219

Zheng, J., Ma, J., Wang, Z., Xu, S., Waite, T. D., & Wu, Z. (2017). Contaminant Removal from Source Waters Using Cathodic Electrochemical Membrane Filtration: Mechanisms and Implications. *Environmental Science and Technology*, *51*(5), 2757–2765. https://doi.org/10.1021/acs.est.6b05625

Zhou, Y., Lu, J., Zhou, Y., & Liu, Y. (2019). Recent advances for dyes removal using novel adsorbents: A review. *Environmental Pollution*, *252*, 352–365. https://doi.org/10.1016/J.ENVPOL.2019.05.072

Zhu, L., Du, L., Cao, G., & Cai, Z. (2023). AI-guided electro-decomposition of persistent organic pollutants: a long-awaited vision becoming reality? *Environmental Science: Advances*, *2*(10), 1302–1305. https://doi.org/10.1039/D3VA00175J

Appendix

Table A1. Various isotherm models with their linear and non-linear equations.

Isotherm Model	Linear equation	Non-linear equation	Description
Langmuir Isotherm	$\frac{C_e}{q_e} = \frac{1}{K_L Q_0} + \frac{C_e}{Q_0}$	$q_e = \frac{Q_0 K_L C_e}{1 + K_L Ce}$	**qe** is the quantity of adsorbate adsorbed (mg/g), **Q_0** denotes the amount of adsorbate adsorbed monolayer capacity (mg/g), **C_e** is the adsorbate equilibrium concentration (mg/L), **K_L** is the Langmuir isotherm constant (L/mg).
Freundlich Isotherm	$\log q_e = \log K_F + \frac{1}{n} \log C_e$	$q_e = k_F C_e^{1/n}$	**K_F** is the Freundlich isotherm constant (L/g), **n** represents the exponent of Freundlich constant.
Dubinin-Radushkevich Isotherm	$\ln q_e = \ln q_m - \beta \varepsilon^2$	$q_e = q_m e^{-\beta \varepsilon^2}$	**q_m** is the maximum adsorption capacity (mg/g), **β** corresponds to the activity coefficient (mol2/J2), **ε** represents the Polanyi potential.
Temkin Isotherm	$q_e = \frac{RT}{b_T} \ln K_T + \frac{RT}{b_T} \ln C_e$	$q_e = \frac{RT}{b_T} \ln(K_T C_e)$	**K_T** is the equilibrium binding constant (L/g), **b_T** is Temkin constant for the heat of adsorption (kJ/mol).

Table A2. Various kinetic models with their equations.

Kinetic Model	Equation	Description
Pseudo-first-order model	$\log(q_e - q_t) = logq_e - \frac{k_1 t}{2.303}$	$\mathbf{q_e}$ and $\mathbf{q_t}$ represents the equilibrium adsorption capacity and adsorption capacity at time t (mg/g), $\mathbf{k_1}$ is the pseudo-first-order rate constant (min^{-1}).
Pseudo-second-order model	$\frac{t}{q_t} = \frac{1}{k_2 q_e^2} + \frac{t}{q_e}$	$\mathbf{k_2}$ is the pseudo-second-order rate constant (g/mg min).
Elovich model	$q_t = \frac{1}{\beta}\ln \alpha\beta + \frac{1}{\beta}\ln t$	**α** (g/mg min) and **β** (mg/g) corresponds to the Elovich constants.
Intra-particle diffusion model	$q_t = K_{ID}\sqrt{t} + c$	$\mathbf{K_{ID}}$ (mg/g min 1/2) is the rate constant, **c** is the intra-particle diffusion model constant.

Table A3. Various characterization techniques.

Analysis	Characterization techniques	Make and Model
Morphological, topological, and surface analysis	Field Emission Scanning Electron Microscopy, FESEM	Zeiss-Gemini
	Field Emission Transmission Electron Microscopy, FETEM	JEOL-2100F
	Atomic Force Microscopy, AFM	Oxford-Cypher
Elemental analysis	Energy Dispersive X-Ray Analysis, EDX	Zeiss-Sigma
Functional group determination	Fourier Transform Infrared Spectroscopy, FTIR	PerkinElmer- Spectrum 2
	Raman Spectroscopy, RS	Horiba Jobin Vyon-LabRam HR
Nature of crystallinity	X-ray powder Diffraction, XRD	Rigaku- Micromax-007HF
Magnetic nature	Vibrating Sample Magnetometer, VSM	Lakeshore-7410 series
To measure the absorbance	UV–Visible Spectrophotometry	Tecan-Infinite M200 PRO

A4. Packed bed column parameters

Various column adsorption parameters and their equations are as follows as:

$$m_{total} = \frac{FC_o t_{total}}{1000} \quad \text{(A.1)}$$

$$q_{total} = \frac{C_o F}{1000} \times (t_{total} - \int_{t=0}^{t=t_{total}} \frac{C_t}{C_o} dt \quad \text{(A.2)}$$

$$V_{eff} = Q \times t_{total} \quad \text{(A.3)}$$

$$q_{e(exp)} = \frac{Q_{total}}{w} \quad \text{(A.4)}$$

$$R\ \% = \frac{q_{total}}{m_{total}} \times 100 \quad \text{(A.5)}$$

Were,

F (mL/h): Flow rate

C_o (mg/L): Initial dye concentration

C_t (mg/L): Dye concentration at time t

t_{total} (min): Total time for column saturation

m_{total} (mg): Total amount of dye introduced into the column

Q_{total} (mg): amount of dye molecules adsorbed by adsorbent in the column experiment

$q_{e(exp)}$ (mg/g): Maximum adsorption capacity in column studies

V_{eff} (mL): Total volume of the effluent

R (%): Removal percentage of dye

List of Publications and Conferences

LIST OF PUBLICATIONS FROM THESIS WORK

1. **Ajit Kumar**, Chandi Patra, Shravan Kumar, Selvaraju Narayanasamy (2022). Effect of magnetization on the adsorptive removal of an emerging contaminant ciprofloxacin by magnetic acid activated carbon, **Environmental Research**, 206, 112604, https://doi.org/10.1016/j.envres.2021.112604 (**Elsevier; SCI IF 2022: 8.3)**.
2. **Ajit Kumar**, Chandi Patra, Harish Kumar, Selvaraju Narayanasamy (2022). Activated carbon-chitosan based adsorbent for the efficient removal of the emerging contaminant diclofenac: Synthesis, characterization and phytotoxicity studies, **Chemosphere**, 307, Part 2, 135806, https://doi.org/10.1016/j.chemosphere.2022.135806 **(Elsevier; SCI IF 2022: 8.8)**.
3. **Ajit Kumar**, Vishnu Priyan V, Jothika Jayabalan, Selvaraju Narayanasamy (2023). Fabrication of a novel bio-polymer adsorbent with high adsorptive capacity towards organic dyes, **Industrial Crops and Products** https://doi.org/10.1016/j.indcrop.2023.117166 **(Elsevier; SCI IF 2023: 5.9)**

LIST OF PUBLICATIONS FROM COLLABORATIVE WORK

1. Jothika Jeyabalan, Ajithkumar Veluchamy, **Ajit Kumar**, Ragavan Chandrasekar, Selvaraju Narayanasamy, (2023). A review on the laccase assisted decolourization of dyes: Recent trends and research progress **Journal of the Taiwan Institute of Chemical Engineers** https://doi.org/10.1016/j.jtice.2023.105081 (**Elsevier; SCI IF 2023: 5.7**)
2. Vishnu Priyan Varadharaj, Ghurupreya Ramesh, **Ajit Kumar**, Jothika Jeyabalan, Selvaraju Narayanasamy, (2023). Synthesis, characterization, and application of oxidant-modified biochar prepared from sawdust for sequestration of basic fuchsin: isotherm, kinetics, and toxicity studies **Biomass Conversion and Biorefinery** https://doi.org/10.1007/s13399-023-04210-z (**Elsevier; SCI IF 2023: 4.00**)
3. Ragavan Chandrasekar, Das Bedadeep, Tasrin Shahnaz, Vishnu Priyan Varadharaj, **Ajit Kumar**, Harish Kumar Rajendran, Selvaraju Narayanasamy, (2023). Graphene-Based Materials in Effective Remediation of Wastewater **Book: Graphene and its Derivatives (Volume 2)** https://doi.org/10.1007/978-981-99-4382-1_3
4. Vishnu Priyan V, Jeevanantham Sathasivam, **Ajit Kumar**, Selvaraju Narayanasamy, (2024). Chapter 6: Valorisation of Agricultural waste into a Low Cost-Adsorbent: Perspective of Reutilization. **Book: Agricultural Waste to Value-Added Products:**

Bioproducts and its Applications https://link.springer.com/book/10.1007/978-981-97-2535-9

PRESENTATIONS IN INTERNATIONAL AND NATIONAL CONFERENCES

1. Chandi Patra, **Ajit Kumar**, Selvaraju Narayanasamy "Surface porosity modified biopolymer for enhanced sequestration of dye from simulated water", REFLUX 2019, IIT Guwahati (Assam), **28-29 September 2019**.
2. **Ajit Kumar**, Chandi Patra, Selvaraju Narayanasamy "Effect of magnetization on activated carbon for the remediation of antibiotics from aqueous solution" **International Conference on Biotechnology for Resource Efficiency, Energy, Environment, Chemicals and Health** (BRE3CH-2021), CSIR-Indian Institute of Petroleum Dehradun (Uttarakhand), India, **01-04 December 2021**.
3. Chandi Patra, **Ajit Kumar**, Selvaraju Narayanasamy "Polypyrrole doped acid activated carbon for efficient removal of emerging antibiotic contaminant from simulated wastewater setups" **International Conference on Biotechnology for Resource Efficiency, Energy, Environment, Chemicals and Health** (BRE3CH-2021), CSIR-Indian Institute of Petroleum Dehradun (Uttarakhand), India, **01-04 December 2021**.

WORKSHOP

1. Online workshop on **"Scanning Electron Microscopy: Technique and its Applications"** organized by Northeast Centre for Biological Sciences and Healthcare Engineering (NECBH), IIT Guwahati, Assam. **29-30 July 2021**.
2. Online workshop on **"Nuclear Magnetic Resonance: Technique and its Applications"** organized by Northeast Centre for Biological Sciences and Healthcare Engineering (NECBH), IIT Guwahati, Assam. **23-24 August 2021**.
3. Online workshop on **"Scientific Writing"** organized by ACS Publications in collaboration with IIT Bhilai. **20th September 2021**.